University of Stuttgart
Germany

Functions of protein kinase D in β-cell regulation and breast cancer stem cell maintenance

Von der Fakultät Energie-, Verfahrens- und Biotechnik der

Universität Stuttgart zur Erlangung der Würde eines

Doktors der Naturwissenschaften (Dr. rer. nat.)

genehmigte Abhandlung

vorgelegt von

Wolfgang-Sebastian Lieb

aus Ulm

Erstprüferin: Prof. Dr. Monilola Olayioye

Zweitprüfer: Prof. Dr. Tilman Brummer

Prüfungsvorsitzender: Prof. Dr. Roland Kontermann

Tag der mündlichen Prüfung: 03.07.2020

Institut für Zellbiologie und Immunologie

Universität Stuttgart

2020

to my loved ones

Affidavit

I hereby confirm that my thesis entitled “Functions of protein kinase D in β-cell regulation and breast cancer stem cell maintenance” is the result of my own work. All sources and/ or materials applied are listed and specified in the thesis. Furthermore, I confirm that this thesis has not yet been submitted as part of another examination process neither in identical nor in similar form.

Wolfgang-Sebastian Lieb	Ulm, 03.10.2020 Ort, Datum

Table of Content

Zusammenfassung

Die Proteinkinase D (PKD)-Familie besteht aus den drei Isoformen PKD1, PKD2 und PKD3, die am besten für die Regulierung des Aktin-Umbaus und die Kontrolle der Vesikelabschnürung am Golgi-Komplex bekannt sind. Bislang ist die Signalübertragung der PKD-Familie gut verstanden, aber ihre Beiträge zu Krankheiten wie Diabetes und dreifach negativem Brustkrebs (TNBC) müssen noch weiter aufgeklärt werden.

Die Anpassung von β-Zellen an Insulinresistenz ist ein essenzieller Prozess, um die Glukosehomöostase während der Alterung und bei Adipositas zu erhalten. Es ist daher wichtig, die Signalwege zu verstehen welche die β-Zellfunktion regulieren. In dieser Arbeit zeige ich, dass die PKD die β-Zellfunktion während des Alterns und bei Adipositas über den Prozess der zellulären Seneszenz reguliert. Dafür verwendete ich einen β-Zell-spezifischen funktionellen PKD-Knockout oder den PKD-Inhibitor CRT0066101 und analysierte sowohl die alters- als auch die adipositasabhängige Glukosehomöostase. Der Verlust der PKD-Funktion verbesserte die Glukosetoleranz, die Glukose-stimulierte Insulinsekretion (GSIS) und schützte vor Hochfettdiät (HFD)-induzierter Insulin- und Glukoseintoleranz *in vivo*. Die Behandlung von Mäusen mit CRT0066101 führte zu den gleichen Effekten. Ich fand außerdem heraus, dass der Verlust bzw. die Inhibition von PKD die Expression der Superoxid Dismutase 2 (SOD2) verminderte, die Prävalenz von reaktiven Sauerstoffspezies (ROS) erhöhte und die p16 Expression verstärkte. Das hatte zur Folge, dass Seneszenzmarker wie erhöhte Zellgröße und β-Galaktosidase-Aktivität zu finden waren. Zusätzlich wurde durch die Verabreichung von CRT0066101 an Tiere mit nachgewiesener Glukose- und Insulinintoleranz die β-Zellfunktion vollständig wiederhergestellt. Diese Ergebnisse zeigen, dass PKD eine wesentliche Rolle bei der Aufrechterhaltung der β-Zellfunktion während des Alterns und der Adipositas spielen (Figure 1A).

Die Proteinkinase D3 (PKD3) ist bei TNBC hochreguliert und unterstützt die Zellproliferation sowie die Entwicklung von Metastasen. Hier zeige ich, dass PKD3 für die Aufrechterhaltung der TNBC-Stammzellpopulation erforderlich ist. TNBC Stammzellen repräsentieren eine Teilgesamtheit aus undifferenzierten Zellen, welche in direktem Zusammenhang mit frühzeitiger Metastasierung, Tumorrezidiv und schlechterem Gesamtüberleben stehen. Die Depletion von PKD3 in MDA-MB-231-

Zellen verringerte die Häufigkeit von Krebsstammzellen *in vitro* und das Tumorinitiationspotential *in vivo*. Ich führe ferner den Beweis, dass das RhoGEF GEF-H1 der PKD3-Aktivierung in TNBC-Stammzellen vorgeschaltet ist. Am wichtigsten ist, dass die pharmakologische PKD3-Hemmung, in Kombination mit dem Chemotherapeutikum Paclitaxel, die Onkosphären- und Koloniebildungseffizienz *in vitro* und das Tumorrezidiv *in vivo* synergistisch verminderte. Auf der Grundlage dieser Ergebnisse schlage ich vor, dass die gezielte Inhibition des GEF-H1/PKD3-Signalweges eine effiziente therapeutische Option für TNBC darstellt (Figure 1B).

Abstract

The protein kinase D family consists of three isoforms, PKD1, PKD2 and PKD3, which are best known for regulating actin remodeling and controlling vesicle fission at the Golgi complex. So far, the signaling of PKD is well understood but its contributions to diseases such as diabetes and triple negative breast cancer (TNCB) must be further elucidated.

β-cell adaption to insulin resistance is essential during aging and obesity to preserve glucose homeostasis. It is therefore important to understand the pathways regulating β-cell function. Here I show that protein kinase D (PKD) controls β-cell function during aging and obesity through regulating cellular senescence. I employed a β-cell specific functional PKD knockout or the PKD inhibitor CRT0066101 and analyzed aging- as well as obesity-dependent glucose homeostasis. The loss of PKD function improved glucose tolerance, glucose-stimulated insulin secretion (GSIS) and protected from high-fat-diet (HFD)-induced insulin and glucose intolerance *in vivo.* Treating mice with CRT0066101 resulted in the same effects. I further found that the depletion/inhibition of PKD decreased superoxide dismutase 2 (SOD2) expression, increased reactive oxygen species (ROS) and induced p16 expression. Furthermore, other senescence markers, such as cellular size and β-galactosidase activity, were increased as well. Additionally, the administration of CRT0066101 to animals with established glucose and insulin intolerance completely rescued β-cell function. These findings reveal an essential role for PKD in maintaining β-cell function during aging and obesity (Figure 1A).

Protein kinase D3 (PKD3) is upregulated in TNBC supporting cell proliferation and metastasis development. Here I show that PKD3 is required for the maintenance of the TNBC stem cell population. Stem cells represent a subpopulation of undifferentiated cells linked to early metastases, faster tumor recurrence, worse overall survival and higher-stage tumors. Depletion of PKD3 in the TNBC cell line MDA-MB-231 cells reduced the cancer stem cell frequency *in vitro* and tumor initiation potential *in* vivo. I further provide evidence that the RhoGEF GEF-H1 is upstream of PKD3 activation in TNBC stem cells. Most importantly, pharmacological PKD3 inhibition in combination with the chemotherapeutic paclitaxel synergistically decreased oncosphere and colony formation efficiency *in vitro* and xenograft recurrence *in vivo*. Based on these results I

propose that targeting the GEF-H1/PKD3 signaling pathway provides a potential therapeutic option for TNBC (Figure 1B).

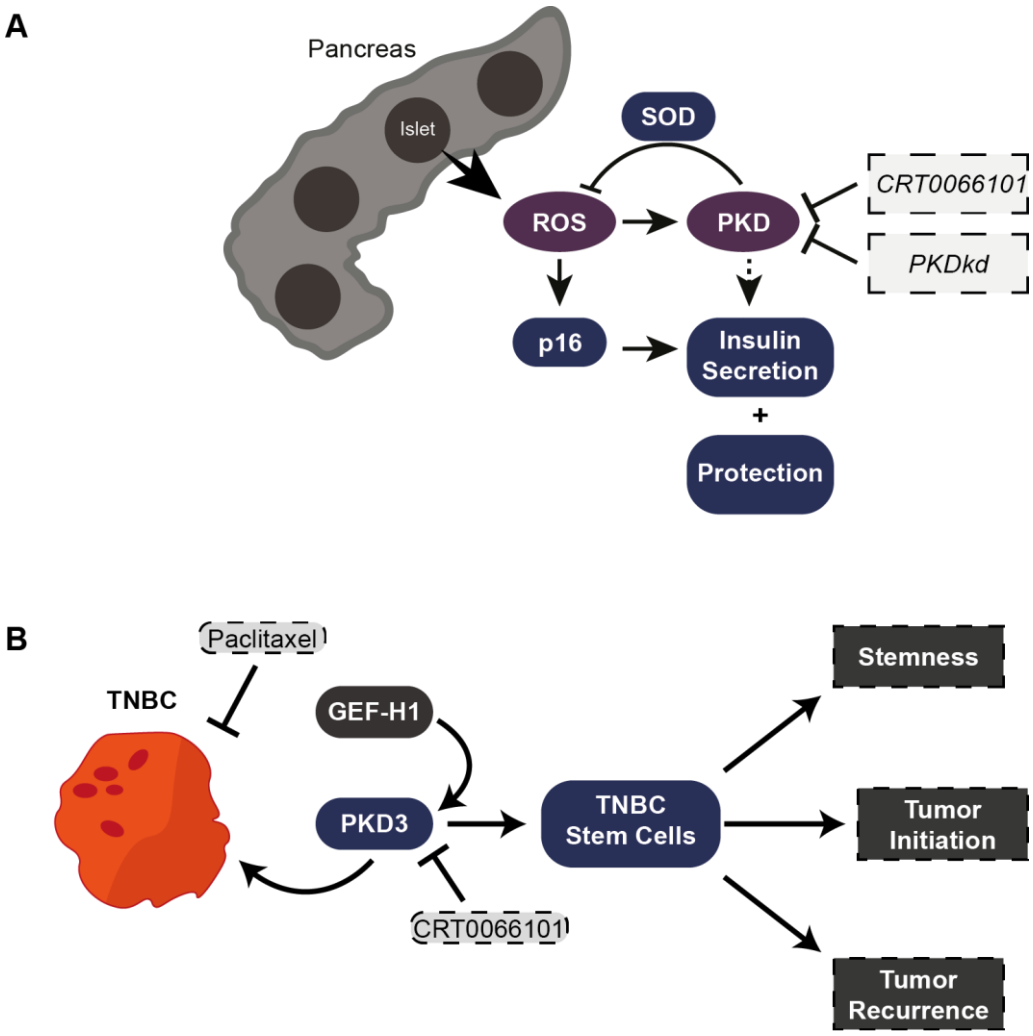

Figure 1 | Graphical abstracts. (A) Inhibition of protein kinase D induces β-cell senescence and thereby protects from high-fat-diet-induced glucose and insulin intolerance. **(B)** The GEF-H1/PKD3 signaling pathway promotes the maintenance of triple negative breast cancer stem cells.

Abbreviations

ABCG2	ATP-binding cassette super-family G member 2
ABL	Abelson murine leukemia viral oncogene homolog 1
ALDH	Aldehyde dehydrogenase
ALDH1	Aldehyde dehydrogenase 1
ARHGEF2	Rho guanine nucleotide exchange factor 2/ GEF-H1
cAMP	Cyclic adenosine monophosphate
CCF	Cytoplasmic chromatin fragments
CDK	Cyclin dependent kinase
CERT	Ceramide transfer protein
CSC	Cancer stem cells
CTGF	Connective tissue growth factor
CXCL2	C-X-C motif chemokine 2
DAG	Diacylglycerol
DDR	DNA damage response
DMEM	Dulbecco modified eagle medium
DMSO	Dimethyl sulfoxide
DNMT	DNA-methyl-transferase
Dox	Doxycyclin
EDTA	Ethylendiaminetetraacetic acid
EGF	Epidermal growth factor
EGFP	Enhanced green fluorescent protein
EGFR	Epidermal growth factor receptor
ELDA	Extreme limiting dilution assay
ELISA	Enzyme-linked immunosorbent assay
ELF2A	Eukaryotic initiation factor 2a
EMT	Epithelia-to-mesenchymal transition
ER	Estrogen receptor
ERK	Extracellular-signal-regulated kinase
FACS	Fluorescence-activated cell sorting
FCS	Fetal calf serum
GABP	GA-binding protein transcription factor

GEF-H1	Guanine exchange factor H1/ ARHGEF2
GIT1	ARF GTPase-activating protein
GLP-1	Glucagon-like peptide 1
GPCR	G-protein coupled receptor
GPR40	G-protein-coupled receptor 40
GSIS	Glucose stimulated insulin secretion
GTT	Glucose tolerance test
h	Hour
HDAC	Histone deacetylase
HER2	Human epidermal growth factor 2
HFD	High fat diet
i.p.	Intra peritoneal
ITT	Insulin tolerance test
KCl	Potassium chloride
KH_2PO_4	Potassium dihydrogen phosphate
LFD	Low fat diet
LIM	LIM domain kinase 1
MET	Mesenchymal-to-epithelial transition
MFI	Mean fluorescence intensity
min	Minute
MMS	Mammosphere medium
SOD	Superoxide dismutase
mTORC1	Mammalian target of rapamycin complex1
Na_2HPO_4	Sodium dihydrogen phosphate
NaCl	Sodium chloride
NaDOC	Sodium deoxychylate
NaN_3	Sodium azide
NANOG	Homeobox protein NANOG
NEUROD1	Neurogenic differentiation factor 1
NF-κB	nuclear factor 'kappa-light-chain-enhancer' of activated B-cells
NOTCH	Notch homolog, translocation-associated
NUR77	Nerve growth factor IB

OCT3/4	Octamer-binding transcription factor 3/4
OSBP	oxysterol binding protein
p16	Cyclin dependent kinase inhibitor $p16^{Ink4a}$
PBS	Phosphate buffered saline
PERK	Pancreatic endoplasmic reticulum kinase
PDK	Phosphoinositide-dependent kinase
PD-L1	Programmed death ligand 1
PDX-1	Duodenal homeobox-1
PDZ	Postsynaptic density-95/discs large/zonula occludens
PH	Pleckstrin-homology
PI	Propidium iodide
PI3K	Phosphoinositide 3-kinase
PI4KIIIβ	Phosphatidylinositol 4-kinase
PIP_2	Phosphatidylinositol (4,5)-bisphosphat
PKC	Protein kinase C
PKD	Protein Kinase D
PKDkd-EGFP	Protein Kinase D kinase dead-EGFP
PLC	Phosholipase C
p.o.	Per oral
poly-HEMA	Poly(2-hydroxymethylmethacrylate)
PR	Progesterone receptor
PRC	Polycomb repressive complexes
PRKD	Protein kinase D gene
qPCR	Quantitative real time polymerase chain reaction
RFP	Red fluorescent protein
RIN1	Rab interactor 1
ROS	Reactive oxygen species
rtTA	Tet activator protein
SA β-galactosidase	Senescence associated β-galactosidase
SAHF	Senescence- associated heterochromatic foci
SASP	Senescence-associated secretory phenotype
SDS	Sodium dodecyl sulfate
sec	Second

SFE	Sphere formation efficiency
SLUG	Zinc finger protein SNAI2
SNAIL	Zinc finger protein SNAI1
SOX2	Sex determining region Y
SRC	Proto-oncogene tyrosine-protein kinase
SSH1L	Slingshot-1L
spGEF-H1	Smart pool human RNA against GEF-H1
spPKD3	Smart pool human RNA against PKD3
spRNA	Smart pool human RNA
T1D	Type 1 diabetes
T2D	Type 2 diabetes
TAZ	Tafazzin
TGF-β	Transforming growth factor β
TNBC	Triple negative breast cancer
TRE	Tetracycline responsive promoter element
Tris	Tris-hydoxymehtyl-aminomethane
TWIST1	Twist-related protein 1
VEGF	Vascular endothelial growth factor
WAVE2	Wiskott-Aldrich syndrome protein family member 2
WHO	World health organization
WNT	Wingless-type MMTV integration site family
YAP	Yes-associated protein
ZEB1/2	Zinc finger E-box-binding homeobox 1/2

List of Figures

List of Tables

1 Introduction

The human genome encodes 518 kinases, which phosphorylate one-third of the proteome[1,2]. Highly dependent on spatial and temporal distribution, kinases are responsible for almost every signal transduction process and thereby virtually regulate every aspect of cell function[3]. Apart from immunological, infectious, metabolic, degenerative and inflammatory diseases, deregulation of kinases has been confirmed to play key roles in cancer development[4,5].

The Protein Kinase D (PKD) family of serine/threonine kinases belongs to the superfamily of calcium/calmodulin-dependent kinases[6] and consists of three isoforms in mammals: PKD1[7,8], PKD2[9] and PKD3[10]. PKDs have been described to play important roles in many cellular processes, such as vesicular transport, migration, invasion and proliferation[11-14]. Most studies in the recent years focused on PKD1 and PKD2 and therefore little is known about the functions of PKD3. The following sections will describe the structure and activation of the PKD isoforms, their localization and functions.

1.1 Structure of PKD

All PKD isoforms are structurally divided into an N-terminal regulatory domain as well as a C-terminal catalytic domain (Figure 2). The regulatory domain contains cysteine rich zinc finger motives (C1a, C1b) and a pleckstrin homology (PH) domain, which both have inhibitory effects on PKD activity[15,16]. By binding to the lipid diacylglycerol (DAG) via the zinc finger motives, PKD is recruited to the Golgi apparatus and the plasma membrane[17,18]. The catalytic domain (kinase domain) is responsible for PKD's kinase activity and targets the following motif: (L/V/I)X(R/K)XX(S/T)XX[19-21] (where X is any amino acid). Although the PKD isoforms share high homology within the catalytic and C1 domains, structural differences within the flanking regions of the C1 and PH domains indicate isoform-specific functions[6,13]. For example, only PKD1 and PKD2 contain an N-terminal apolar (rich in alanine/proline) region, which contributes to their translocation to the Golgi network[22]. Moreover, PKD3 lacks the C-terminal autophosphorylation site as well as a postsynaptic density-95/discs large/zonula occludens (PDZ)-binding domain, which has been demonstrated to directly regulate the transport of target proteins[23]. These structural differences might account for

different subcellular localizations and also contribute to the different substrate spectra of the PKD isoforms[24].

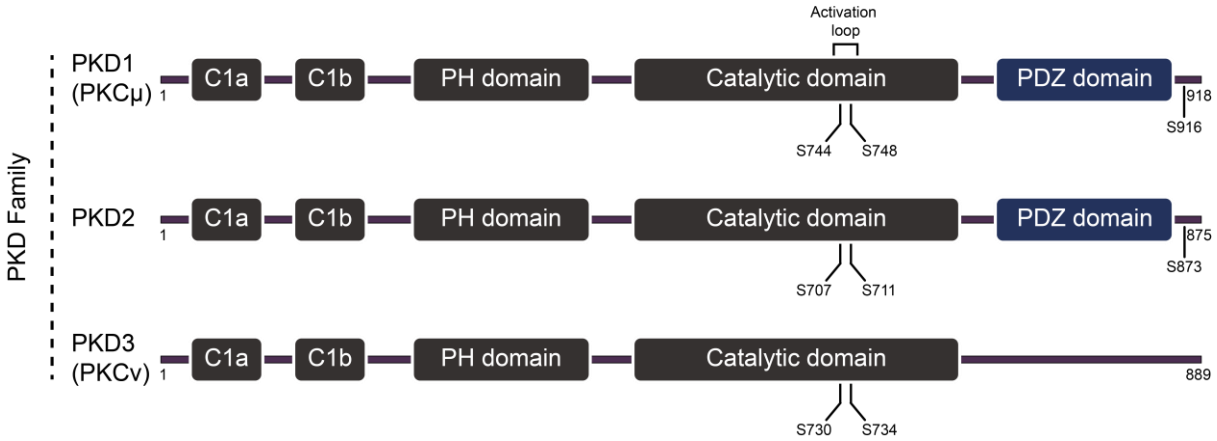

Figure 2 | The PKD family and its functional domains. C1a, C1b: zinc finger motive; PH domain: pleckstrin homology domain; PDZ domain: postsynaptic density-95/discs large/zonula occludens domain. Adapted from Roy et al.[25].

1.2 Activation of PKD

The activation of PKD requires DAG and the members of the protein kinase C (PKC) family[26]. DAG is generated by phospholipase C (PLC)-mediated phosphatidylinositol (4,5)-bisphosphate (PIP_2) hydrolysis. PLC activation and subsequent PIP_2-hydrolysis is initiated by ligand binding to G-protein coupled receptors (GPCR), growth receptors, or lymphocyte receptors. Apart from regulating PKD's localization via binding to its C1 domain, DAG binds and activates analogues members of the PKC family[27-31]. As a result, PKCs phosphorylate two distinct serine residues (Figure 2) of the "activation loop" of PKD thereby relieving the autoinhibition by the PH domain[32,33]. Additionally, a C-terminal autophosphorylated serine residue increases and stabilizes the active state of PKD1 (S916) and PKD2 (S873)[34]. PKC-mediated activation of PKD is mainly conducted by novel PKCs (PKCδ, ε, η, θ) but also by classical PKCs such as PKCα[35]. Upstream of PKC, the rho guanine nucleotide exchange factor 2 (ARHGEF2, also GEFH1) has recently been shown to activate PKD at trans-Golgi membranes upon microtubule disruption via the RhoA/PLC/PKC pathway[36]. PKC independent activation of PKD was observed in response to oxidative stress via SRC-ABL, in osteoblasts via bone morphogenetic protein 2 and in myeloid leukemia via caspase-3[37-39]. Thus, PKD activation occurs via various interaction partners, which strongly indicates a

multidimensional signaling network, controlled by PKD. This further reinforces the theory of isotype-selectivity, depending on cellular context and stimuli[28,40].

1.3 Signaling and biological functions of PKD

Under basal conditions, PKD is mainly distributed in the cytosol, and a small portion is localized at the Golgi complex, mitochondria and in the nucleus[6,34]. Upon stimulation with GPCR agonists, phorbol esters and growth factors, PKD enriches at DAG-rich membranes where it is further activated by PKC-mediated phosphorylation[18]. Depending on the cellular location, PKD regulates various cellular processes including vesicular protein transport[41], actin cytoskeleton remodeling and cell migration[42,43], oxidative stress response[44], and gene transcription[45].

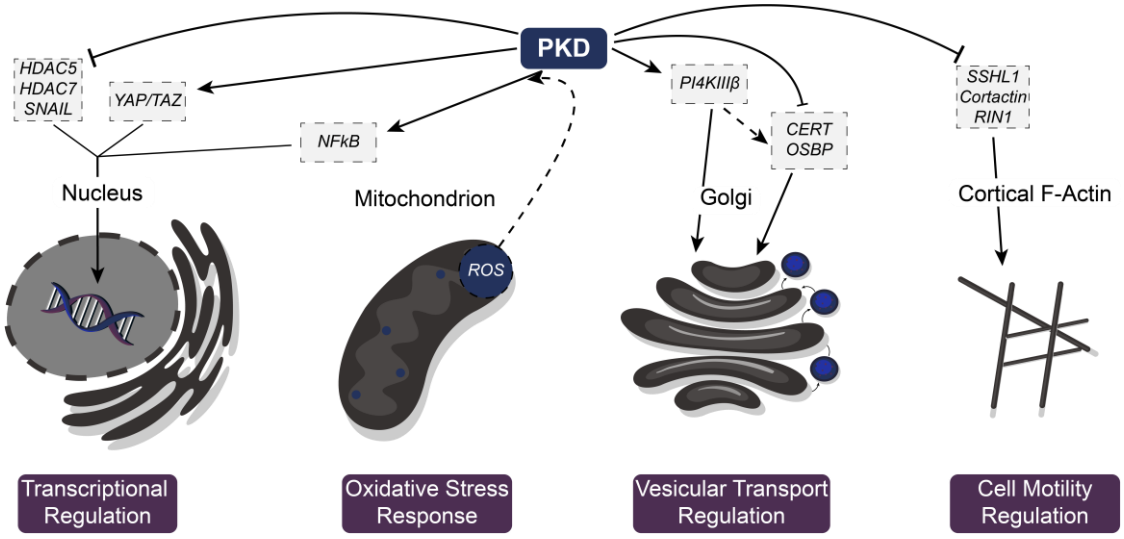

Figure 3 | PKD has diverse cellular functions. For explanations see text.

The most important molecular functions are depicted in Figure 3 and described below. At the plasma membrane, PKD negatively controls cell migration through regulation of the actin cytoskeleton remodeling[46]. Specifically, PKD decelerates F-actin polymerization by inactivating the cofilin-phosphatase slingshot-1L (SSH1L)[42,47,48], inhibiting rab interactor 1 (RIN1)[49] and cortactin[43,50] by direct phosphorylation. Apart from inhibiting migration, PKD strengthens cell-cell-contacts by stabilizing and upregulating E-CADHERIN[51,52]. Together, increased cell adhesion and inhibition of cell migration suppress epithelial to mesenchymal transition (EMT), an essential process during the development of metastasis in cancer[53].

Basolateral protein exit from the TGN is regulated by PKD through the regulation of the lipid metabolism[54]. Therefore, PKD activates phosphatidylinositol 4-kinase (PI4KIIIβ) via phosphorylation at S294. To stabilize the activity of the lipid kinase PI4KIIIβ, 14-3-3 proteins can protect the phosphorylated serine 294 from dephosphorylation[55]. PI4KIIIβ phosphorylates phosphatidylinositol at position D-4, resulting in the Golgi membrane specific signal lipid PI4P[56], which recruits two lipid transfer proteins, ceramide transfer protein (CERT) and oxysterol binding protein (OSBP), to the TGN[57,58]. CERT transports ceramide from the endoplasmic reticulum to the TGN, where it is converted to sphingomyelin and the PKD-recruiting/activating DAG[59]. In a negative feedback loop, PKD phosphorylates CERT (S132) and OSBP (S240) leading to their dissociation from the TGN-membrane[60,61]. Finally, the BAR (Bin/Amphiphysin/Rvs) domain protein arfaptin-1 is also recruited through interaction with PI4P to the TGN membrane and this recruitment is regulated by PKD-mediated phosphorylation of arfaptin-1 at S132. Notably, this phosphorylation disrupts the ability of arfaptin-1 to inhibit the small GTPase Arf1 thereby allowing for vesicle fission to occur. This signaling pathway is especially required for the biogenesis of secretory storage granules containing cargo such as insulin and chromogranin[62,63].

Additionally, PKD protects cells from mitochondria-derived reactive oxygen species (ROS). Studies show that oxidative stress induces a SRC/ABL/PKC-dependent activation of PKD (T463/T95/S744/S748), which enables the kinase to signal to NFκB (nuclear factor 'kappa-light-chain-enhancer' of activated B-cells) via the IKK (IκB kinase) complex, which results in the degradation of IκBα (inhibitor of κB). Accordingly, NFκB translocates to the nucleus and facilitates the transcription of superoxide dismutase 2 (SOD2), which detoxifies the cells from ROS[64].

In terms of transcriptional regulation, PKD-mediated phosphorylation of HDAC5[65] and HDAC7[45] shuttles these proteins out of the nucleus. Thereby, PKD mediates e.g. T cell receptor-induced NUR77 expression and apoptosis as well as vascular endothelial growth factor (VEGF)-induced gene expression and angiogenesis[45,65]. Angiogenesis describes the process of de novo formation of blood capillaries, to e.g. support tumor growth [66]. Via a signaling pathway composed of VEGF receptor 2-PLCγ-PKC, PKD is activated resulting in an activation of ERK1/2 and cell proliferation[33]. Moreover, by promoting the expression of angiogenic factors, PKD e.g. induces the tumor angiogenesis in prostate cancer[67].

The above described functions clearly show that the spatial and temporal distribution of PKD family members determines their substrate spectra and thus the cellular outcome.

1.4 Regulation of the glucose homeostasis

Glucose homeostasis is dependent on the balance between hepatic glucose production and glucose utilization by organs such as the liver, adipose tissue and muscle. This balance is regulated by the pancreatic hormone insulin. Under normal circumstances, an upregulation of blood glucose levels results in increased insulin secretion into the blood stream via pancreatic β-cells. The circulating insulin facilitates the uptake and storage of glucose in peripheral tissues and inhibits hepatic gluconeogenesis[68].

1.4.1 Insulin Signaling and Diabetes

β-cells are endocrine cells and produce, store as well as release insulin. Insulin is an anti-hyperglycemic hormone, which keeps blood glucose levels at physiological range and antagonizes epinephrine, glucagon and other hyperglycemic hormones. As part of the Langerhans islets (referred to as islets), β-cells comprise up to 80% of all endocrine cells within islets[69].

The biosynthesis and fast regulation of insulin is regulated on transcriptional and translational level. Transcription of insulin is regulated by transcription factors such as duodenal homeobox-1 (PDX-1)[70], neurogenic differentiation factor 1 (NEUROD1)[71] and MAFA[72]. Insulin translation is upregulated by exposure to nutrients. Pancreatic endoplasmic reticulum kinase (PERK) plays an important role and regulates insulin translational processes via the phosphorylation of the eukaryotic initiation factor 2a (EIF2A)[73]. PERK-deficiency was shown to induce defects in insulin synthesis especially in neonatal development[74,75].

Upon glucose exposure, β-cells start the oxidative metabolism of glucose, thereby boosting the ATP/ADP ratio. This event depolarizes the plasma membrane through the closure of K^{+}_{ATP} channels. Moreover, calcium channels increase intracellular calcium concentrations and the exocytosis of insulin vesicles is triggered. Additionally, insulin release can be enhanced by: i) fatty acids via the G-protein-coupled receptor (GPR40), ii) incretin glucagon-like peptide 1 (GLP1) via its GPCR, iii) release of acetylcholine via

the M2 muscarinic receptor, which induces insulin release through DAG and PKC, iv) β-adrenergic agonists via increased cAMP levels, and v) increase of β-cell mass via insulin/ insulin-like growth factor 1 dependent pathways[76].

Once in the blood stream, insulin binds to the insulin receptor tyrosine kinase on e.g. muscle and fat cells, causing phosphorylation of the insulin receptor substrate, which allows the binding of phosphoinositide 3-kinase (PI3K). Subsequently, PI3K synthesizes phosphatidylinositol (3,4,5)-trisphosphate at the plasma membrane, which facilitates phosphoinositide-dependent kinase (PDK) to phosphorylate Thr308 and mTORC2 to phosphorylate Ser473 of AKT (protein kinase B). Activated AKT leads to glucose uptake (via AS160 and glucose transporter 4), glycogen synthesis (via glycogen synthase kinase 3β) and protein as well as lipid synthesis (via mTORC1)[77].

Impairment of the glucose homeostasis leads to diabetes mellitus, which is defined by a group of diseases that are characterized by insulin intolerance and defects in insulin secretion. Especially insulin resistance of peripheral tissues, failure in signal transduction and genetic alterations are responsible for these metabolic deviations. If untreated, hyperglycemia and insulin deficiency cause severe diseases, such as vision loss, kidney failure, heart attacks and finally death[78-80]. According to the world health organization (WHO), 8.5 % of adults were diagnosed with diabetes in 2014, tendency rising. Apart from gestational diabetes, type 1 (T1D) and type 2 diabetes (T2D) are mainly diagnosed[81]. Whereas T1D is characterized by absent insulin production due to an autoimmune destruction of β-cells, T2D results from developing insulin resistance and subsequent β-cell failure[82,83]. With 90-95% of all diagnosed patients, T2D is the most prevalent form of diabetes and therefore treatment developments are under intensive investigation[84].

1.4.2 Risk Factors of T2D: Aging and Obesity

Aging and obesity are major risk factors for the development of T2D and go hand in hand with developing glucose dys-homeostasis in both animal and human studies[85-87]. Obesity is defined by excess accumulation of fat tissue to an extent that both psychological and physical health are disturbed[88]. Obesity is highly linked to the development of metabolic diseases and for example caused by the upregulated release of free fatty acids into the blood stream, which can be taken up for instance by muscle cells[89]. Excess fatty acids activate protein kinase Cθ, which prevents the

activation of the insulin receptor substrate by insulin and thereby inhibits glucose uptake[90-92]. In turn, hyperglycemia develops, and β-cells continue sensing glucose and therefore continuously secrete insulin. Initially β-cells produce excess insulin (hyperinsulinemia) to compensate for glucolipotoxicity but fail in the end, which leads to T2D manifestation[93].

Aging leads to oxidative stress, DNA damage, decreased mitochondrial function, inflammation and senescence, which all contribute to metabolic diseases[94]. Importantly, several studies have demonstrated that aging (i) induces β-cell death by mitochondrial failure, (ii) causes decreased insulin secretion and (iii) promotes insulin resistance[95]. During the aging process, increased insulin resistance and decreased insulin secretion lead to impaired glucose tolerance, which manifests in diabetes[96]. However, recent studies revealed that aging dependent β-cell senescence rescues from decreased insulin production[97].

1.4.3 Senescence and β-Cell Function

If cells are exposed to stress or reach the limit of their replicative potential, they enter a stable growth arrest[98,99]. This state of stable cell cycle arrest is called senescence and limits the replication of old or damaged cells. Apart from leaving the cell cycle, senescent cells go through several phenotypic changes, like chromatin rearrangement, metabolic reprogramming and the secretion of specific factors called senescence-associated secretory phenotype (SASP) (Figure 4).

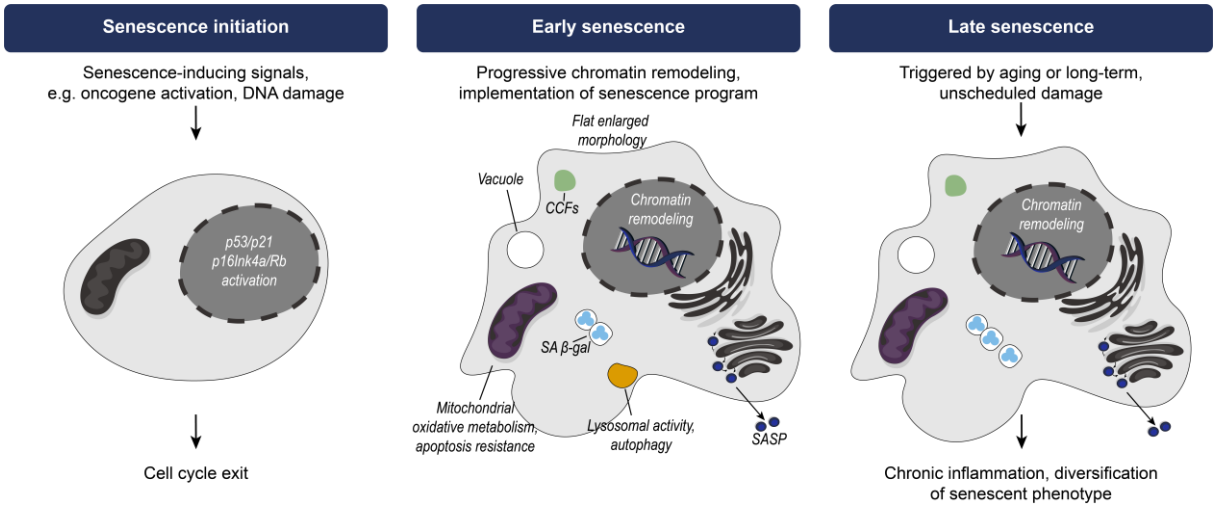

Figure 4 | Senescence and phenotypic alterations. Adapted from[100]. CCF: cytomplasmic chromatin fragments; SA β-gal: senescence associated β-galactosidase; SASP: senescence-associated secretory phenotype;

Physiologically, senescence is required for tissue homeostasis during development, tissue remodeling (e.g. wound healing)[101-103] and protects against cancer[104].

Senescence can be triggered by DNA damage, induction of the p53/p21 pathway and the activation of the INK4/ARF locus. DNA damage response (DDR) (e.g. via chemotherapeutics) is characterized by deposition of γ-H2Ax and p53-binding protein 1 (53BP1) in the chromatin. Moreover, the kinases ATM, ATR, CHK1 and CHK2 result in the activation of the p53/p21 axis[105,106]. Upon activation, p53 promotes the transcription of cyclin-dependent kinase (CDK) inhibitor p21, resulting in CDK2 inhibition, Rb hyperphosphorylation and cell cycle exit[105]. Additionally, incessant stress induces the CDK4/6 inhibitor $p16^{Ink4a}$, which results in a persistent growth arrest[107]. $p16^{Ink4a}$ is encoded by the INK4/ARF locus, which is controlled by epigenetic regulators, such as the polycomb repressive complexes 1/2 (PRC1/2)[107,108]. Importantly, $p16^{Ink4a}$ levels strongly increase during aging and tumorigenesis and $p16^{Ink4a}$ is therefore a specific marker for senescence *in vivo*[109-111]. Considered as the hallmark of senescence markers, senescence associated β-galactosidase (SA β-galactosidase) activity is enhanced during senescence due to increased lysosomal content and allows the precise detection of senescent cells[112,113]. Senescence induces chromatin rearrangements, e.g. the formation of senescence-associated heterochromatic foci (SAHFs)[114,115]. SAHFs are enriched in repressive marks and result in a loss of structure and decompaction of the DNA in the SAHF core[116]. Interestingly, senescence induces the blebbing of cytoplasmic chromatin fragments (CCFs), which promote a pro-inflammatory phenotype during senescence and cancer[117,118]. Furthermore, senescent cells exhibit reduced levels of mitophagy, resulting in a dysfunctional mitochondrial network during aging and ROS dependent senescence [119,120].

During aging, pancreatic β-cell proliferation declines dramatically in mice and in humans[121,122]. This reduction in β-cell mass manifests in a dysregulated insulin homeostasis, which causes reduced glucose tolerance and contributes to an increased risk of T2D development at later stages[123]. The decreased replicative capacity of β-cells is promoted by $p16^{Ink4a}$ (referred to as p16), which increases with age in mouse islets and predisposes mice to diabetes[124,125]. Additionally, high blood concentrations of free fatty acids, e.g. upregulated by high-fat-diet (HFD), reduce β-cell proliferation by inducing the expression of p16[126]. Although p16 expression drives a decline in β-

cell regenerative capacity, it remained elusive whether the increase of p16 levels actually caused cellular senescence and whether such cells were still functional. Surprisingly, a recent study observed that p16 drives β-cell senescence during normal aging and thereby enhances the glucose stimulated insulin secretion (GSIS) capacity of β-cells[97]. Thus, during healthy aging p16-dependent β-cell senescence promotes GSIS to compensate for the reduction in β-cell mass. Signaling pathways controlling the expression of p16 in β-cells during healthy aging, however, are still poorly addressed.

1.4.4 Protein Kinase D and β-Cell Regulation

In pancreatic β-cells, especially the role of PKD1 has intensively been studied: PKD1 localizes at the Golgi compartment, stimulates insulin secretion through phosphorylation of arfaptin-1[62,127] and controls starvation induced lysosomal degradation of nascent insulin granules[128] *in vitro*. Mitogen-activated protein kinase p38δ negatively controls PKD activity through direct phosphorylation. Accordingly, p38δ-deficient mice showed high constitutive PKD activity, GSIS as well as protection against high-fat-feeding induced insulin resistance. Using isolated islets from PKD1 KO mice, it was shown that the loss of PKD1 diminished the release of insulin upon fatty acid induced GPR40 stimulation[129]. Additionally, it was demonstrated that the M3-Muscarinic receptor promotes insulin release from β-cells via activation of PKD1[130]. However, the loss of PKD1 only abrogated the potentiation of GSIS without affecting physiological GSIS. In line with this, a β-cell-specific PKD1 knockout showed that the kinase is dispensable for β-cells under basal conditions but necessary for the compensatory increase in GSIS in response to high-fat feeding[131]. So far, the roles of PKD2 and PKD3 in β-cell regulation have not been addressed yet.

1.5 Breast Cancer Stem Cell Maintenance

1.5.1 TNBC and TNBC Stem Cells

Breast cancer is the most diagnosed and aggressive cancer among women worldwide[132,133]. About 12% of women suffer from breast cancer throughout their life[134]. The most invasive form of breast cancer is TNBC constituting 12% – 20% of all breast cancer cases[135]. Despite improved early detection and the development of novel therapeutics, triple-negative breast cancer (TNBC) still is associated with a high

mortality rate. TNBC is characterized by the lack of estrogen receptor (ER), progesterone receptor (PR) and HER2 overexpression[136,137]. Compared to HER2 and ER/PR positive breast cancers, TNBC is associated with worse outcome, increased risk for metastasis and lower 5-year survival[138-140]. Apart from surgery, TNBC treatment is mainly based on chemotherapeutics such as anthracyclines and taxanes, however, many TNBCs rapidly develop resistance to these drugs[141].

Notably, after the treatment with taxanes an expansion of $CD44^+/CD24^-$ and aldehyde dehydrogenase 1 (ALDH)-positive TNBC cells with tumor-initiating ability was observed[142-144]. Expression of these markers is characteristic of so-called cancer stem cells, which represent a subpopulation of undifferentiated cells linked to early metastases, faster tumor recurrence, worse overall survival and higher-stage tumors [145-148]. The theory of cancer stem cells states that only 1 – 10 % of cells within a tumor are responsible for proliferation, migration and relapse after treatment[149,150].

CD24 is not expressed in highly aggressive breast cancer subtypes and therefore, its expression is not an ideal indicator for breast cancer stem cells[151]. Thus, other markers are important for identifying breast cancer stem cells. Aldehyde dehydrogenase 1 (ALDH1) is an enzyme of the aldehyde dehydrogenase (ALDH) superfamily and oxidizes endogenous and exogenous aldehydes[152]. ALDH oxidizes retinol to retinoic acid during the early differentiation of stem cells[153] and high levels of ALDH are correlated with a poor prognosis and metastasis[154].

Moreover, apart from infinite proliferation and self-renewal, cancer stem cells have the capability to initiate tumor formation[155]. Notably, it was shown that only one cancer stem cell is sufficient to initiate a tumor formation[156]. Furthermore, cancer stem cells are characterized by plasticity, which indicates that they are able to move up and down the cell hierarchy within the tumor tissue, depending on signals provided by the environment[157].

Cancer stem cells can further be characterized by transcription factors and additional surface markers. Characteristic transcription factors include the Yamanaka factors Oct3/4, Sox2 and Nanog. Those are also known to be highly expressed in embryonic stem cells and are important for maintaining pluripotency and self-renewal[158,159]. Various signaling pathways are dysregulated in breast cancer stem cells as well. One example is the Notch signaling pathway, which is important in cell to cell

communication, helps cancer stem cells to maintain their population and is involved in acquiring chemoresistance[160,161]. Additionally, Notch signaling is involved in epithelial to mesenchymal transition (EMT), a process that helps generating and maintaining stem cell features in cancer stem cells, and is required for metastases formation[162]. Other important signaling pathways include Hedgehog signaling or the WNT/β-catenin pathway[158,163].

Understanding the mechanisms that underlie the self-renewal behavior and survival of cancer stem cells is thus of great importance for the discovery and development of anticancer drugs targeting cancer stem cells.

1.5.2 Protein Kinase D, GEF-H1 and TNBC

As described before, depending on the spatial and temporal distribution, PKD has isoform specific biological functions. Especially in cancer progression different expression patterns and functions of PKD isoforms have been observed[164,165]. This is exemplified in breast cancer where PKD1 acts as tumor suppressor by maintaining the epithelial phenotype and blocking invasion and metastasis[164] whereas PKD2 and PKD3 rather function as oncoproteins through driving growth and chemoresistance[165,166].

In normal breast tissue, PKD1 is the predominant isoform but its gene expression is suppressed during breast cancer progression by epigenetic silencing[164]. Another function of activated PKD1 is the downregulation of matrix metalloproteinases at the mRNA level and the prevention of E-CADHERIN degradation via SNAIL. Thus, PKD1 prevents invasion and EMT[52,167]. While the exact mechanism of PKD2 regulation is unknown, GA-binding protein transcription factor (GABP) is a potential regulator of PKD2 expression[168]. High PKD2 levels further correlate with a high amount of P-glycoprotein, a protein generating efflux pumps for various drugs. Hence, PKD2 is considered to be responsible for chemoresistance[166].

In TNBC, an isoform switch towards high PKD3 expression occurs, which can be traced back to the lack of ER, a repressor of PKD3 gene expression[133,165]. Elevated PKD3 levels are associated with increased proliferation and cell motility, metastatic progression, as well as poor prognosis, supporting a pro-oncogenic function of the kinase in TNBC[14,24,133]. Indeed, an orthotopic TNBC mouse model showed that both the knockdown of PKD3 and its pharmacological inhibition using the PKD inhibitor

CRT0066101, decreased tumor growth, lymph node infiltration and the number and size of lung metastases[133]. On the molecular level, PKD3 was shown to increase proliferation through activating the mammalian target of rapamycin complex 1 (mTORC1) signaling cascade[14]. However, molecular pathways controlling the activity of PKD3 and its precise pro-oncogenic function in TNBC have remained elusive. Interestingly, a recent study revealed, that PKD can be activated by the Rho guanidine exchange factor (GEF) GEF-H1[36], which is also highly expressed in TNBC[169].

GEF-H1 is a RhoGEF sequestered by microtubules and activated downstream of G-protein coupled receptor (GPCR) ligands[36,170]. GEF-H1 is important for exocytosis, response to mechanical forces, cell migration, and cell polarity. It was previously shown that GEF-H1 increases RhoA and RhoB activity after being released from microtubules. The chemical compound nocodazole dissociates microtubules leading to GEF-H1 activation and subsequently induction of PKD activation via Rho and the Rho effector PLCε[36].

1.5.3 Utilizing the GEF-H1/PKD3-Axis in TNBC

The hormone receptors for estrogen and progesterone are not expressed in TNBC and HER2 is not amplified. Thus, a targeted therapy (e.g. with the monoclonal antibody trastuzumab targeting HER2 in HER2 amplified breast cancers[171]) was not possible for a long time. Just recently, the programmed death ligand 1 (PD-L1) therapeutic antibody atezolizumab was approved for PD-L1 positive unresectable locally advanced or metastatic TNBC[172]. However, TNBC patients are usually treated via surgery, radiation therapy and chemotherapy with taxanes such as paclitaxel[173-175].

Due to the limited therapeutic options it is important to identify new treatment strategies against TNBC. The high levels of oncogenic PKD3 make this kinase a valid target for further investigations. Notably, treating mice with the pan-PKD inhibitor CRT0066101 reduced TNBC xenograft growth and the number of metastases[133]. Additionally, the chemotherapeutic agent paclitaxel was reported to inhibit the activation of GEF-H1 via microtubule stabilization[176]. Thus, inhibiting the potential GEF-H1/PKD3-axis in TNBC by combining paclitaxel and CRT0066101 could be superior to the respective single treatment[133].

1.6 Objective

The molecular functions of PKD are well understood but its physiological role *in vivo* remains elusive. Importantly, the impact of PKD dysregulation on diseases such as diabetes and TNBC warrants investigation.

The prevalence of adults living with diabetes will rise to 629 million by 2045. Major risk factors are obesity and aging, which facilitate β-cell failure. In order to further understand the role of PKD in β-cells during aging and obesity, a functional PKD knockout (PKDkd-EGFP) mouse model was employed and juvenile as well as adult mice were studied. Moreover, the PKD inhibitor CRT0066101 was used to confirm the link between PKD, aging, senescence and β-cell function. To verify senescence, biological markers like enhanced SA β-galactosidase activity, increased cell size and decreased Ki67 levels were employed. Another hallmark of senescence is p16 upregulation, which can be triggered by increased ROS levels. Notably, PKD is known to regulate mitochondrial ROS. Thus, I examined p16 as well as ROS levels during aging and obesity, to link PKD to ROS/p16-dependent senescence. Additionally, I analyzed the performance of PKDkd-EGFP mice during HFD. Finally, the efficacy and therapeutic potential of CRT0066101 on pre-diabetic HFD-fed wildtype mice was tested.

PKD3 is upregulated in TNBC and correlates with worse patient outcome. Thus, I aimed to further unravel the role of PKD3 in TNBC, especially in TNBC stem cell regulation. First, I analyzed the stem cell potential of PKD3 knockdown MDA-MB-231 cells, using *in* vitro sphere formation and Aldefluor assays, and in *vivo* limiting dilution experiments. Next, the regulation of the PKD3-TNBC stem cell connection by GEF-H1 was analyzed by sphere formation assay. To further understand the role of PKD3, a transgenic, PKD3-overexpressing cell line was used and studied. Moreover, colony formation assays were employed to examine the effect of PKD3 on the clonogenic activity. Finally, I focused on developing a treatment strategy against TNBC stem cells, using the pan-PKD inhibitor CRT0066101 and the chemotherapeutic paclitaxel, *in* vitro and *in vivo* in an orthotopic mouse model.

2 Materials and Methods

2.1 Key Resource Table

REAGENT or RESOURCE	SOURCE	IDENTIFIER
Antibodies		
Anti-αTubulin	Cell Signaling Technology	Cat# 3873, RRID:AB_1904178
Anti-GAPDH	Cell Signaling Technology	Cat# 2118, RRID:AB_561053
Anti-GEF-H1	Cell Signaling Technology	Cat# 4076, RRID:AB_2060032
Anti-GFP	Roche	Cat# 11814460001, RRID:AB_390913
Anti-Glucagon	CST	Cat# 2760 RRID:AB_659831
Anti-Insulin + Proinsulin	Acris	Cat# AM20166PU-N RRID:AB_10696052
Anti-Ki67-APC	Biolegend	Cat# 652405 RRID:AB_2561929
Anti-Phospho-(Ser744/748)-PKD	Cell Signaling Technology	Cat# 2054, RRID:AB_2172539
Anti-Phospho-S6 Ribosomal Protein (Ser240/244)	CST	Cat# 5364 RRID:AB_10694233
Anti-p16INK4A	Thermo Fisher Scientific	Cat# PA5-20379 RRID:AB_11157205
Anti-Rabbit-Alexa-Fluor-546 secondary	Invitrogen	Cat# A-11035 RRID:AB_143051
Bacterial and Virus Strains		
Platinum-A (Plat-A) Retroviral Packaging Cell Line	Cell Biolabs	RV-101
Chemicals and Peptides		
Cholera toxin	Merck	Cat# C8052
Collagenase P	Roche	Cat# 11213865001
CRT0066101 (*in vivo*)	Selleckchem	Cat# S8366

CRT0066101 (cell culture)	Tocris	Cat# 4975
Crystal violet	Merck	Cat# C0775
Dextrose	Merck	Cat# D9434
Doxycycline (*in vivo*)	Yancheng Suhai Pharmaceutical	Cat# 137087-0008
Doxycycline (cell culture)	Calbiochem	Cat# 324385
EGF	R&D Systems	Cat# 236-EG
G418	Carl Roth	Cat# CP11.1
Glucose	Roth	Cat# 6887.1
Hydrocortisone	Merck	Cat# 3867
Insulin (*in vivo*)	Lilly	Cat# HI0210
Insulin (cell culture)	Merck	Cat# I5500
Lipofectamine™ RNAiMAX	Thermo Fisher Scientific	Cat# 13778030
Paclitaxel (cell culture)	Merck	Cat# T7402
Paclitaxel (*in vivo*)	Fresenius Kabi	6 mg/ml infusion solution
Paraformaldehyde	Merck	Cat# P6148
Poly(2-hydroxyethyl methacrylate) (pHEMA)	Merck	Cat# P3932
Polysorbate	Roth	Cat# 9139.1
Critical Commercial Assays		
ALDEFLUOR	STEMCELL Technologies	Cat# 01700
CellROX™ Deep Red	Thermo Fisher Scientific	Cat# C10422
IL6 ELISA	Biolegend	Cat# 431301
Insulin ELISA High Range	Alpco	Cat# 80-INSMSH-E01
Insulin ELISA Ultrasensitive	Alpco	Cat# 80-INSMSU-E01
LegendScreen (human)	BioLegend	Cat# 700007
NucleoSpin® miRNA	Macherey-Nagel	Cat# 740971
Power SYBR® Green RNA-to-CTTM 1-Step kit	Thermo Fisher Scientific	Cat# 4389986

Senescence β-Galactosidase Staining Kit	CST	Cat# 9860
Triglyceride Detection Kit	Thermo Fisher Scientific	Cat# TR22421
Tumor dissociation kit	Miltenyi Biotec	Cat# 130-096-730
Experimental Models: Cell Lines		
BT-549	CLS	Cat# 300132/p770_BT-549, RRID:CVCL_1092
HCC1806	ATCC	Cat# CRL-2335, RRID:CVCL_1258
MCF7	Institute of Clinical Pharmacology (IKP) Stuttgart	-
MCF10A	Department of Biomedicine, University of Basel	-
MCF10A_EcoR_PKD3WT-EGFP	IZI, University of Stuttgart	-
MDA-MB-231	CLS	Cat# 300275/NA, RRID:CVCL_0062
MDA-MB-468	CLS	Cat# 300279/NA, RRID:CVCL_0419
MDA-MB-436	Institute of Clinical Pharmacology (IKP) Stuttgart	-
Experimental Models: Mouse-Strains		
ntg/ +/-: Tg(Ins2-rtTA)2Efr/J; CD57BL/6	The Jackson Laboratory	Cat# 008250
PKDkd-EGFP: Tg(TetO-PKDkd-EGFP) x Tg(Ins2-rtTA)2Efr/J); CD57BL/6	University of Stuttgart, IZI	-
SCID Mice	Charles River Laboratories	IMSR Cat# CRL:236, RRID:IMSR_CRL:236
Tg(TetO-PKDkd-EGFP); CD57BL/6	University of Stuttgart, IZI	Ellwanger et al.[177]
Wildtype: CD57BL/6	University of Stuttgart, IZI	-

Oligonucleotides (qPCR; F: Forward; R: Reverse;)		
ABCG2 F: CAGGTGGAGGCAAATCTTCGT; R: TCCAGACACACCACGGATAAA	Microsynth	-
Actin	Qiagen	Cat# Mm_Actb_1_SG
ALDH1A1 F: GCACGCCAGACTTACCTGTC R: CCTCCTCAGTTGCAGGATTAAAG	Microsynth	-
CD44 F: CTGCCGCTTTGCAGGTGTA R: CATTGTGGGCAAGGTGCTATT	Microsynth	-
HES1 F: TGAAGAAAGATAGCTCGCGG R: GGTACTTCCCCAGCACACTT	Microsynth	-
HEY1 F: TGGATCACCTGAAAATGCTG R: TTGTTGAGATGCGAAACCAG	Microsynth	-
SOD2 F: ggccaagggagatgttacaa R: gaaccttggactcccaca	Microsynth	-
NANOG F: CAGAAGGCCTCAGCACCTAC R: CTGTTCCAGGCCTGATTGTT	Microsynth	-
NOTCH4 F: AACTCCTCCCCAGGAATCTG R: CCTCCATCCAGCAGAGGTT	Microsynth	-
OCT3/4 F: GAAGCTGGAGAAGGAGAAGCTG R: CAAGGGCCGCAGCTTACACATGTTC	Microsynth	-
PKD1	Qiagen	Cat# Mm_Prkd1_1_SG
PKD2	Qiagen	Cat# Mm_Prkd2_1_SG
PKD3	Qiagen	Cat# Mm_Prkd3_1_SG

SNAIL F: CACTATGCCGCGCTCTTTC R: GCTGGAAGGTAAACTCTGGATTAGA	Microsynth	-
SOX2 F: AGTCTCCAAGCGACGAAAAA R: GGAAAGTTGGGATCGAACAA	Microsynth	-
Oligonucleotides (siRNA)		
spNon: ON-Target plus non-targeting control pool	Dharmacon	Cat# D-001810–10
spGEF-H1: ON-Target plus SMARTpool human ARHGEF2	Dharmacon	Cat# L-009883
spPKD3: ON-Target plus SMARTpool human PRKD3	Dharmacon	Cat# L-005029
Recombinant DNA		
pWPXLd-rtTA3-IRES-EcoR-PGK-Puro	IBTB, University of Stuttgart	-
pCMV-Gag-Pol	Cell Biolabs	Cat# RV-111
TRE3G-PGK-NEO retroviral backbone	IBTB, University of Stuttgart	-
Software		
FlowJo	FlowJo	RRID:SCR_008520
GraphPad Prism	GraphPad	RRID:SCR_002798
ImageJ	ImageJ	RRID:SCR_003070
ZEN	Zeiss	-
Other		
0.9 % NaCl injection solution	Braun	Cat# 2246244
Accutase	Thermo Fisher Scientific	Cat# 00-4555-56
B27 Supplement	Thermo Fisher Scientific	Cat# 17504-044
Diet: Low Fat (LFD)	Altromin	Cat# C1090-10
Diet: High Fat (HFD)	Altromin	Cat# C1090-60
DMEM high glucose	Thermo Fisher Scientific	Cat# 11965092

DMEM low glucose	Thermo Fisher Scientific	Cat# 31885023
DMEM/F12 GlutaMAX	Thermo Fisher Scientific	Cat# 31331028
HBSS	Thermo Fisher Scientific	Cat# 14025092
Horse serum	Thermo Fisher Scientific	Cat# 16050122
NuPage Novex 4–12% Bis-Tris gels	Thermo Fisher Scientific	Cat# NP0336
PBS	Thermo Fisher Scientific	Cat# 70011036
RPMI-1640	Thermo Fisher Scientific	Cat# 11875093

2.2 Cell Culture

MDA-MB-231 cells and MDA-MB-231-based knockdown cell lines (shNon_CTRL, shPKD3_1, shPKD3_2; [133]) were cultured in DMEM low glucose. MDA-MB-436 cells were cultured in DMEM high glucose. MDA-MB-468, BT-549, HCC1806 and MCF7 cells were cultured in RPMI-1640. All media were supplemented with 10 % fetal bovine serum (PAA Laboratories). MCF10A_EcoR_PKD3WT-EGFP cells were cultured in DMEM/F12 GlutaMAX supplemented with 5 % horse serum, 20 ng/ml EGF, 0.5 µg/ml hydrocortisone, 100 ng/ml cholera toxin and 10 µg/ml insulin. All cell lines were cultured at 37°C in a humidified chamber with 5 % CO_2, were regularly tested for *Mycoplasma* contamination (Lonza, LT07-318) and authenticated (Multiplexion GmbH).

2.3 Orthotopic Tumor Models

Animal experiments had been approved by state authorities and were carried out in accordance to federal guidelines. For the limiting dilution assay (ELDA), 8-week-old female SCID mice were injected with the appropriate number of MDA-MB-231 shNon_CTRL or shPKD3_1 cells in 100 µl PBS into the right fat pad of the 4th nipple. Tumor growth was analyzed by caliper measurements. Mice were sacrificed after 8 weeks. Multiple group comparison and estimated stem cell frequency was analyzed using the ELDA software [178]. Tumors were imaged and processed for oncosphere

formation assays as well as ALDEFLUOR™ analysis. Tumor dissociation was performed according to manufacturer's instructions.

For combined paclitaxel and CRT0066101 treatment, 8-week-old female SCID mice were injected with $2x10^6$ MDA-MB-231 cells in 100 µl PBS into the right fat pad of the 4th nipple. Tumor growth was analyzed by caliper measurements ((length x width^2)/2). After the tumors had reached 100 mm^3 mice were assigned to control and 3 treatment groups (n=7 mice per group). During the following treatment-phase (21 days), mice were treated with either *(a)* CRT0066101 (peroral, 80 mg/kg diluted in a 5 % dextrose saline solution), *(b)* paclitaxel (intraperitoneal injection, 10 mg/kg body weight diluted in a 10 % polysorbate PBS solution), *(c)* CRT0066101 in combination with paclitaxel or *(d)* the combination of the respective carriers (control). Paclitaxel was injected at day 23, 30, 37 and 44. CRT0066101 was given once daily from day 23 to day 43. After the treatment-phase, mice were observed for another 20 days and analyzed for tumor recurrence. At the end point, mice were sacrificed and imaged.

2.4 Animal Models: Islets & High Fat Diet

Animal experiments had been approved by state authorities and were carried out in accordance to federal guidelines. To generate Tg(TetO-PKDkd-EGFP) x Tg(Ins2-rtTA)2Efr/J) mice (called "PKDkd-EGFP" from now on), Tg(Ins2-rtTA)2Efr/J mice (called "ntg/ +/-" from now on) were crossbred with Tg(TetO-PKDkd-EGFP) mice.

For short-term *in vivo* and *ex vivo* (isolated islets) studies, 4-15 months old PKDkd-EGFP and control (ntg/ +/-) mice were continuously treated with doxycycline (2 mg/ml, 5 % sucrose) infused drinking water, for 7 days. On day 7, mice were used for a glucose tolerance test (GTT), insulin tolerance test (ITT) or were immediately euthanized for islet isolation. For short-term studies with per oral (p.o.) CRT0066101 treatment, 4-6 months old wildtype mice were treated with CRT0066101 (80 mg/kg; 5 % dextrose in 0.9 % NaCl) for 7 days, once daily, followed by GTT, ITT or islet isolation.

2.4.1 Glucose Tolerance Test

Mice were fasted for 16 h before the GTT. On the next day, the basal glucose level was determined via blood sampling from the tail. For measurements, I used a blood glucose meter (STADA Gluco Result, STADAPHARM GmbH) and STADA Gluco Result (STADAPHARM GmbH) blood glucose test strips. After intraperitoneal (i.p.)

glucose injection (2g/kg body weight (bw) in 0.9 % NaCl; HFD studies: 1g/kg bw in 0.9 % NaCl), I measured the blood glucose concentration after 15, 30, 60, 90, 120 and 240 min via blood sampling from the tail.

2.4.2 Insulin Tolerance Test

Mice were fasted for 6 h before the ITT. On the same day, the basal glucose level was determined via blood sampling from the tail. For measurements, I used a blood glucose meter (STADA Gluco Result, STADAPHARM GmbH) and STADA Gluco Result (STADAPHARM GmbH) blood glucose test strips. After intraperitoneal (i.p.) insulin injection (0.75 IU/kg bw in 0.9 % NaCl), I measured the blood glucose concentration after 15, 30, 60 and 90 min via blood sampling from the tail.

2.4.3 Islet Isolation

Mice were euthanized and disinfected with EtOH. Next, the abdominal cavity was uncovered and the bile duct as well as the gall bladder were localized. The small intestine was clamped to the right and to the left of the sphincter of Oddi and the gall bladder was disconnected from the bile duct. Then, a syringe (injection cannula: 30G, BD Microlance, Cat# 304000) was inserted into the gall bladder and moved down the bile duct, as close as possible towards the sphincter of Oddi. 2 ml collagenase P (1 mg/ml) were slowly injected into the pancreatic duct and the inflation of the pancreas was closely monitored. The inflated pancreas was removed and transferred into a 10 cm dish, where it was cut in small pieces with scissors. Next, 1 ml of collagenase P was added, and the entire solution was transferred to a 15 ml falcon. After a 10 min incubation at 37°C, the digestion was stopped with 10 ml of ice-cold PBS. Further on, the tissue pellet was washed twice with 10 ml PBS and dissolved in 15 ml HBSS. After filtering the solution through a 70 µm cell strainer (Falcon, Cat# 352350), islets were handpicked and transferred (mouth pipette) to a 3.5 cm petri dish with 5 ml HBSS. For ex vivo glucose stimulated insulin secretion (GSIS), islets were cultured overnight in 5 ml RPMI (10 % fetal calf serum (FCS) and 1 % penicillin/ streptomycin (P/S)). For all other *ex vivo* studies, islets were processed on the same day.

2.4.4 Glucose Stimulated Insulin Secretion

For *ex vivo* GSIS, 10 overnight cultured (RPMI, 10 % FCS, 1 % P/S) islets per mouse were transferred into a 200 µl KBHB (120 mM NaCl, 4.7 mM KCl, 2.5 mM $CaCl_2$, 1mM

KH_2PO_4, 1.2 mM $MgSO_4$, 10 mM HEPES, 20 mM $NaHCO_3$, 0.5 mg/ml BSA, pH 7.4) drop containing 5 mM glucose. All further steps were carried out in 200 µl KBHB. After 60 min of equilibration at 37°C, the islets were transferred to 3 mM glucose for another 60 min to mimic starvation. Next, islets were transferred to 16 mM glucose for 60 min. Finally, the islets were transferred to 200 µl 1.5 % HCl in 70 % EtOH and stored at –80°C. The supernatants of 3 mM and 16 mM glucose incubation were collected and stored at -80°C. The insulin concentration was assessed via ELISA.

For *in vivo* GSIS, mice were starved for 16 hours. The baseline glucose concentration was measured (blood glucose meter, via tail), glucose was injected i.p. (2 g/kg bw) and after 15 min the blood glucose concentration was analyzed. Additionally, blood was collected before and after the glucose challenge, to analyze the plasma insulin concentration via ELISA.

2.4.5 High-Fat-Diet

For classic high-fat-diet with PKD-EGFP and ntg/ +/- mice, 2 months old mice received either HFD or LFD (control diet) for 16 weeks ad libitium and were continuously treated with doxycycline (200 µg/ml) infused drinking water. Blood was sampled via the tail once per week for triglyceride and interleukin 6 (IL6) analysis. Weight was monitored weekly. After 16 weeks, GTT, ITT or islet isolation was performed.

For the high-fat-diet rescue experiment, wildtype CD57BL/6 mice received high-fat-diet (HFD) during the first 16 weeks, followed by GTT or ITT. Afterwards, all mice received normal diet and were either treated p.o. with CRT0066101 (80 mg/kg; 5 % dextrose in 0.9 % NaCl; 5 days per week, once daily) or the carrier (5 % dextrose in 0.9 % NaCl; 5 days per week, once daily) during the weeks 17-20, again followed by ITT or GTT.

2.5 Triglyceride Assay

Triglyceride determination was conducted according to manufacturer’s instructions.

2.6 Enzyme-Linked Immunosorbent Assay

ELISA was performed according to manufacturer’s instructions. For *ex vivo* GSIS insulin ELISA, samples were diluted 1:5 (5 mM, 16 mM glucose) or 1:200 (total insulin content). For *in vivo* GSIS insulin ELISA, plasma samples remained undiluted. For IL6 ELISA, plasma samples were pre-diluted 1:10.

2.7 Reactive Oxygen Species

10 islets per mouse were transferred to 96-well plates and incubated for 10 min in 100 µl trypsin (1x) at 37°C. Next, cells were singularized using a syringe (injection cannula: 27G) and washed once with PBA (2 % FCS, 0.2 % NaN_3 in PBS). Cells were diluted in 200 µl PBA, the CellRox reagent (5 µM) was added and plates were incubated for 30 min at 37 °C. Afterwards, cells were washed 3 times with PBA and analyzed via flow cytometry. Data was evaluated using FlowJo. Relative mean fluorescence intensities (rel. MFI) were calculated with the following formula: rel. MFI = MFI_{sample}/MFI_{cells}.

2.8 Ki67 Proliferation Assay

10 islets per mouse were transferred to 1.5 ml Eppendorf tubes and incubated for 10 min in 200 µl trypsin (1x) at 37°C. Next, cells were singularized using a syringe (injection cannula: 27G) and washed once with PBS. For fixation, cells were resuspended in 300 µl ice-cold 70 % EtOH, vortexed and incubated on ice for 30 min. Cells were again washed and stained with Ki67-APC antibody for 30 min at 4°C. Afterwards, cells were washed once and analyzed via flow cytometry. Data was evaluated using FlowJo. Data is presented as percent positive cells compared to isotype control or as relative mean fluorescence intensity (rel. MFI). rel. MFI = $[MFI_{sample} – (MFI_{isotype} – MFI_{cells})] / MFI_{cells}$.

2.9 Cell/ Islet Size

For β-cell size, 10 islets per mouse were transferred to 96-well plates and incubated for 10 min in 100 µl trypsin (1x) at 37°C. Next, cells were singularized using a syringe (injection cannula: 27G) and washed once with PBA (2 % FCS, 0.2 % NaN_3 in PBS). Cells were resuspended and analyzed via flow cytometry. Data was evaluated using FlowJo. Data is presented as Median FSC-A.

For islet area, 30 islets per genotype were imaged and the area was measured via ImageJ.

For cryosectioning, whole pancreata were fixed in PBS/ 4 % paraformaldehyde at 4°C overnight, followed by incubation in PBS/ 30 % sucrose at 4 °C for 24 h. After perfusion, the pancreata were mounted with cryostat embedding medium, frozen on dry ice and stored at -80°C. Frozen pancreata were cut into 10-12 µm sections using a cryostat. Tissue sections were mounted on poly-lysine-coated microscope slides and stained

for immunofluorescence microscopy. Images were obtained using a confocal laser scanning microscope. β-cell area was calculated by dividing the cross-section area of an islet by the nuclei number.

2.10 Senescence β-Galactosidase

5 islets per mouse were transferred to 12-well plates and analyzed with the senescence β-galactosidase kit according to manufacturer's instructions. Next day, pictures of the islets were taken with the Zeiss AXIO Zoom V16 microscope (objective ApoZ 1.5x 10.37 FWD 30mm). The blue intensity of each islet was assessed using the ZEN software.

2.11 Quantitative Real-Time PCR

RNA was isolated from 50 islets per mouse, using the NucleoSpin® miRNA kit according to manufacturer's instructions. 10-100 ng RNA were used for real-time PCR, using the Power SYBR® Green RNA-to-C_T™ 1-Step kit. Analysis was performed using the CFX96 Touch Real-Time PCR Detection System (Bio-RAD, 1855196). To analyze the fold change gene expression, the double delta Ct analysis was used (fold change = $2^{(-\Delta\Delta Ct)}$). Actin served as control gene.

2.12 Immunoblotting

Western blot was conducted like previously reported[36]. In short, cells were lysed, samples were loaded on NuPage Novex 4–12% Bis-Tris gels and proteins were blotted using the iBlot™ system (Thermo Fisher Scientific). Membranes were incubated with specific primary antibodies and proteins were visualized with HRP-secondary antibodies.

2.13 Cell Surface Protein Screen

LEGENDScreen kit was used according to manufacturer's instructions. In brief, MDA-MB-231 shNon_CTRL or shPKD3_1 cells were detached with accutase and seeded ($3x10^4$ cells) into 96-well plates containing the pre-diluted PE-labelled antibodies. After 40 min of incubation at 4°C, cells were fixed for 10 min at room temperature using the fixation solution. Subsequently, cells were washed and analyzed by flow cytometry using MACSQuant® Analyzer 10 (Miltenyi Biotec). Data was evaluated using FlowJo. Relative mean fluorescence intensities (rel. MFI) were calculated with the following

formula: rel. MFI = [MFI_{sample} – ($MFI_{isotype}$ – MFI_{cells})] / MFI_{cells}. The threshold was set to rel. MFI > 1.5. All values below were not considered. After normalizing to shNon_CTRL, all values ≤ 0.9 were considered downregulation and values ≥ 1.1 were considered upregulation.

2.14 Sphere Formation Assay

For extreme limiting dilution assays (ELDA), MDA-MB-231 shNon_CTRL or shPKD3_1 cells were trypsinized, singularized using a 27G needle and 1, 10 or 100 cells were seeded onto Poly(2-hydroxyethyl methacrylate)-(pHEMA)-treated 96-well plates, respectively. Cells were cultured in 300 µl sphere formation medium containing DMEM/F12 GlutaMAX supplemented with 10 µg/ml insulin, 20 ng/ml EGF, 1 µg/ml hydrocortisone and 1x B27-supplement at 37°C in a humidified chamber with 5 % CO_2. 20 technical replicates per condition were cultured for 10 days. Only wells positive for spheres, no matter the actual number of spheres, were regarded as a positive result. Multiple group comparison and estimated stem cell frequency was analyzed using the ELDA software [178].

For primary oncosphere/ sphere formation assays, cells were trypsinized, singularized using a 27G needle, seeded onto pHEMA-treated plates in sphere formation medium and cultured for 5 days at 37°C in a humidified chamber with 5 % CO_2. Afterwards, formed spheres were imaged and the sphere area was analyzed using ImageJ. Only spheres larger than 2,500 µm^2 were taken into consideration. For secondary oncosphere/ sphere formation assays, primary spheres were collected, trypsinized, singularized using a 27G needle, re-seeded onto pHEMA-treated plates in sphere formation medium and cultured for 5 days at 37°C in a humidified chamber with 5 % CO_2. Formed spheres were imaged and the sphere area was analyzed using ImageJ. Only spheres larger than 2,500 µm^2 were taken into consideration. Data is presented as sphere area (mm^2) or sphere formation efficiency (SFE; spheres formed per 1000 cells seeded). shNon, shPKD3_1, shPKD3_2, MDA-MB-231, MDA-MB-468, MDA-MB-436, HCC1806 and MCF7 cells were seeded onto 12-well plates (primary assay: 3x10^3 cells; secondary assay: 1x10^3 cells) in 1.5 ml sphere formation medium. BT-549 cells were seeded onto 6-well plates (primary/ secondary assay: 5x10^3 cells) in 3 ml sphere formation medium.

MCF10A_EcoR_PKD3WT-EGFP cells were pre-treated with Dox for 24 h before the cells were singularized and seeded ($5x10^3$ cells) onto 6-well plates in 3 ml sphere formation medium. Subsequently, the sphere formation medium was supplemented with Dox and cells were cultured for 5 days. Dox was not replenished. Formed spheres were imaged and the sphere area was analyzed using ImageJ. Only spheres larger than 2,500 μm^2 were taken into consideration. Data is presented as sphere area (mm^2) or sphere formation efficiency (SFE; spheres formed per 1000 cells seeded).

For western blot or flow cytometry of primary and secondary oncospheres/spheres, cells were trypsinized, singularized using a 27G needle, seeded ($2x10^5$ cells) onto pHEMA-treated 10 cm plates in sphere formation medium and cultured for 5 days at 37°C in a humidified chamber with 5 % CO_2. Afterwards, oncospheres/spheres were collected and prepared for western blot or flow cytometry.

2.15 ALDEFLUOR Assay

For the ALDEFLUOR™ Assay, $1x10^5$ singularized cells (monolayer cells or secondary oncospheres) were diluted in 100 µl Assay Buffer containing 1.5 µl of activated ALDEFLUOR™ Reagent. Subsequently, 50 µl were removed and mixed with 1.5 µl DEAB Reagent (control). Control and test samples were incubated at 37°C for 30 min, followed by flow cytometry analysis using MACSQuant® Analyzer 10 (Miltenyi Biotec). Data was evaluated using FlowJo. DEAB treated samples served as internal controls.

2.16 Transient siRNA Transfection

Cells were transfected with Lipofectamine™ RNAiMAX according to manufacturer's instructions. For primary oncosphere formation assays, cells were transfected with siRNAs 24 h prior to seeding. For primary sphere formation assays using MCF10A_EcoR_PKD3WT-EGFP cells, transfection was carried out 48 h prior to seeding. siRNAs were purchased from Dharmacon: spNon negative control, spGEF-H1 and spPKD3.

2.17 Generation of Retroviral Constructs

The sequence encoding for PKD3WT-EGFP was amplified by PCR (5'-GCTTGCGTTGGATCCCATGTCTGCAAATAATTCCCCTCCATC-3', 5'-GTATCGATAAGCTTGATAATTCTTAATTTACTTGTACAGCTCGTCCATGC-3') and

sub-cloned via Gibson Assembly (NEB) into the TRE3G-PGK-NEO retroviral backbone. All constructs were validated by Sanger sequencing.

2.18 Generation of MCF10A_EcoR_PKD3WT-EGFP cells

MCF10A cells were modified by retroviral transduction of pWPXLd-RIEP (pWPXLd-rtTA3-IRES-EcoR-PGK-Puro) to stably co-express the ecotropic receptor (EcoR) and rtTA3 [179,180]. Stable cell pools were obtained by drug selection with 1 µg/mL puromycine for 2 weeks. Subsequently, the cells were transduced with ecotropically packaged retroviruses containing PKD3-EGFP. Retroviral gene transfer was performed using 20 µg plasmid DNA and 5 µg helper plasmid (pCMV-Gag-Pol) for each calcium phosphate transfection [181]. Retroviral packaging was performed using PlatiniumE cells. Transduced cells were selected for 5 days with 750 µg/mL G418, followed by a 24 h pulse with 1 µg/mL doxycycline and FACS-enrichment (BD Biosciences, FACSAria III). The pools were maintained in the absence of doxycycline. For experiments, the expression of PKD3WT-EGFP was induced using 1 µg/ml doxycycline.

2.19 Colony Formation Assay

For colony formation, $2x10^3$ (MDA-MB-231, MDA-MB-436, BT-549) or $3x10^3$ (MDA-MB-468) cells were seeded per 6-well in cell culture medium. 24 h later, cells were treated with *(a)* DMSO, *(b)* paclitaxel, *(c)* CRT0066101 or *(d)* paclitaxel+CRT0066101 for 48 h. After the treatment, cells were further cultured for 14 days, followed by fixation with 4 % paraformaldehyde (10 min at room temperature) and staining with crystal violet (20 min at room temperature). Colonies were analyzed using the Odyssey imaging system (LI-COR). Signals were corrected for background noise and normalized to the DMSO control.

2.20 Statistical Analysis

All values are presented as mean ± SEM. Significance between multiple groups was determined by one-way or two-way ANOVA and Bonferroni's test for multiple comparison. Significance between two groups was determined by t-test. Data was analyzed, using GraphPad Prism 7. P-values: $P \leq 0.05$ (*), $P \leq 0.01$ (**), $P \leq 0.001$ (***), $P \leq 0.0001$ (****). Combination index (CI) values were calculated using Webb's

fractional product method. CI<1 indicates synergism. 1≤CI≤1.09 indicates addition. CI>1.09 indicates antagonism.

3 Results

3.1 Regulation of glucose homeostasis

3.1.1 PKDkd-EGFP expression is specific to β-cells

To create a functional PKD knockout, transgenic mice inducibly expressing a PKDkd (kinase dead)–EGFP protein, that acts dominant-negative on all three PKD isoforms, were generated by Kornelia Ellwanger[46,47,60,182]. To express PKDkd–EGFP in an inducible and conditional manner, the tetracycline-dependent gene expression system was used[183]. In this system, the tet activator protein (rtTA) is expressed constitutively from the activator transgene. In the presence of the tetracycline analogue doxycycline, the rtTA protein binds to the TRE (tetracycline responsive promoter element), inducing the expression of the transgene. *In vivo*, doxycycline is administered in the drinking water.

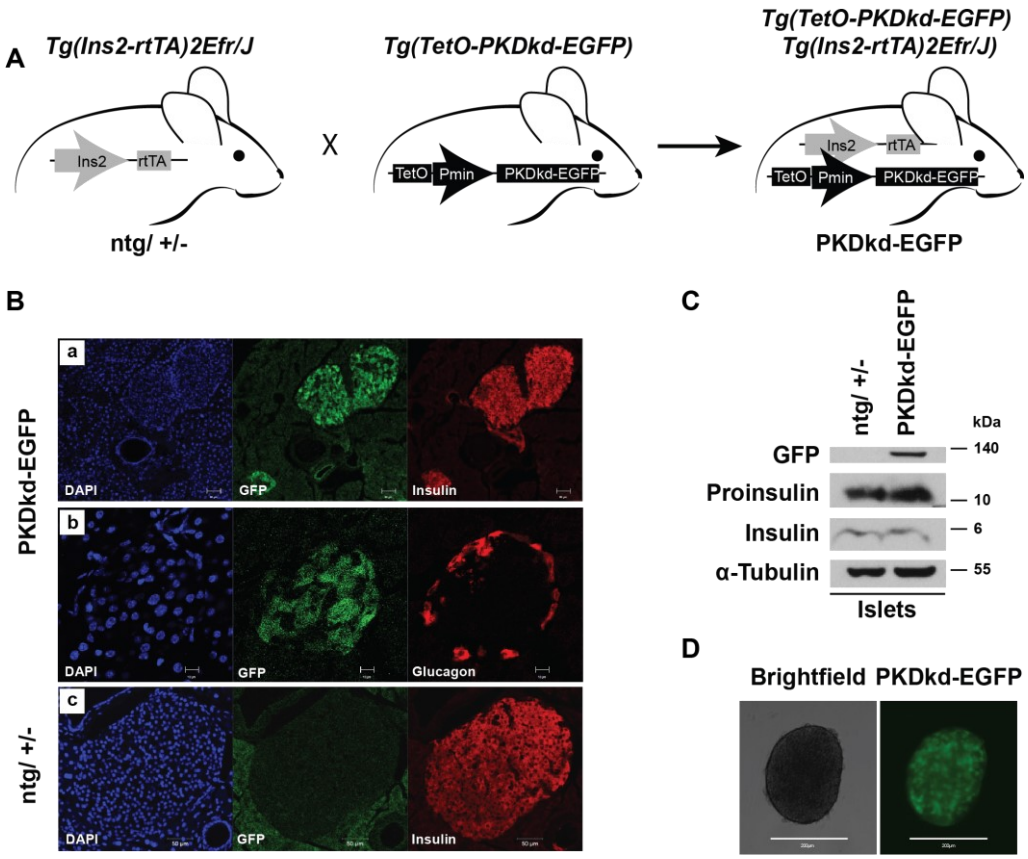

Figure 5 | Specific expression of PKDkd-GFP in pancreatic β-cells. (A) Breeding scheme of functional PKD knockout mice. The offspring expresses PKDkd-EGFP in a time (via TetOn-System) and tissue (Ins2 promotor exclusively induces PKDkd-EGFP expression in β-cells) dependent manner. **(B)** Selective expression of PKDkd-EGFP in β-cells. The pancreata of doxycycline-treated PKDkd-EGFP transgenic mice or control mice (ntg/ +/-) were

cryosectioned and stained for immunofluorescence microscopy. Scale bar, 50 µm (a, c) or 10 µm (b); Nuclei: DAPI (blue); Insulin (red; a, c); Glucagon (red; b); PKDkd-EGFP: transgene (green; a, b). Experiment performed and pictures taken by Claudia Koch. **(C)** Western blot of Langerhans islets. Immunoblotting was conducted, and membranes were probed with specific antibodies as indicated. α-Tubulin was used as loading control. Experiment performed by Claudia Koch[184]. **(D)** Microscopy of islets. *Left panel:* brightfield. *Right panel:* GFP channel showing the expression of PKDkd-EGFP in β-cells.

To analyze the role of PKD in β-cells, double transgenic mice were generated in which the expression of PKDkd-EGFP is induced in pancreatic β-cells. The Tg(Ins2-rtTA)2Efr/J mice express the reverse tetracycline-controlled transactivator (rtTA) protein under the control of the rat insulin 2 (*Ins2*) promoter (Figure 5A). In preliminary experiments conducted by Claudia Koch[184] and Kornelia Ellwanger, a selective expression of PKDkd-EGFP in the islets of Langerhans was observed upon 1 week of doxycycline administration in the drinking water. Staining of insulin and glucagon in pancreatic tissue revealed a β-cell specific expression of the transgene, which was not observed in α-cells (Figure 5B). PKDkd-EGFP expression was detectable at day one after doxycycline treatment and constantly increased over time, reaching a maximum after one week (Supplemental Figure S1A). The expression of PKDkd-EGFP did not per se interfere with insulin or proinsulin levels and remained stable in isolated islets (Figure 5C, D).

3.1.2 PKDkd-EGFP promotes a senescent phenotype in β-cells

Aging is associated with a reduction in β-cell mass, upregulated senescence and results in reduced glucose tolerance at later stages[123]. p16 is the master senescence gene in β-cells reducing their regenerative capacity[97,109]. p16 overexpression in β-cells strongly enhances GSIS, indicating that endogenous p16 drives GSIS with age[97]. Interestingly, β-cell function is improved in aged mice, which correlates with an epigenetic silencing of PKD3 gene expression[185]. To corroborate this finding, RT-qPCR analysis of islets isolated from juvenile (4-6 month) and adult (12-15 month) mice was performed to measure the expression of PKD1, PKD2, and PKD3. The analysis showed that compared to PKD2 and PKD3, PKD1 was expressed at a low level. Strikingly, during aging, the expression of both PKD2 and PKD3 declined, indicating a potential connection between aging and PKD function (Figure 6A).

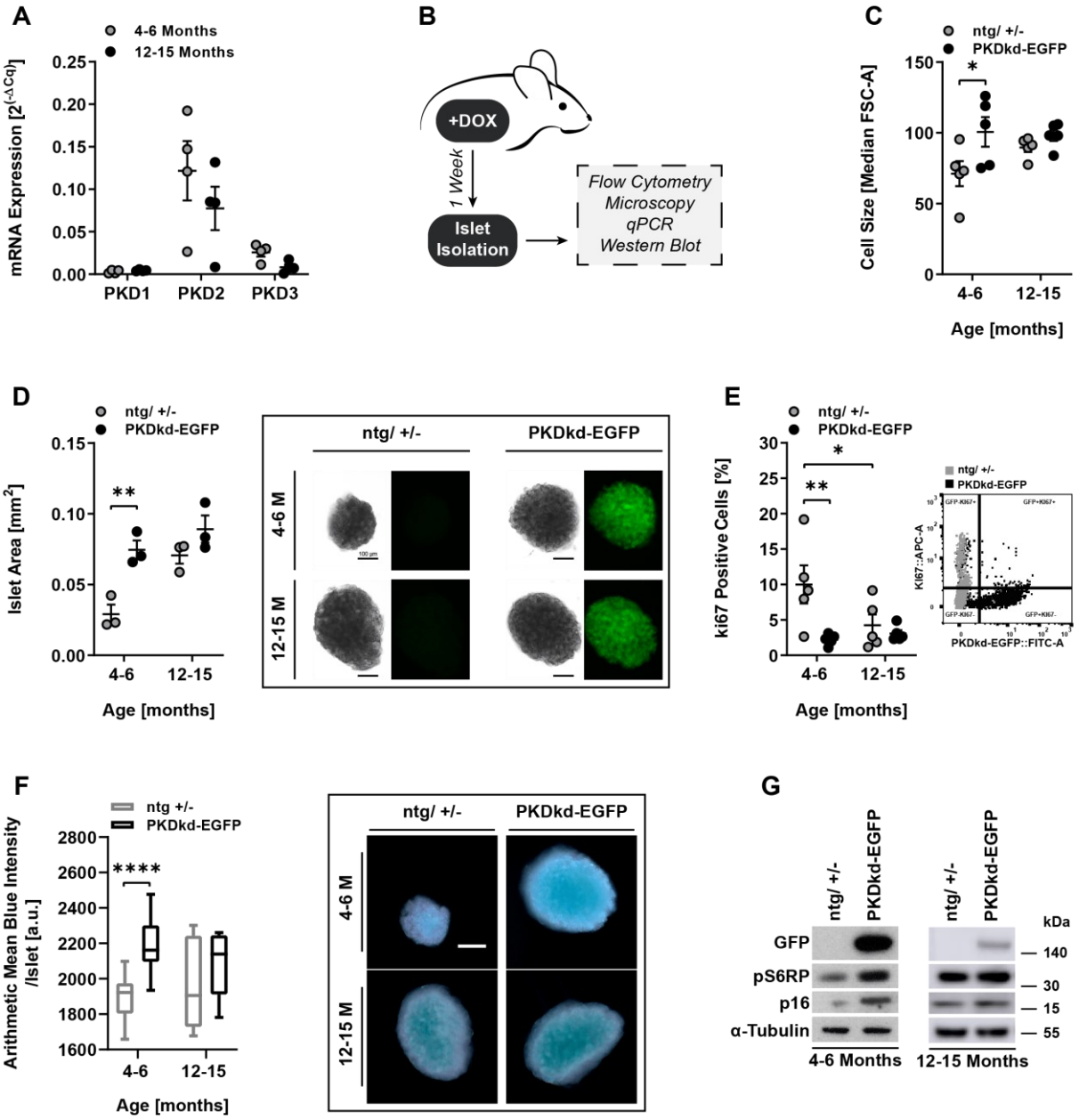

Figure 6 | PKDkd expression promotes a senescent phenotype in pancreatic ß-cells. (A) qPCR analysis of PKD isoforms in islets. Data is presented as mean mRNA expression ± SEM, n=4. **(B)** Workflow of doxycycline treated mice. **(C)** Flow cytometry-based cell size analysis. Islets were isolated and singularized into single cells. Data is presented as median FSC-A ± SEM, n=5. **(D)** Islet area. Left panel: 10 islets per mouse were analyzed via ImageJ. Data is presented as mean islet area (mm2) ± SEM, n=3. Statistical comparison by one-way ANOVA and Bonferroni-test. Right panel: Representative islet pictures. Bar represents 100 µm. **(E)** Flow cytometry-based proliferation analysis. Left panel: Islets were isolated and singularized into single cells. Data is presented as mean percent Ki67 positive cells ± SEM, n=5. Statistical comparison by one-way ANOVA and Bonferroni-test. Right panel: Dot plot of Ki67 analysis. Experiment and analysis conducted by Carlos Omar Oueslati Morales. **(F)** Senescence β-galactosidase staining. Left panel: Islets were isolated and stained for β-galactosidase, followed by imaging and analysis via the ZEN software. Data is presented as box and whiskers plot (Tukey). Center lines represent the median. Arithmetic mean blue intensity ± SEM, n=9 (12-15 months), n=24 (4-6 months). Statistical comparison by t-test. Right panel: Representative islet pictures. Bar represents 100 µm. **(G)** Western blot of islets.

Immunoblotting was conducted, and membranes were probed with specific antibodies as indicated. α-Tubulin was used as loading control.

The observed downregulation of PKD2 and PKD3 gene expression in islets during aging might indicate a potential function for the kinases in cellular senescence. To address this, young and adult PKDkd-EGFP and control (ntg/ +/-) mice received doxycycline for 7 days, followed by islet isolation and immediate analysis for hallmarks of senescence such as increased cell size, decreased proliferation and SA-β-galactosidase activity (Figure 6B). PKDkd-EGFP expression increased β-cell and islet size in juvenile mice but had limited effects in adult mice (Figure 6C, D; Supplemental Figure S1B). Additionally, proliferation was downregulated and SA β-galactosidase activity upregulated in juvenile mice (Figure 6E, F). Importantly, the β-cell size regulator ribosomal protein S6 (S6RP) was activated and p16 was upregulated upon PKDkd-EGFP expression in juvenile mice, clearly connecting PKD levels with p16 expression and senescence (Figure 6G).

3.1.3 The functional PKD knockout improves glucose tolerance and GSIS

Transgenic expression of p16 in β-cells of young mice strongly improved glucose tolerance and enhanced GSIS[97]. As PKDkd-EGFP expression increased p16 levels (Figure 6G), I analyzed whether PKDkd-EGFP mice showed an improved β-cell function and therefore performed glucose tolerance test (GTT), insulin tolerance test (ITT) as well as GSIS. After one week of doxycycline treatment, mice were starved for 16 hours, followed by an intraperitoneal injection of glucose. Blood samples were collected from the tail tip and blood glucose was measured. Although insulin tolerance was not affected, juvenile PKDkd-EGFP expressing mice showed a significantly improved glucose tolerance, compared to adult mice (Figure 7A-D). Interestingly, the fasting blood glucose levels were already reduced in juvenile PKDkd-EGFP expressing mice (Figure 7E). Moreover, the *in vivo* GSIS revealed upregulated insulin levels in juvenile PKDkd-EGFP expressing mice, before the glucose injection and 15 min afterwards (Figure 7F-G). Thus, it appeared that the expression of PKDkd-EGFP increased insulin secretion into the blood stream in juvenile mice. To further understand our findings, islets of control (ntg/ +/-) and PKDkd-EGFP expressing mice were isolated and *ex vivo* GSIS experiments were conducted. Here, PKDkd-EGFP

expression resulted in significantly amplified insulin secretion in juvenile, but not in adult islets (Figure 7H-K).

Current literature shows that ROS promotes senescence via p16 upregulation in human epidermal keratinocytes[186] and mouse fibroblasts[187]. Interestingly, Sasaki and colleagues linked ROS-induced cellular senescence to a demethylation of the p16 promotor in human epidermal keratinocytes[186]. Furthermore, ROS-induced deficiency of mitochondrial dynamics modifies mitochondrial homeostasis and promotes β-cell senescence[188-190]. Notably, mitochondrial ROS activates PKD, which initiates the NFκB pathway and facilitates the expression of the ROS scavenging protein superoxide dismutase 2 (SOD2)[64]. The loss of SOD2 increases mitochondrial oxidative damage and promotes p16-dependent cellular senescence[191]. Additionally, aging mice show reduced SOD2 expression[192] and a polymorphism in the human SOD2 gene is associated with T2D[193].

To address whether the functional knock-out of PKD impacts ROS levels in β-cells, I analyzed the expression of SOD2 by qPCR and examined the ROS content in isolated islets via flow cytometry. Indeed, I observed that SOD2 was downregulated and ROS levels were upregulated in PKDkd-EGFP expressing islets from juvenile mice (Figure 7L-M). Moreover, I observed, that SOD2 expression declined during aging, which confirms the study of Tirosh et al.[192] (Figure 7M).

These findings clearly demonstrated that the functional knockout of PKD reduced SOD2 gene expression and facilitated ROS upregulation.

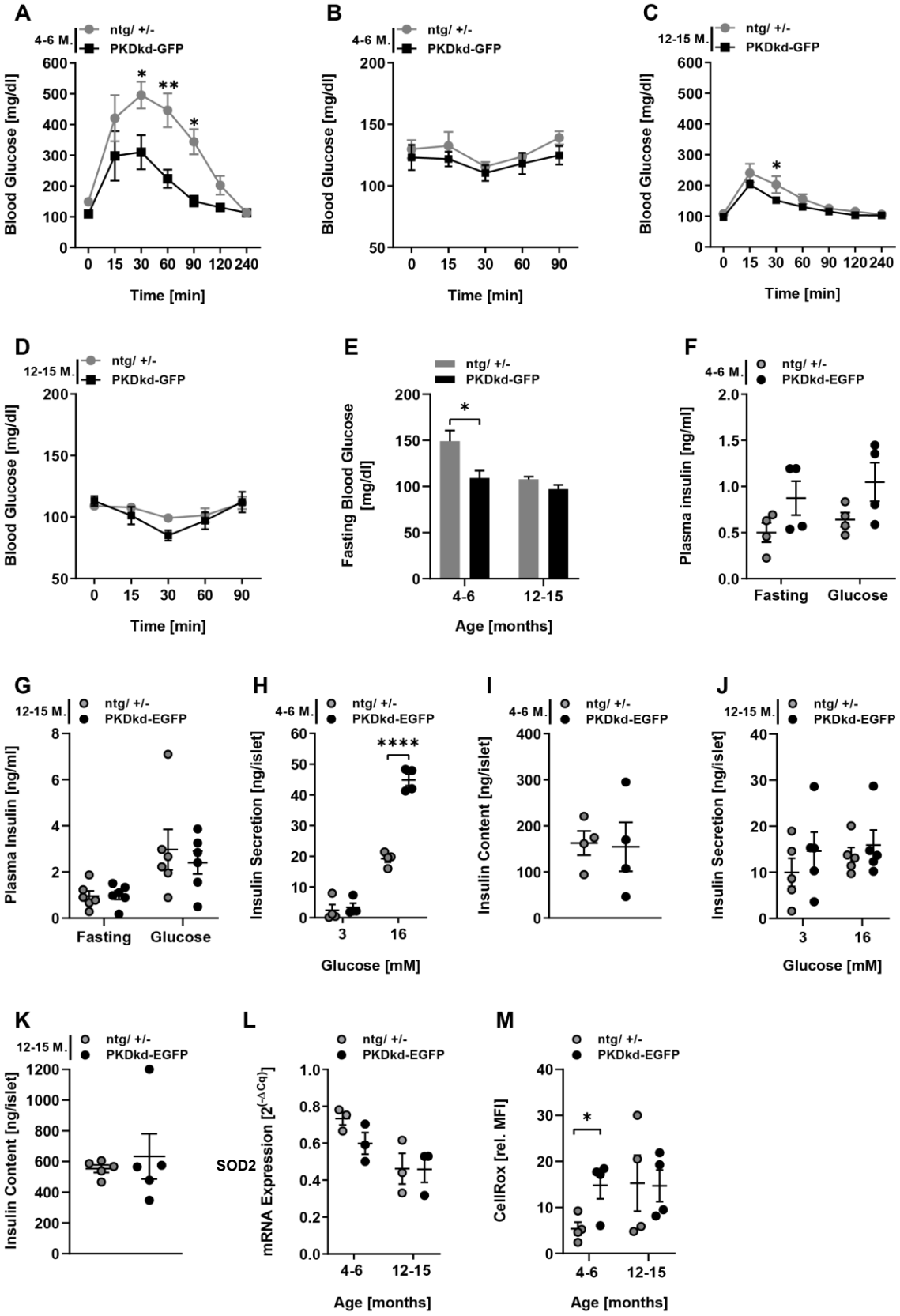

Figure 7 | PKDkd expression improves glucose tolerance in vivo and enhances GSIS in isolated islets. (A) GTT of 4-6 months old mice. After glucose injection, the blood glucose levels were measured at indicated time points. Data are presented as mean blood glucose concentration (mg/dl) ± SEM, n=5. Statistical comparison by two-way ANOVA. **(B)** ITT of 4-6

months old mice. After insulin injection, the blood glucose levels were measured at indicated time points. Data is presented as mean blood glucose concentration (mg/dl) ± SEM, n=5-6. Statistical comparison by two-way ANOVA. **(C)** GTT of 12-15 months old mice. After glucose injection, the blood glucose levels were measured at indicated time points. Data is presented as mean blood glucose concentration (mg/dl) ± SEM, n=7. Statistical comparison by two-way ANOVA. **(D)** ITT of 12-15 months old mice. After insulin injection, the blood glucose levels were measured at indicated time points. Data is presented as mean blood glucose concentration (mg/dl) ± SEM, n=5. Statistical comparison by two-way ANOVA. **(E)** Blood glucose levels after 16 h of fasting. Data is presented as mean blood glucose concentration (mg/dl) ± SEM, n=5-7. Statistical comparison by t-test. **(F-G)** Plasma insulin levels of mice via ELISA, before and 15 min after glucose injection. 4-6 months (F) and 12-15 months (G) old mice were fasted overnight and challenged with glucose to assess the insulin secretion capacity. Data is presented as mean plasma insulin concentration (ng/ml) ± SEM, n=4-6. Experiment in graph (F) was performed by Claudia Koch. **(H)** Insulin secretion during *ex vivo* GSIS using 4-6 months old animals. 10 size-matched islets were handpicked, cultured overnight in medium and on the next day transferred into KBHB buffer containing 5 mM glucose and for 30 min. The supernatant was discarded and KBHB containing 3 mM glucose was added for 1 h. Afterwards, the supernatant was collected and KBHB containing 16 mM glucose was added for 1 h, supernatants were collected, and insulin was quantified by ELISA. Data is presented as mean insulin secretion per islet (ng/islet) concentration ± SEM, n=4. Statistical comparison by one-way ANOVA. **(I)** Islets of 4-6 months old mice were incubated with ice cold acidic (1.5 % HCl) ethanol at -20 °C to determine total insulin content. Insulin levels were quantified by ELISA. Data is presented as mean insulin content per islet (ng/islet) ± SEM, n=4. Statistical comparison by t-test. **(J)** Insulin secretion during ex vivo GSIS using 12-15 months old animals. 10 size-matched islets were handpicked, cultured overnight in medium and on the next day transferred into KBHB buffer containing 5 mM glucose and for 30 min. The supernatant was discarded and KBHB containing 3 mM glucose was added for 1 h. Afterwards, the supernatant was collected and KBHB containing 16 mM glucose was added for 1 h, supernatants were collected, and insulin was quantified by ELISA. Data is presented as mean insulin secretion per islet (ng/islet) concentration ± SEM, n=5. Statistical comparison by one-way ANOVA. **(K)** Islets of 12-15 months old mice were incubated with ice cold acidic (1.5 % HCl) ethanol at -20 °C to determine total insulin content. Insulin levels were quantified by ELISA. Data is presented as mean insulin content per islet (ng/islet) ± SEM, n=5. Statistical comparison by t-test. **(L)** qPCR analysis of SOD2 in islets. Data is presented as mean mRNA expression ± SEM, n=3. Statistical comparison by one-way ANOVA. **(M)** Flow cytometry-based ROS detection. Islets were singularized into single cells and stained with the CellRox reagent. Data is presented as mean CellRox intensity (rel. MFI) ± SEM, n=4. Statistical comparison by t-test.

3.1.4 CRT0066101 improves glucose tolerance

To validate prior findings in a more clinically relevant setting and to exclude off-target effects by the PKDkd-EGFP transgene, I employed a pharmacologically selective inhibitor of PKD, CRT0066101, in wildtype mice. The inhibitor was administered p.o. once daily, for 7 days. Afterwards I analyzed glucose tolerance, insulin tolerance and markers of senescence, such as cellular size, Ki67 expression and SA β-galactosidase activity in β-cells and islets (Figure 8A). While insulin tolerance remained unaffected, CRT0066101 significantly improved glucose tolerance (Figure 8B) in wildtype mice. Moreover, PKD inhibition improved *in vivo* GSIS (Figure 8D) and triggered markers of

cellular senescence. Cellular size and SA β-galactosidase were upregulated upon PKD inhibition and Ki67 expression was downregulated (Figure 8E-G). In line with prior findings, I could show that the pharmacological inhibition of PKD decreased SOD2 expression, which in turn increased ROS in β-cells (Figure 8H-I).

Thus, these findings confirmed that the functional knockdown of PKD as well as its pharmacological inhibition decreased SOD2, increased ROS and thereby activated senescence.

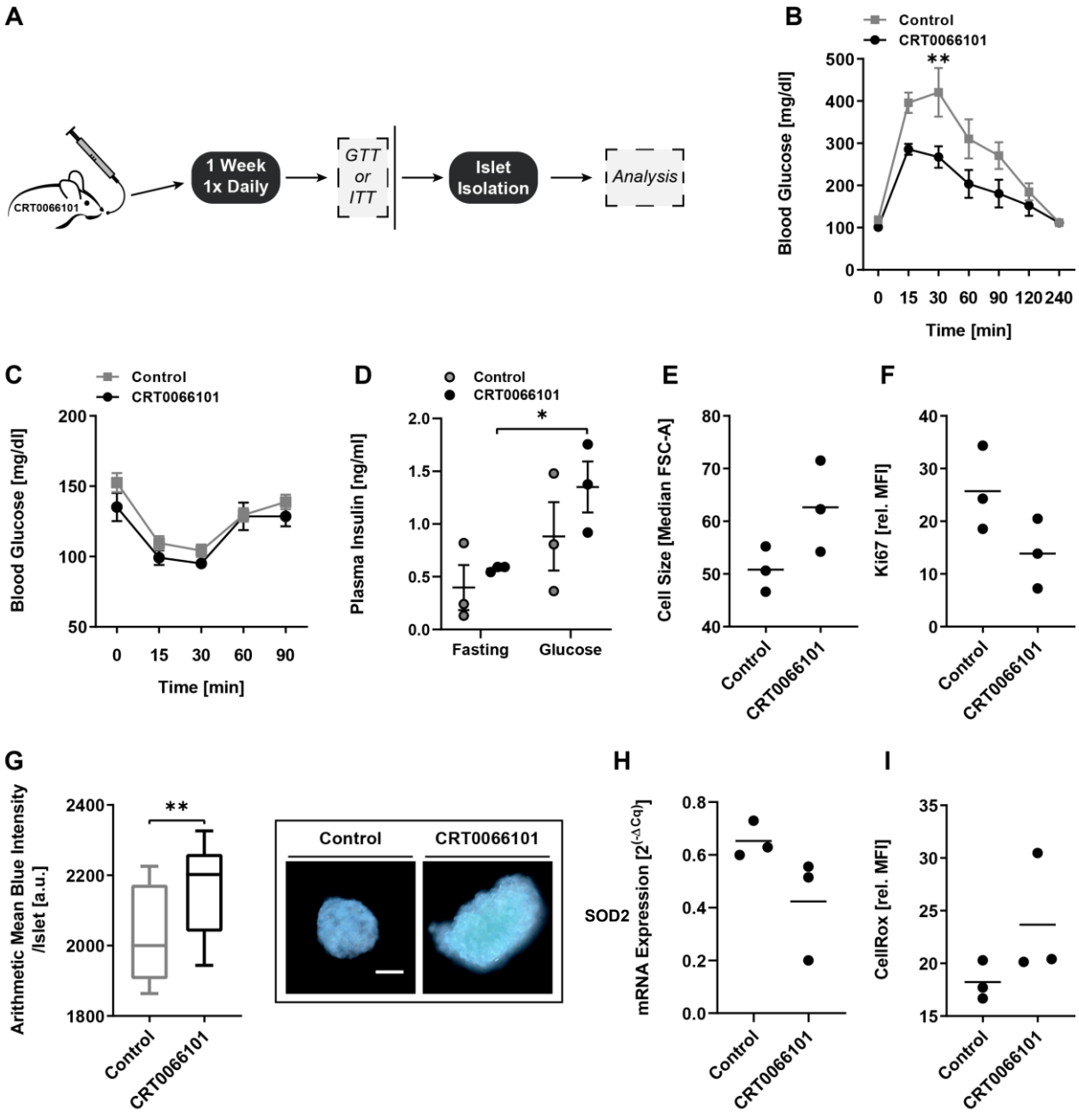

Figure 8 | CRT0066101 treatment improves glucose tolerance in vivo and induces a senescent phenotype in pancreatic islets. (A) Workflow of CRT0066101 treated mice. **(B)** GTT of 4-6 months old wildtype mice. Mice were treated as indicated for 1 week, followed by testing the glucose tolerance. After glucose injection, blood glucose levels were analyzed at

indicated time points. Data is presented as mean blood glucose concentration (mg/dl) ± SEM, n=5. Statistical comparison by two-way ANOVA. **(C)** ITT of 4-6 months old wildtype mice. Mice were treated as indicated for 1 week, followed by testing the insulin tolerance. After insulin injection, the blood glucose levels were measured at indicated time points. Data is presented as mean blood glucose concentration (mg/dl) ± SEM, n=5-6. Statistical comparison by two-way ANOVA. **(D)** Plasma insulin levels of mice via ELISA, before and 15 min after glucose injection. 4-6 months old wildtype mice were fasted overnight and challenged with glucose to assess the insulin secretion capacity. Data is presented as mean plasma insulin concentration (ng/ml) ± SEM, n=3. **(E)** Flow cytometry-based cell size analysis. Islets were isolated and singularized into single cells. Data is presented as median FSC-A ± SEM, n=3. **(F)** Flow cytometry-based proliferation analysis. Islets were isolated and singularized into single cells. Data is presented as mean percent Ki67 positive cells ± SEM, n=3. Statistical comparison by one-way ANOVA and Bonferroni-test. **(G)** Senescence SA β-galactosidase staining of 4-6 months old wildtype animals. Left panel: Mice were treated, and islets were isolated and stained for SA β-galactosidase , followed by imaging and analysis via the ZEN software. Data is presented as box and whiskers plot (Tukey). Center lines represent the median. Arithmetic mean blue intensity ± SEM, n=15-18. Statistical comparison by t-test. Right panel: Representative islet pictures. Bar represents 100 µm. **(H)** qPCR analysis of SOD2 in islets. Data is presented as mean mRNA expression ± SEM, n=3. Statistical comparison by one-way ANOVA. **(I)** Flow cytometry-based ROS detection. Islets were singularized into single cells and stained with the CellRox reagent. Data is presented as mean CellRox intensity (rel. MFI) ± SEM, n=3. Statistical comparison by t-test.

3.1.5 PKDkd-EGFP expression protects from high-fat-diet-induced insulin resistance

To test the improved glucose tolerance in a disease setting, I placed PKDkd-EGFP expressing and control (ntg/ +/-) mice on a high-fat-diet (HFD) (Figure 9A). The high-fat-diet model is a widely accepted model for lipid-induced insulin resistance[194]. Mice fed with a low-fat purified diet (LFD) containing the same ingredients with a closely matched composition to the high-fat formula were used as control groups. As expected, body weight of HFD mice drastically increased over time, however, weight gain of PKDkd-EGFP mice was markedly decreased compared to control mice. Weight gain of mice on LFD, however, was similar for both genotypes (Figure 9B). Food intake was not altered by PKDkd-EGFP expression (data not shown). After 16 weeks, the fasting blood glucose levels were tested and GTT as well as ITT were performed. The PKDkd-EGFP expressing mice showed decreased fasting blood glucose levels (Figure 9C). Strikingly, the glucose tolerance of HFD-fed and LFD-fed PKDkd-EGFP animals was significantly improved compared to control HFD and LFD animals' levels. The difference was more pronounced in HFD-fed mice (Figure 9D).

LFD-fed control and PKDkd-EGFP animals did not significantly differ in insulin tolerance. However, while HFD-fed control animals displayed a strong insulin resistance, compared to the respective LFD-fed animals, this effect was not as pronounced in PKDkd-EGFP animals (Figure 9E).

Strikingly, HFD-fed PKDkd-EGFP animals showed a protection against lipid-induced insulin resistance when compared to HFD-fed control animals indicating that the β-cell specific loss of PKD activity improved glucose tolerance and protected from insulin resistance. In line with our previous data, islets from HFD-fed PKDkd-GFP mice contained increased levels of p16 compared to control mice, pointing to the development of a senescence program (Figure 9F).

HFD is accompanied by a systemic inflammation due to increased free fatty acid (FFA) levels, which in turn elevate the production of cytokines like interleukin (IL) 6[195-197]. This low grade inflammation reduces the insulin sensitivity of metabolic organs such as fat and muscle[198]. I therefore analyzed IL6 levels in the plasma of HFD-/ LFD-fed PKDkd-EGFP and control mice after 8 and 16 weeks. IL6 was upregulated in HFD- and LFD-fed mice after 8 and 16 weeks, however, PKDkd-EGFP mice had slightly reduced IL6 levels (Supplemental Figure S1C). Moreover, HFD increases the levels of triglycerides in the blood stream[199], which can be converted to FFAs and thereby increase insulin resistance[200,201]. I observed that the blood triglyceride concentration did not differ in HFD-fed animals. However, in LFD-fed mice, the expression of PKDkd-EGFP reduced the triglyceride content, compared to control mice (Figure 9G).

Hence, PKDkd-EGFP expression increases glucose sensitivity, decreases insulin resistance and slightly reduces IL6 blood concentration and thereby protects from the HFD-induced metabolic syndrome.

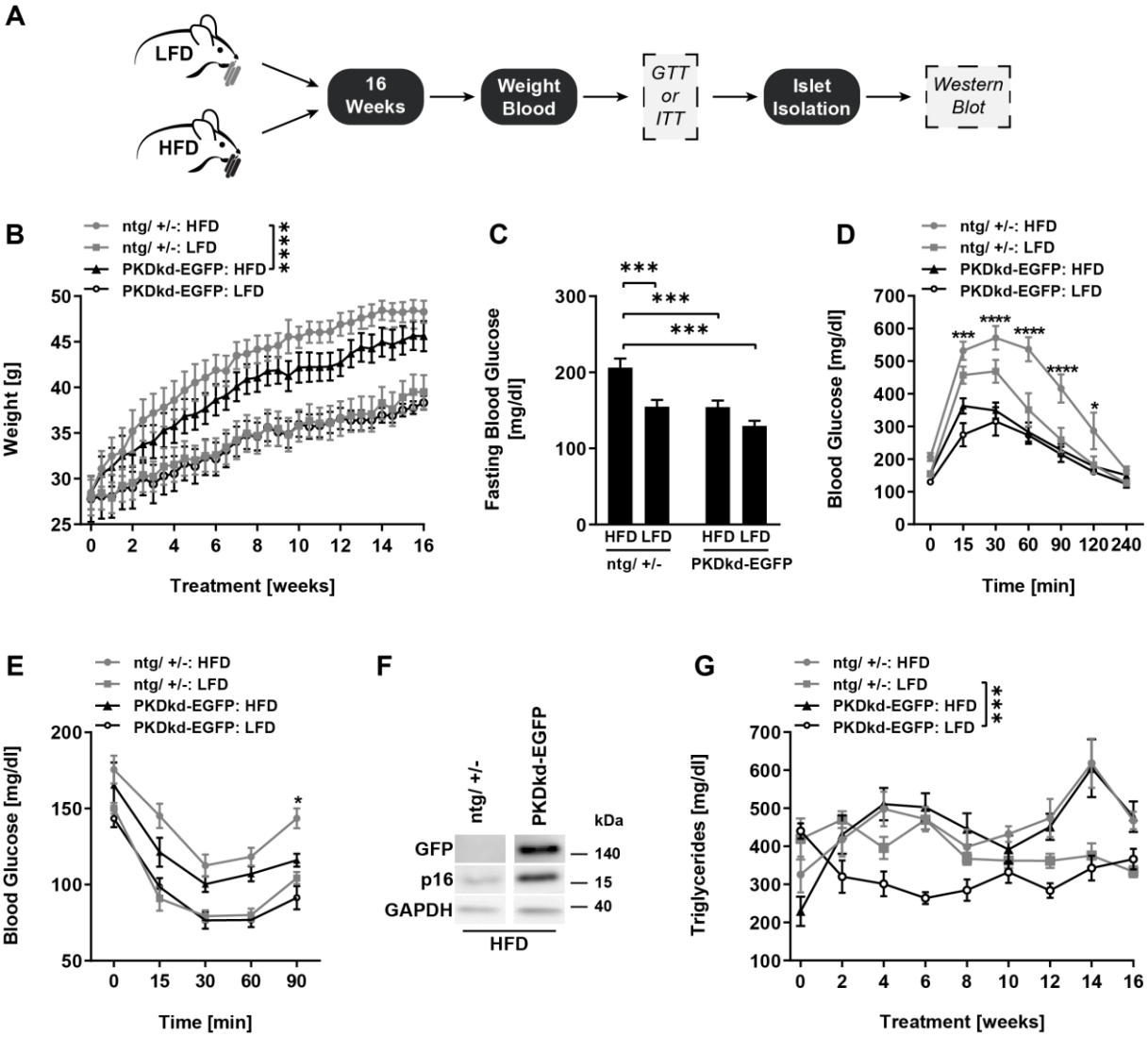

Figure 9 | PKDkd expression improves glucose tolerance and protects from induced insulin resistance in high-fat-diet mice. (A) Workflow of high fat diet. **(B)** Body weight of LFD and HFD fed transgenic mice. Data is presented as mean weight (g) ± SEM, n=7. Statistical comparison by two-way ANOVA. **(C)** Fasting blood glucose concentration of HFD and LFD fed transgenic mice, after 16 weeks. Data is presented as fasting blood glucose (mg/dl) ± SEM, n=7. Statistical comparison by one-way ANOVA and Bonferroni-test. **(D)** GTT of LFD and HFD fed transgenic mice. After glucose injection, blood glucose levels were analyzed at indicated time points. Data is presented as mean blood glucose (mg/dl) ± SEM, n=7. Statistical comparison by two-way ANOVA. **(E)** ITT of LFD and HFD fed transgenic mice. After insulin injection, blood glucose levels were analyzed at indicated time points. Data is presented as mean blood glucose (mg/dl) ± SEM, n=6. Statistical comparison by two-way ANOVA. **(F)** Western blot of islets. Immunoblotting was conducted, and membranes were probed with specific antibodies as indicated. α-Tubulin was used as loading control. **(G)** Plasma triglyceride analysis of HFD and LFD fed transgenic mice. Data is presented as mean triglyceride concentration (mg/dl) ± SEM, n=7. Statistical comparison by two-way ANOVA.

3.1.6 Rescue of high-fat-diet mice via pharmacological PKD inhibition

Next, I tested if PKD inhibition rescues already existing HFD-induced insulin and glucose intolerance. Thus, I put wildtype mice on HFD for 16 weeks and performed ITT or GTT. After HFD, mice were placed on normal diet and treated with CRT0066101 (or carrier) from week 17-20, again followed by GTT or ITT (Figure 10A). During the treatment phase, CRT0066101-treated mice decreased in weight, compared to control mice (Figure 10B). Food consumption did not differ (data not shown). Strikingly, the HFD-induced glucose and insulin intolerance were significantly reduced in CRT0066101-treated mice (Figure 10C-F). Interestingly, the treatment also reduced blood triglyceride concentration but did not alter IL6 levels (Figure 10G, Supplemental Figure S1D). Moreover, I analyzed SA β-galactosidase activity and observed an upregulation of senescence upon PKD inhibition (Figure 10F).

In sum, these data suggest that the functional knockdown (PKDkd-EGFP) and the pharmacological inhibition (CRT0066101) of PKD induced a senescent phenotype via a downregulation of SOD2 and an upregulation of ROS as well as p16. Moreover, both approaches protected from HFD-induced obesity, glucose intolerance as well as insulin resistance. Strikingly, in a pre-conditioned glucose/insulin resistant mouse model, CRT0066101 reversed the HFD-induced metabolic syndrome.

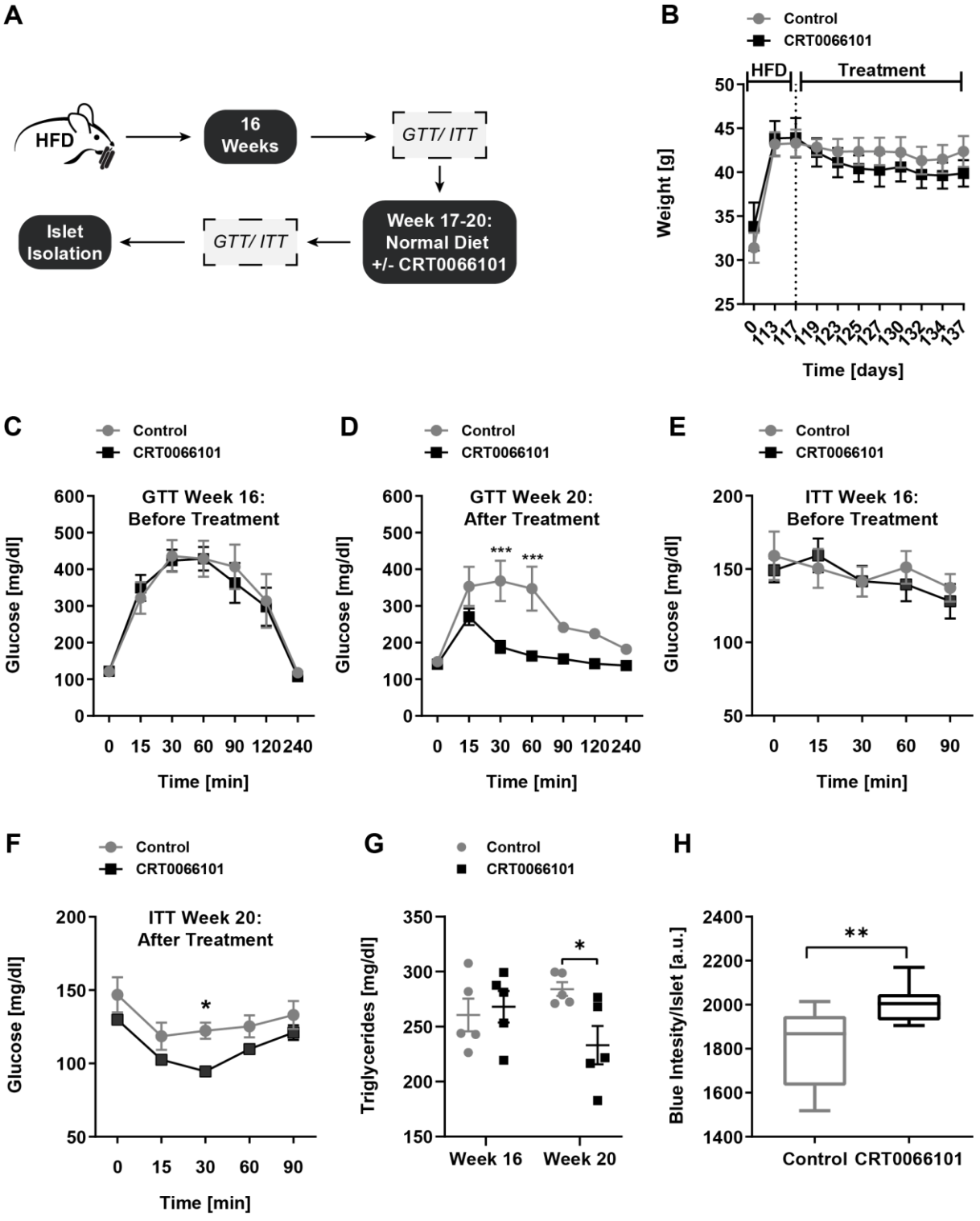

Figure 10 | PKD inhibition via CRT0066101-treatment improves glucose and insulin tolerance in pre-diabetic mice. (A) Workflow of CRT0066101 treated wildtype mice. **(B)** Body weight before and after CRT0066101 treatment. Data is presented as mean weight (g) ± SEM, n=5-6. Statistical comparison by two-way ANOVA. **(C-D)** GTT before (C) and after (D) CRT0066101 treatment. After glucose injection, blood glucose levels were analyzed at indicated time points. Data is presented as mean blood glucose (mg/dl) ± SEM, n=5-6. Statistical comparison by two-way ANOVA. **(E-F)** ITT before (E) and after (F) CRT0066101 treatment. After insulin injection, blood glucose levels were analyzed at indicated time points.

Data is presented as mean blood glucose (mg/dl) ± SEM, n=5. Statistical comparison by two-way ANOVA. **(G)** Plasma triglyceride analysis before (week 16) and after (week 20) CRT0066101 treatment. Data is presented as mean triglyceride concentration (mg/dl) ± SEM, n=5. Statistical comparison by t-test. **(H)** Senescence SA β-galactosidase staining of 4-6 months old wildtype animals. Mice were treated, and islets were isolated and stained for SA β-galactosidase , followed by imaging and analysis via the ZEN software. Data is presented as box and whiskers plot (Tukey). Center lines represent the median. Arithmetic mean blue intensity ± SEM, n=9-12. Statistical comparison by t-test.

3.2 PKD3 signaling in TNBC stem cells

The studies in this chapter were published in the International Journal of Cancer (Lieb et al. 2019)[202].

3.2.1 PKD3 depletion decreases cancer stem cell-like properties in MDA-MB-231 cells

It is well established that PKD3 controls vesicular trafficking to the plasma membrane thereby modulating the expression of cell surface proteins[203]. To analyze how PKD3 controls the cell surface phenotype of breast cancer cells, the previously described TNBC cell line MDA-MB-231 stably depleted of PKD3 (shPKD3_1)[133] was used and a flow cytometry-based screening of 332 molecules (Figure 11A) was performed. As a control, I used MDA-MB-231 cells stably expressing a scrambled shRNA (shNon_CTRL) (Figure 12A-B). Of the 332 cell surface proteins, 102 were above the detection threshold and are listed in Table 1. In the PKD3 deficient cells, 68 proteins displayed dysregulated surface levels with respect to the control (24 upregulated and 44 downregulated). Several of the proteins with decreased cell surface expression have been associated with the maintenance of breast cancer stem cells, such as CD44, CD184, CD61, NOTCH2, NOTCH4, and CD304[142,143,204-208] (Figure 11B, Figure 12C-H, Table 1). This prompted me to measure the stem cell frequency of the stable MDA-MB-231 cell lines by performing extreme limiting dilution assays (ELDA) (Figure 11C). Indeed, the estimated stem cell frequency was significantly decreased in PKD3 depleted cells when compared to the stem cell frequency of the control cells (Figure 11D). I then analyzed the gene expression of a panel of breast cancer stemness markers including SOX2, OCT3/4, NANOG, NOTCH4, CD44, SNAIL and ALDH in monolayer (2D)-cultured shPKD3_1 and shNon_CTRL cells[147,209]. Compared to the control cells, I observed a significant downregulation of the corresponding genes in shPKD3_1 cells (Figure 11E). Enhanced ALDH activity is considered a hallmark of

breast cancer stem cells[210,211]. When comparing MDA-MB-231 shPKD3_1 cells with shNon_CTRL cells, I observed that PKD3 depletion caused a significant decrease in ALDH activity as measured by Aldefluor assay (Figure 11F), which further substantiated a potential role of the kinase in stem cell regulation. Finally, I investigated the formation of primary and secondary oncospheres as a measure of cancer stem cell activity[212]. Here, the depletion of PKD3 caused an up to 70 % decrease in primary and secondary sphere forming efficiency (SFE) (Figure 11G) in comparison to the control. Remarkably, the knockdown of PKD3 neither changed the size of the oncospheres (Figure 11H), nor did it induce cell death by anoikis, excluding anti-proliferative and pro-apoptotic effects (Figure 12I-J).

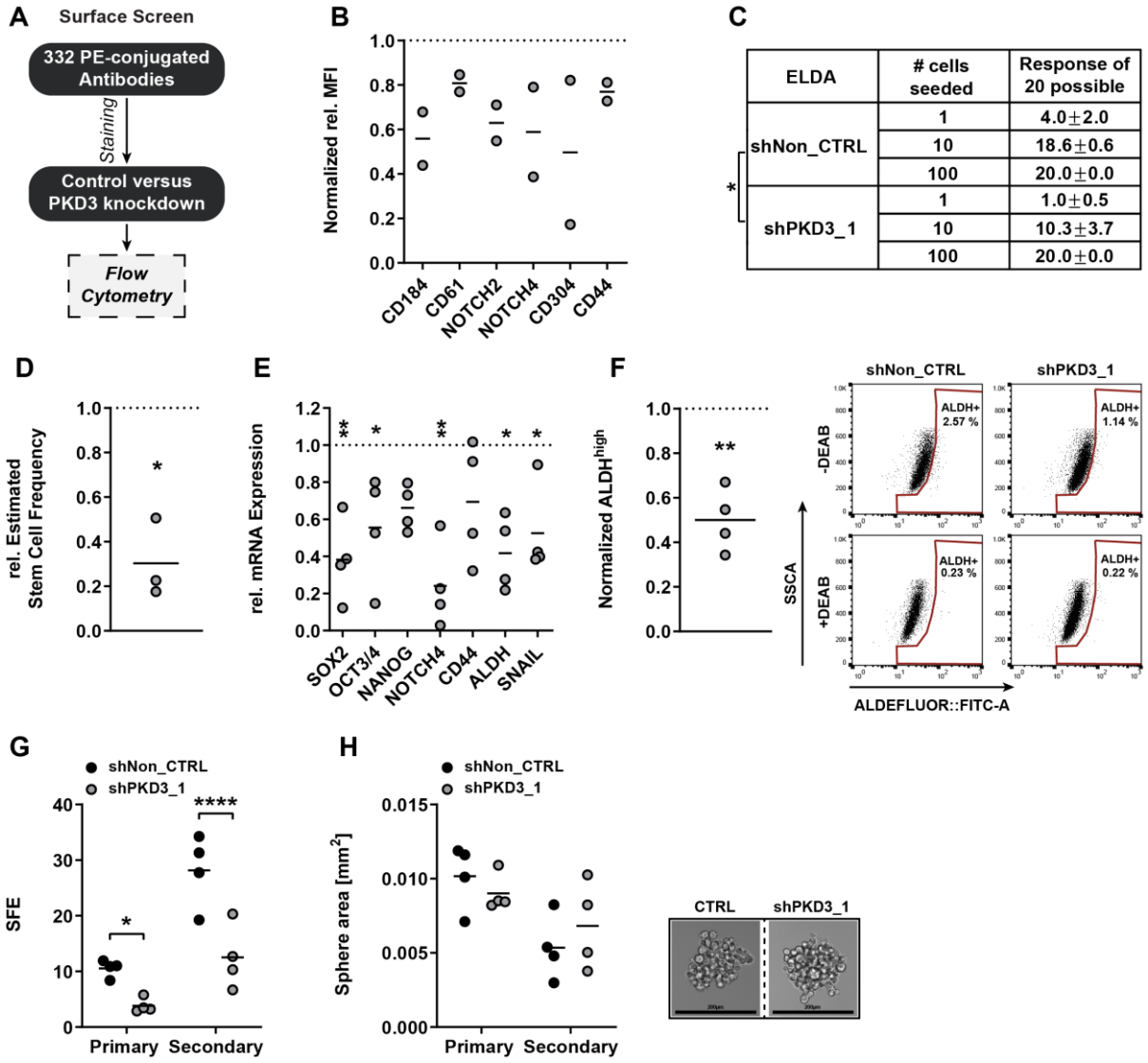

Figure 11 | Loss of PKD3 reduces stemness in MDA-MB-231 cells. (A) Cell surface screen workflow. **(B)** Flow cytometry-based surface protein screening. Monolayer-cultured cells. Data is presented as relative mean fluorescence intensity (rel. MFI) normalized to shNon_CTRL,

n=2. **(C)** Extreme limiting dilution assay (ELDA). Analysis of 20 wells of a 96-well plate per condition. Only sphere-positive wells were considered. Data is presented as mean ± SEM, n=3. Statistical comparison by ELDA multiple group analysis. **(D)** ELDA-based estimated stem cell frequency. Data is presented as mean estimated stem cell frequency normalized to shNon_CTRL, n=3. Statistical comparison by t-test. **(E)** qPCR analysis of stemness markers. Monolayer-cultured cells. Data is presented as mean mRNA expression normalized to shNon_CTRL, n=4. Statistical comparison by t-test. **(F)** Left panel: flow cytometry-based stemness analysis via ALDEFLUOR. Monolayer-cultured cells. Data is presented as mean ALDHhigh population normalized to shNon_CTRL, n=4. Statistical comparison by t-test. Right panel: Dot plot of ALDEFLUOR measurements. DEAB-treated samples served as internal control. **(G)** Oncosphere count of primary and secondary oncosphere assays. Data is presented as mean sphere formation efficiency (SFE), n=4. Statistical comparison by one-way ANOVA and Bonferroni-test. **(H)** Left panel: sphere area of primary and secondary oncospheres. Data is presented as mean square millimeters (mm2), n=4. Statistical comparison by one-way ANOVA and Bonferroni-test. Right panel: representative oncosphere pictures. Bar represents 200 µm.

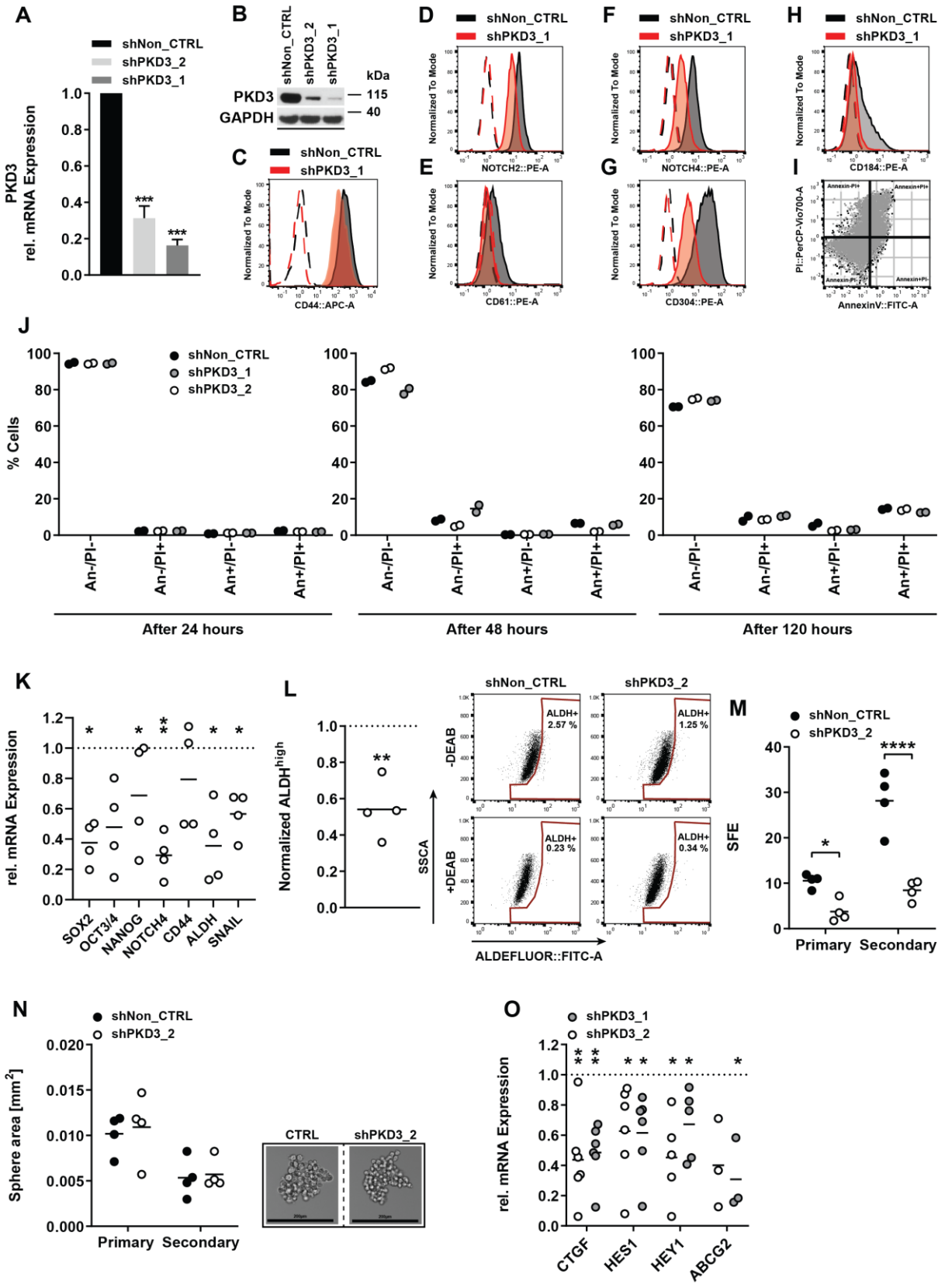

Figure 12 | PKD3 knockdown cells are not prone to anoikis but show decreased stemness related signaling. (A) qPCR analysis of PKD3 knockdown. Data is presented as mRNA expression normalized to shNon_CTRL, mean ± SEM, n=6. Statistical comparison by t-test. **(B)** PKD3 knockdown control. Western blot of indicated cell lines. Immunoblotting was

conducted, and membranes were probed with specific antibodies as indicated. GAPDH was used as loading control. **(C-H)** Histograms of indicated surface proteins. Dashed lines: isotype control. Solid lines: antibodies against indicated antigens. **(I)** Dot blot of AnnexinV/ PI stained cells from (I) after 120 h. **(J)** Flow cytometry-based annexin V (An) and propidium iodine (PI) apoptosis assay. Indicated cell lines were seeded ($2x10^5$ cells in 10 cm pHEMA-treated plates) into primary oncosphere assays and incubated for 24, 48 or 120 h. Oncospheres were harvested, singularized and 30,000 cells per sample were stained with AnnexinV and PI, according to manufacturer's instructions. After 10 min, cells were analyzed using a flow cytometer. Data is presented as mean percent cells, n=2. **(K)** qPCR analysis of stemness markers. Monolayer-cultured cells. Data is presented as mean mRNA expression of 2D-cultured shPKD3_2 cells normalized to shNon_CTRL, n=4. Statistical comparison by t-test. **(L)** *Left panel*: flow cytometry-based stemness analysis via ALDEFLUOR™. Data is presented as mean $ALDH^{high}$ population of shPKD3_2 cells normalized to shNon_CTRL, n=4. Statistical comparison by t-test. *Right panel:* Dot plot of ALDEFLUOR measurements. DEAB-treated samples served as internal control. **(M)** Oncosphere count of primary and secondary oncosphere assays. Data is presented as mean sphere formation efficiency (SFE), n=4. Statistical comparison by one-way ANOVA and Bonferroni-test. **(N)** *Left panel:* sphere area of primary and secondary oncospheres. Data is presented as mean square millimeters (mm^2), n=4. Statistical comparison by one-way ANOVA and Bonferroni-test. *Right panel:* representative oncosphere pictures. Bar represents 200 µm. **(O)** qPCR analysis of stemness markers. Monolayer-cultured cells. Data is presented as mean mRNA expression of 2D-cultured shPKD3_2 cells normalized to shNon_CTRL cells, n=3-6. Statistical comparison by t-test.

Table 1 | Surface Protein Screen.

Name	UniProtKB	shPKD3_1 / shNon	SEM
CD304	O14786	0.50	0.324
CD245	Q92614	0.51	0.014
CD63	P08962	0.55	0.021
CD146	P43121	0.55	0.060
CD184 (CXCR4)	P61073	0.56	0.120
CD324 (E-CADHERIN)	P12830	0.57	0.035
CD266 (Fn14)	Q9NP84	0.58	0.146
Notch 4	Q99466	0.59	0.202
CD46	P15529	0.59	0.027
CD148	Q12913	0.62	0.037
CD261 (DR4)	O00220	0.62	0.083
Notch 2	Q04721	0.63	0.081
CD111	Q15223	0.64	0.201
erbB3/ HER-3	P21860	0.64	0.011

CD164	Q04900	0.66	0.007
CD252 (OX40L)	P23510	0.66	0.006
CD167a (DDR1)	Q08345	0.67	0.252
CD166	Q13740	0.68	0.052
CD340 (erbB2)	P04626	0.69	0.027
CD89	P24071	0.70	0.099
CD326 (Ep-CAM)	P16422	0.72	0.127
CD97	P48960	0.76	0.065
CD47	Q08722	0.77	0.067
CD44	P16070	0.77	0.042
CD298	P54709	0.77	0.178
Tim-1	Q96D42	0.80	0.062
CD61	P05106	0.81	0.041
EGFR	P00533	0.81	0.318
CD183	P49682	0.82	0.071
CD49a	P56199	0.83	0.031
CD51	P06756	0.83	0.079
CD51/61	-	0.84	0.054
CD196	P51684	0.84	0.002
CD119 (IFN-γ R α chain)	P15260	0.85	0.077
Notch 1	P46531	0.85	0.242
CD99	P14209	0.85	0.015
CD100	Q92854	0.86	0.291
CD138	P18827	0.88	0.005
CD49d	P13612	0.88	0.167
CD104	P16144	0.88	0.063
HLA-E	P13747	0.89	0.272
CD62P (P-Selectin)	P16109	0.89	0.144
MSC (W7C6)	O60682	0.91	0.015
CD277	O00481	0.90	0.159

CD49c	P26006	0.91	0.141
SSEA-4	-	0.91	0.629
CD218a (IL-18Rα)	Q13478	0.92	0.019
CD64	P12314	0.92	0.105
CD116	P15509	0.92	0.232
CD58	P19256	0.92	0.098
C3AR	Q16581	0.93	0.015
CD40	P25942	0.93	0.009
CD156c (ADAM-10)	O14672	0.93	0.060
CD95	P25445	0.93	0.023
CD221 (IGF-1R)	P08069	0.94	0.255
CD9	P21926	0.95	0.034
CD85d (ILT4)	Q8N423	0.95	0.051
CD257 (BAFF)	Q9Y275	0.95	0.373
DLL1	O00548	0.96	0.030
CXCR7	P25106	0.96	0.063
CD84	Q9UIB8	0.96	0.072
CD49f	P23229	0.98	0.259
CD276	Q5ZPR3	0.98	0.235
CD57	Q96E93	0.99	0.083
β2-microglobulin	P61769	1.00	0.154
HLA-A2	P01892	1.00	0.154
CD71	P02786	1.01	0.147
CD170 (Siglec-5)	O15389	1.01	0.287
CD29	P05556	1.01	0.210
HLA-A,B,C	-	1.01	0.209
CD112 (Nectin-2)	Q92692	1.01	0.077
CD318 (CDCP1)	Q9H5V8	1.01	0.111
CD271	P08138	1.02	0.221
CD107a (LAMP-1)	P11279	1.05	0.035

CD81	P35762	1.07	0.267
CD82	P27701	1.07	0.153
CD274 (B7-H1)	Q9NZQ7	1.08	0.627
CD317	Q10589	1.09	0.498
CD102	P13598	1.11	0.015
CD215 (IL-15Rα)	Q13261	1.13	0.076
CD83	Q01151	1.16	0.022
CD49e	P08648	1.18	0.285
CD262 (DR5)	O14763	1.20	0.007
C5L2	Q9P296	1.21	0.070
CD108	O75326	1.22	0.341
CD201 (EPCR)	Q9UNN8	1.25	0.195
CD85h (ILT1)	Q8N149	1.33	0.284
CD132	P31785	1.36	0.233
CD155 (PVR)	P15151	1.45	0.397
CD59	P13987	1.45	0.769
CD270 (HVEM)	Q92956	1.47	0.523
CD273 (B7-DC)	Q9BQ51	1.55	0.683
CD73	P21589	1.57	0.576
FcRL6	Q6DN72	1.59	0.541
SSEA-5	-	1.76	0.802
CD54	P05362	1.85	0.434
CD55	P08174	2.11	1.316
CD141	P07204	2.34	0.925
CD344 (Frizzled-4)	Q9ULV1	2.76	0.573
CD220	P06213	2.91	1.248
HLA-DR	P01903	6.15	0.016
CD275 (B7-H2)	O75144	6.97	5.294

Table shows all proteins with a rel. MFI > 1.5. Signals with a rel. MFI < 1.5 were not considered. Data is presented as normalized rel. MFI, shPKD3_1 versus shNon, mean±SEM, n=2. Values below 1 indicate downregulation. Values above 1 indicate upregulation

To exclude potential off target effects of the PKD3-specific shRNA, I employed a second, independent MDA-MB-231 PKD3 knockdown cell line, shPKD3_2[133]. Using this cell line, I could confirm a significant downregulation of stemness-related marker gene expression (Figure 12K), ALDH activity (Figure 12L) and oncosphere forming efficiency (Figure 12M-N) upon loss of PKD3 expression. Activation of YAP (yes-associated protein)/TAZ (transcriptional co-activator with PDZ-binding motif) and Notch signaling are required to sustain self-renewal and tumor-initiation capacities in breast cancer stem cells[206,213]. Indeed, in both PKD3 knockdown cell lines, decreased expression of the YAP/TAZ and Notch target genes CTGF and HES1/HEY1, respectively, indicated impaired signaling through these pathways. Furthermore, I observed downregulation of ABCG2, which contributes to drug resistance in breast cancer stem cells (Figure 12O)[144]. Thus, my results univocally show that MDA-MB-231 cells require PKD3 for cancer stem cell maintenance *in vitro*.

3.2.2 PKD3 knockdown decreases the tumor initiation potential *in vivo*.

To prove that PKD3 is also important for maintaining the tumor initiation potential *in vivo*, I implanted four different concentrations of MDA-MB-231 shPKD3_1 and shNon_CTRL cells into the 4th mammary fat pad of immunocompromised mice (Figure 13A). Strikingly, shPKD3_1 cells showed a strongly diminished tumor initiation potential compared to shNon_CTRL cells (Figure 13B-C). In line with the reduced tumor initiation potential, the estimated stem cell frequency of PKD3 deficient tumor cells was significantly lower (Figure 13C). Apart from the lowest cell concentration injected, shNon_CTRL and shPKD3_1 tumors did not differ in size (Figure 13D). I next singularized the tumor cells, analyzed ALDH activity (Figure 13E) and primary as well as secondary oncosphere formation (Figure 13F-G). In agreement with the decreased stem cell frequency, ALDH activity and SFE were significantly reduced in PKD3 deficient MDA-MB-231 tumor cells. My data thus confirm a role for PKD3 in promoting stemness and tumor-initiating capacity of MDA-MB-231 cells.

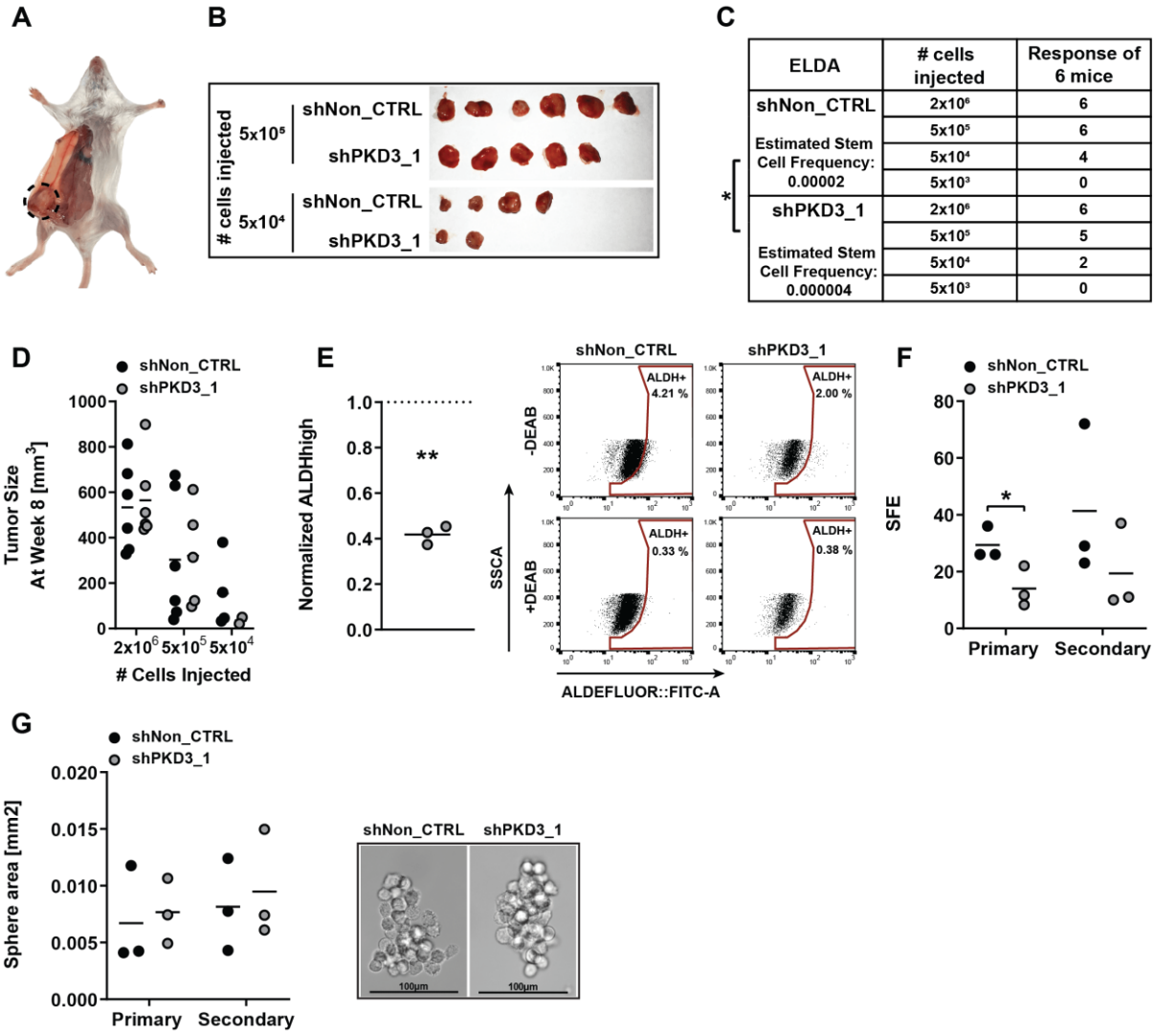

ELDA	# cells injected	Response of 6 mice
shNon_CTRL	$2x10^6$	6
	$5x10^5$	6
Estimated Stem Cell Frequency: 0.00002	$5x10^4$	4
	$5x10^3$	0
shPKD3_1	$2x10^6$	6
	$5x10^5$	5
Estimated Stem Cell Frequency: 0.000004	$5x10^4$	2
	$5x10^3$	0

Figure 13 | *In vivo* tumor initiation potential is decreased in PKD3-depleted TNBC cells. **(A)** Representative picture of orthotopic tumor formation. **(B)** Tumors of mice injected with $5x10^5$ and $5x10^4$ MDA-MB-231 cells expressing the indicated shRNAs. **(C)** Extreme limiting dilution assay (ELDA). 6 mice per condition. Data is presented as tumor bearing mice per injected cell concentration and estimated stem cell frequency. Statistical comparison by ELDA multiple group analysis. **(D)** Tumor size at week 8. Data is presented as mean cubic millimeters (mm^3), n=2-6. Statistical comparison by one-way ANOVA and Bonferroni-test. **(E)** *Left panel:* flow cytometry-based stemness analysis of singularized tumor cells via ALDEFLUOR™. Data is presented as mean $ALDH^{high}$ population of shPKD3_1 normalized to shNon_CTRL, n=3. Statistical comparison by t-test. *Right panel:* Dot plot of ALDEFLUOR measurements. DEAB-treated samples served as internal control. **(F)** Oncosphere count of primary and secondary oncosphere assays, using singularized tumor cells. Data is presented as mean sphere formation efficiency (SFE), n=3. Statistical comparison by t-test. **(G)** *Left panel:* sphere area of primary and secondary oncospheres. Data is presented as mean square millimeters (mm^2), n=3. Statistical comparison by one-way ANOVA and Bonferroni-test. *Right panel:* representative oncosphere pictures. Bar represents 100 µm.

3.2.3 PKD3-mediated TNBC stem cell regulation is dependent on GEF-H1.

The Rho guanine nucleotide exchange factor 2 (ARHGEF2, also GEF-H1) was recently reported to act as an upstream activator of PKD at the Golgi complex in HeLa cells[36]. Interestingly, GEF-H1/Rho signaling contributes to breast cancer metastases[169], which is why I analyzed whether GEF-H1 is required for PKD3 to promote TNBC cell stemness. To trigger Rho-dependent PKD activation I treated MDA-MB-231 cells with nocodazole[36] and detected PKD activity by activation loop phosphorylation (pS744/748), which is conserved in all PKD isoforms. Treatment with phorbol ester (PMA), a potent inducer of PKD activity[214], served as a positive control. Nocodazole strongly increased PKD activity and this was fully abrogated by PKD3 depletion despite the presence of PKD2. Importantly, nocodazole failed to induce PKD activity in the absence of GEF-H1, proving that PKD3, but not PKD2, is activated by GEF-H1 in MDA-MB-231 cells (Figure 14A).

Next, the correlation of GEFH1 and PKD3 expression was analyzed in a panel of breast cancer cell lines. In general, TNBC cell lines with elevated PKD3 expression[14] also expressed higher GEF-H1 levels whereas low PKD3 and GEF-H1 expression was observed in the non-TNBC cell lines (Figure 14B). To verify these findings in clinical patient data, PKD3 and GEF-H1 mRNA levels in human breast cancers from the TCGA database were examined. In accordance with the cell line data, significantly higher GEF-H1 expression was observed in the tumor samples belonging to the high PKD3 expression group (Figure 14C). Next the functional relevance of GEF-H1 and PKD3 expression was addressed in primary oncospheres (3D) obtained from two independent TNBC cell lines (Figure 14D-E). In both MDA-MB-231 and MDA-MB-468 cell lines, GEF-H1 as well as PKD3 expression was upregulated in oncospheres compared to the monolayer culture (2D). To validate a potential functional link between GEF-H1 and PKD3 in cancer stem cells, I performed a transient siRNA-mediated GEF-H1 knockdown prior to seeding of the cells into the primary oncosphere assay and then analyzed PKD3 activation loop phosphorylation. Remarkably, the depletion of GEF-H1 in MDA-MB-231 and MDA-MB-468 cells reduced the phosphorylation of PKD3 in oncospheres by up to 70 % (Figure 14F-H).

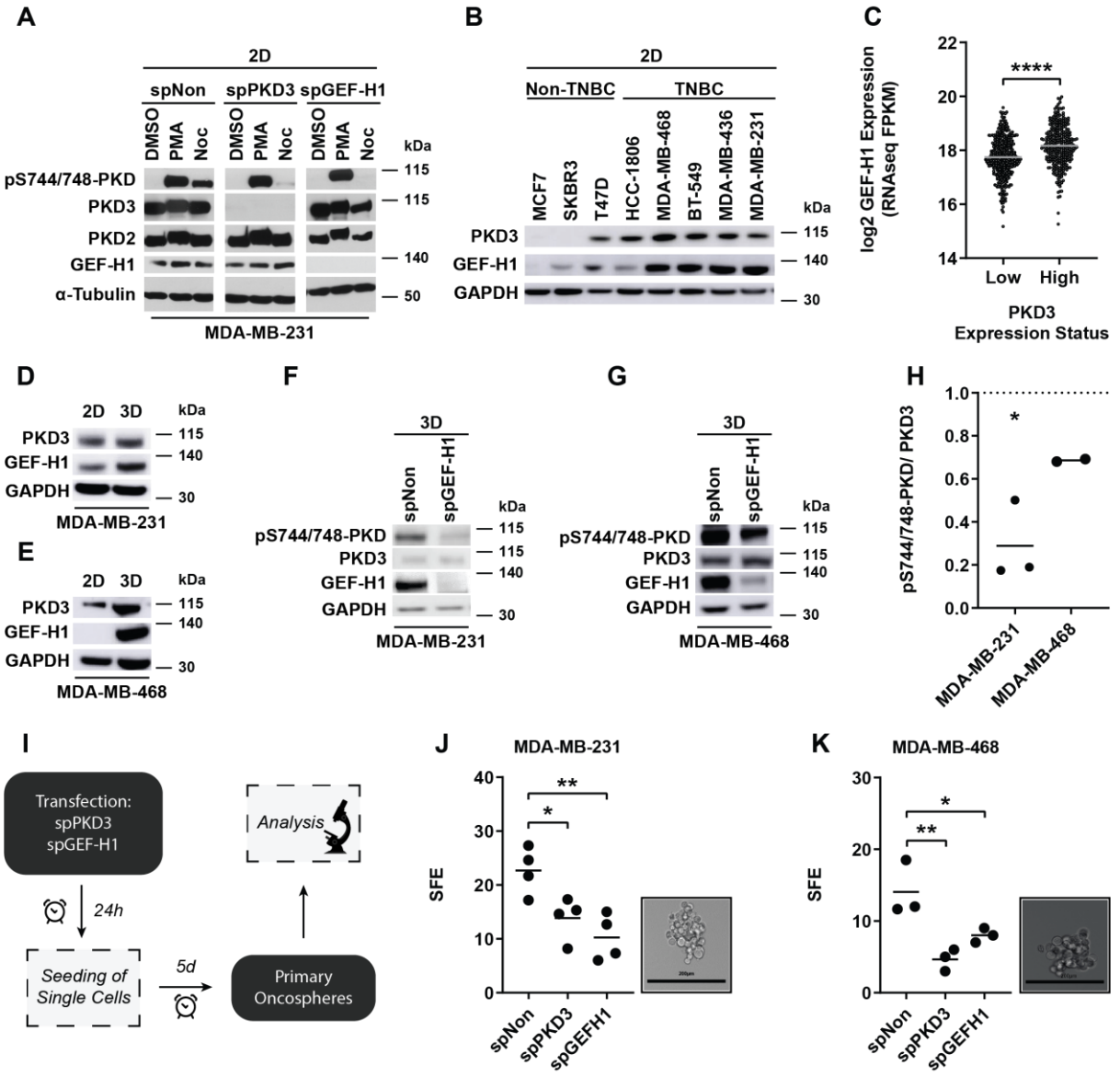

Figure 14 | GEF-H1-mediated activation of PKD3 is crucial for mammosphere formation. **(A)** Western blot of MDA-MB-231 cells treated with nocodazole (Noc) (5 µg/ml, 1 h), phorbol 12-myristate 13-acetate (PMA) (1 µM, 15 min) or the control treatment DMSO. Monolayer-cultured cells. Before treatment, MDA-MB-231 cells were transiently transfected with a smart pool of siRNAs specific for PKD3 (spPKD3), GEF-H1 (spGEF-H1) or a non-targeting control (spNon) for 72 h. Immunoblotting was conducted, and membranes were probed with specific antibodies as indicated. α-Tubulin was used as loading control. **(B)** Western blot of TNBC and non-TNBC cell lines. Monolayer-cultured cells. Immunoblotting was conducted, and membranes were probed with specific antibodies as indicated. GAPDH was used as loading control. Experiment conducted by Hannah Berreth. **(C)** GEF-H1 mRNA expression levels within PKD3 high and low expression groups from the tumor samples belonging to the TCGA-BRCA project. The samples were divided according to PKD3 expression by tertile separation, where “PKD3 low” is represented by the lower tertile (quantile < 0.33, n = 403) and “PKD3 high” by the upper tertile (quantile > 0.67, n = 312), normal tissue samples excluded. GEF-H1 expression is visualized as log2[GEF-H1 expression (FPKM) + 0.01]. Analysis conducted by Raluca Tamas. **(D-E)** Western blot of (D) MDA-MB-231 and (E) MDA-MB-468 cells (MDA-MB-468 experiment conducted by Hannah Berreth), comparing monolayer-cultured cells (2D) with oncospheres (3D). Immunoblotting was conducted, and membranes were probed with specific

antibodies as indicated. GAPDH was used as loading control. **(F-G)** Western blot of (F) MDA-MB-231 or (G) MDA-MB-468 oncospheres. 24 h prior to seeding, MDA-MB-231 or MDA-MB-468 cells were transiently transfected with a smart pool of siRNAs specific for GEF-H1 (spGEF-H1) or a non-targeting control (spNon). Immunoblotting was conducted, and membranes were probed with specific antibodies as indicated. GAPDH was used as loading control. **(H)** Quantification of phosphorylation status of PKD3 of data shown in (E-F), using densitometry analysis. Data is presented as mean line density of spGEF-H1 normalized to spNon, n=2-3. Statistical comparison by t-test. **(I)** Workflow: Oncosphere formation assay of transfected cells. **(J-K)** *Left Panels:* Primary oncosphere assays of (J) MDA-MB-231 and (K) MDA-MB-468 cells. 24 h prior to seeding, MDA-MB-231 and MDA-MB-468 cells were transiently transfected with a smart pool of siRNAs against PKD3 (spPKD3), GEF-H1 (spGEF-H1) or a non-targeting control (spNon). Data is presented as mean sphere formation efficiency (SFE), n=3-4. Statistical comparison by one-way ANOVA and Bonferroni-test. *Right panels:* representative oncosphere pictures. Bar represents 200 µm.

In line with these results, I observed that the transient knockdown of PKD3 or GEF-H1 (Figure 14I) significantly decreased SFE in the TNBC cell lines MDA-MB-231, MDA-MB-468, MDA-MB-436, BT-549 and HCC1806 but not in the luminal A breast cancer cell line MCF7 (Figure 14J-K, Figure 15). This data thus show that GEF-H1 activates PKD3 to promote stem cell maintenance.

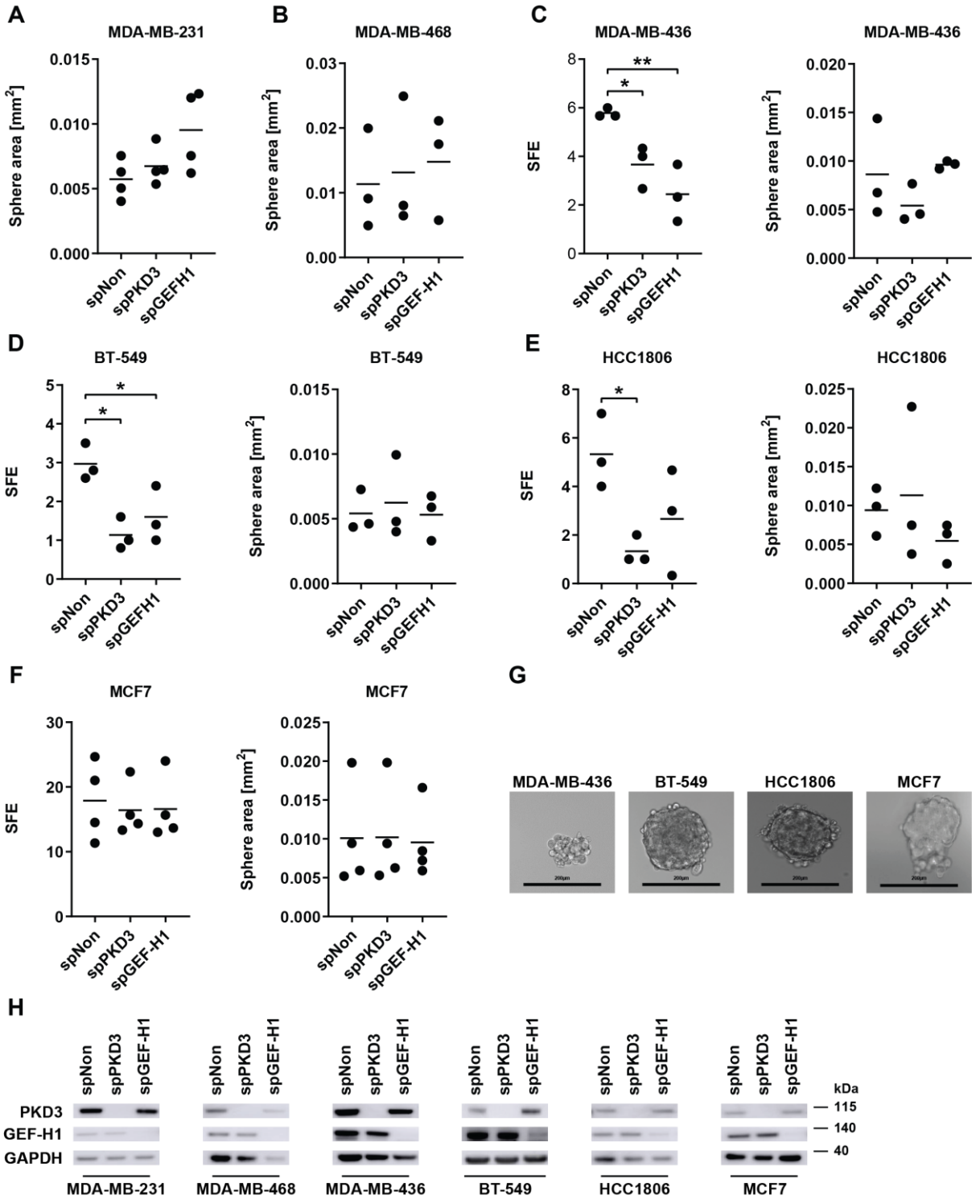

Figure 15 | Loss of PKD3 and GEF-H1 decreases mammosphere formation but not sphere area. (A-B) Sphere area of primary oncosphere assays of (A) MDA-MB-231 and (B) MDA-MB-468 cells. 24 h prior to seeding, MDA-MB-231 and MDA-MB-468 cells were transiently transfected with a smart pool of siRNAs against PKD3 (spPKD3), GEF-H1 (spGEF-H1) or a non-targeting control (spNon). Data is presented as mean square millimeters (mm^2), n=3-4. Statistical comparison by one-way ANOVA and Bonferroni-test. **(C-F)** *Left panels:* primary oncosphere assays of (C) MDA-MB-436, (D) BT-549, (E) HCC1806, (F) MCF7 cells. 24 h prior to seeding, the respective cells were transiently transfected with a smart pool of siRNAs against PKD3 (spPKD3), GEF-H1 (spGEF-H1) or a non-targeting control (spNon).

Data is presented as mean sphere formation efficiency (SFE), n=3-4. Statistical comparison by one-way ANOVA and Bonferroni-test. *Right panels:* Sphere area of primary oncosphere assays of (C) MDA-MB-436, (D) BT-549, (E) HCC1806, (F) MCF7 cells. Data is presented as mean square millimeters (mm^2), n=3-4. Statistical comparison by one-way ANOVA and Bonferroni-test. **(G)** Representative oncospheres of the indicated cell lines. Bar represents 200 µm. **(H)** Western blot-based knockdown control of the indicated cell lines. Immunoblotting was conducted, and membranes were probed with specific antibodies as indicated. GAPDH was used as loading control.

3.2.4 PKD3 overexpression increases cancer stem cell-like properties

I next explored whether ectopic expression of PKD3 is enough to drive oncosphere formation in non-tumorigenic breast epithelial MCF10A cells. Therefore, Cristiana Lungu generated a doxycycline (Dox)-inducible PKD3 (PKD3-EGFP) MCF10A cell line. Next, I analyzed stem cell activity and marker gene expression (Figure 16A). Indeed, the induction of PKD3-EGFP expression in MCF10A cells significantly increased SFE (Figure 16B), without affecting the sphere area (Figure 16C). Additionally, PKD3-EGFP increased the mRNA expression of stemness markers, such as SOX2 and OCT3/4[209,215] (Figure 16D). To verify that GEF-H1 is required for PKD3-mediated stem cell maintenance also in the MCF10A model, I depleted GEF-H1 prior to inducing PKD3-EGFP expression and subjecting the cells to a sphere formation assay. Strikingly, the depletion of GEF-H1 completely blocked the increase in sphere formation mediated by PKD3 (Figure 16E-F), indicating that PKD3-mediated oncosphere formation is strictly dependent on GEF-H1.

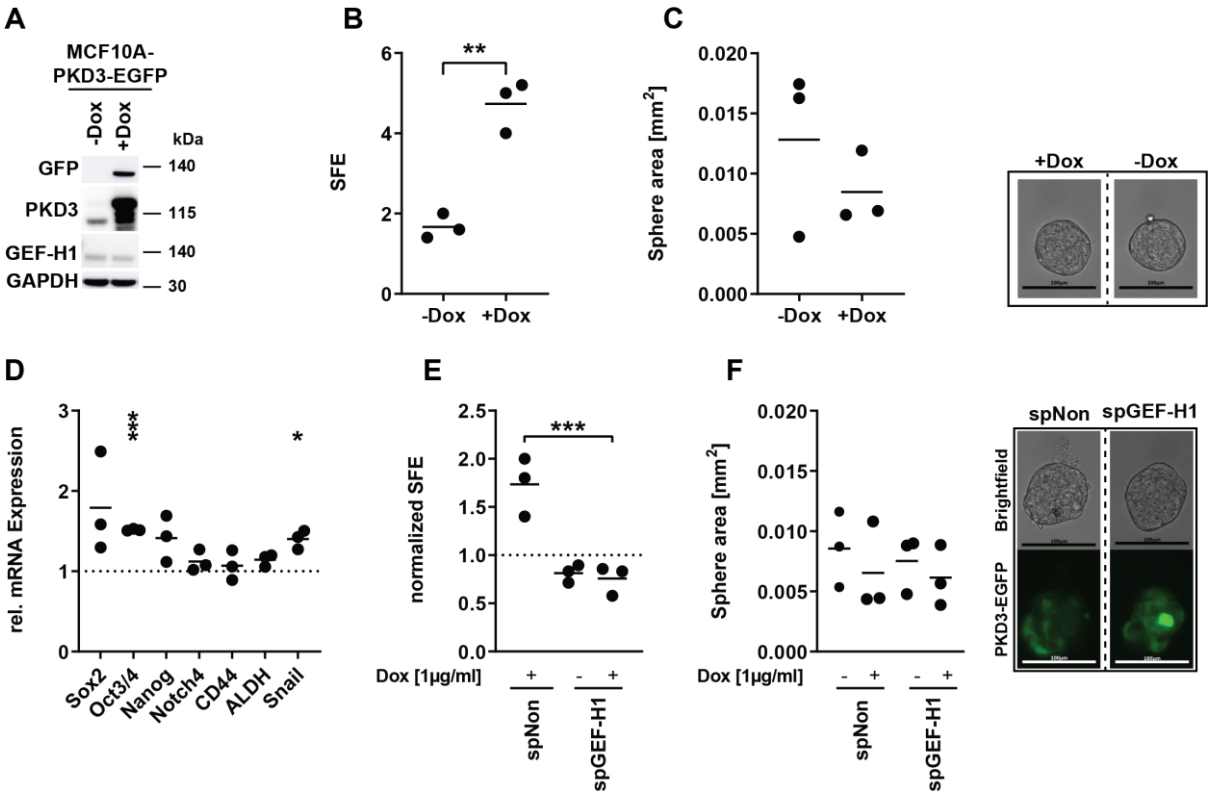

Figure 16 | PKD3 overexpression-induced sphere formation is dependent on GEF-H1. **(A)** Western blot of MCF10A-EcoR-PKD3WT cells. Cells were treated with doxycycline (+Dox) for 48 h. Water served as control (-Dox). Immunoblotting was conducted, and membranes were probed with specific antibodies as indicated. GAPDH was used as loading control. **(B)** Primary oncosphere formation assays of MCF10A-EcoR-PKD3WT-EGFP cells. Prior to seeding cells were treated with Dox for 24 h. Directly after seeding into the oncosphere assay, the medium was supplemented with Dox and the spheres could grow for 5 days. Data is presented as mean sphere formation efficiency (SFE), n=3. Statistical comparison by t-test. **(C)** Left panel: sphere area of primary oncospheres. Data is presented as mean square millimeters (mm2), n=3. Statistical comparison by t-test. Right panel: representative oncosphere pictures. Bar represents 100 µm. **(D)** qPCR analysis of stemness markers. Monolayer-cultured cells. Data is presented as mean mRNA expression of Dox treated cells normalized to untreated control, n=3. Statistical comparison by t-test. **(E)** Primary oncosphere assay. 48 h prior to seeding MCF10A-EcoR-PKD3WT-EGFP monolayer cells were transiently transfected with a smart pool of siRNAs against GEF-H1 (spGEF-H1) or a non-targeting control (spNon). 24h prior to seeding into the oncosphere assay, monolayer cells were treated with Dox. Directly after seeding into the oncosphere assay, cells were treated with Dox. Data is presented as mean sphere formation efficiency (SFE) normalized to untreated spNon, n=3. Statistical comparison by one-way ANOVA and Bonferroni-test. **(F)** Left panel: sphere area of primary spheres. 48 h prior to seeding MCF10A-EcoR-PKD3WT-EGFP monolayer cells were transiently transfected with a smart pool of siRNAs against GEF-H1 (spGEF-H1) or a non-targeting control (spNon). 24h prior to seeding into the oncosphere assay, monolayer cells were treated with Dox. Directly after seeding into the oncosphere assay, cells were treated with Dox. Data is presented as mean square millimeters (mm2), n=3. Statistical comparison by one-way ANOVA and Bonferroni-test. Right panel: representative pictures of transiently transfected and Dox-treated (continuously for 6 days) oncospheres of MCF10A-PKD3-EGFP cells after 5 days in the oncosphere formation assay. Bar represents 100 µm.

3.2.5 Combined paclitaxel treatment and PKD3 inhibition synergistically decreases TNBC stem cell-mediated oncosphere and colony formation

Loss-of-function by stable or transient knockdown of PKD3 in TNBC cell lines revealed a crucial role for the kinase in cancer stem cell maintenance. I thus explored whether pharmacological inhibition of kinase activity using the selective pan-PKD inhibitor CRT0066101[133] would mimic the loss of PKD3 gene expression. First, I tested the efficacy of the inhibitor in oncosphere formation assays. Equally to PKD3 depletion, CRT0066101 treatment of MDA-MB-231, MDA-MB-468, MDA-MB-436 and BT-549 TNBC cells significantly reduced the number of primary and secondary oncospheres without affecting the respective sphere area (Figure 17A-B, Supplemental Figure S2A-D). The chemotherapeutic paclitaxel is widely used in the clinical setting[216]. I therefore asked whether PKD inhibition sensitized TNBC cells to paclitaxel treatment. Firstly, I tested the response behavior of MDA-MB-231 and MDA-MB-468 cells to the combination of paclitaxel and CRT0066101 in a 3D viability assay. Especially low, clinically relevant paclitaxel concentrations[217] as well as low micromolar CRT0066101 concentrations showed synergistic and additive effects (Supplemental Figure S2E-F). Next, I addressed potential synergistic effects of the combinatorial treatment on TNBC stem cells and analyzed ALDH activity as well as sphere forming efficiency. I first performed a primary oncosphere formation assay to enrich for TNBC stem cells (Figure 17C). These oncospheres were singularized, reseeded into a secondary oncosphere formation assay and immediately treated with either CRT0066101, paclitaxel or the combination of both. Both single and combination treatments reduced ALDH activity in MDA-MB-231 and MDA-MB-468 cells (Figure 17D-E). Regarding SFE, the combination was highly synergistic in MDA-MB-231, MDA-MB-468, MDA-MB-436, BT-549 and HCC1806 TNBC cell lines (Figure 17F-G, Supplemental Figure S3) Because clonogenic activity is a sensitive marker of undifferentiated cancer stem cells[218] I tested the combination treatment of CRT0066101 and paclitaxel in a colony formation assay. In line with the previous results, the combinatorial treatment synergistically decreased the clonogenic activity in MDA-MB-231, MDA-MB-468, MDA-MB-436 and BT-549 TNBC cells (Figure 17H-I, Supplemental Figure S4). Thus, combining paclitaxel with CRT0066101 was superior to the single treatments and synergistically reduced the prevalence of cancer stem cells in these TNBC cell lines.

3.2.6 The combination of CRT0066101 and paclitaxel is superior in decreasing tumor recurrence *in vivo*.

Finally, I used an orthotopic xenograft mouse model to investigate the growth and recurrence of MDA-MB-231 tumors after treatment with paclitaxel, CRT0066101 or the combination of both. The cells were transplanted into SCID mice and allowed to form tumors with a size of ~100 mm^3. Compared to the control (vehicle only) CRT0066101 had only little effect on tumor growth. Accordingly, tumor-bearing mice belonging to the control and CRT0066101 groups had to be removed from the study shortly after the end of the treatment period. By contrast, paclitaxel caused an initial inhibition of tumor growth, which was further enhanced by CRT0066101. Upon therapy termination, paclitaxel-treated tumors displayed a strong re-growth. More importantly, in the post-treatment period, animals that had received the combination treatment showed a significant reduction in tumor re-growth compared to paclitaxel treated animals (Figure 17J-K), providing support for the superior targeting of drug-resistant cancer cell subpopulations by paclitaxel plus CRT0066101.

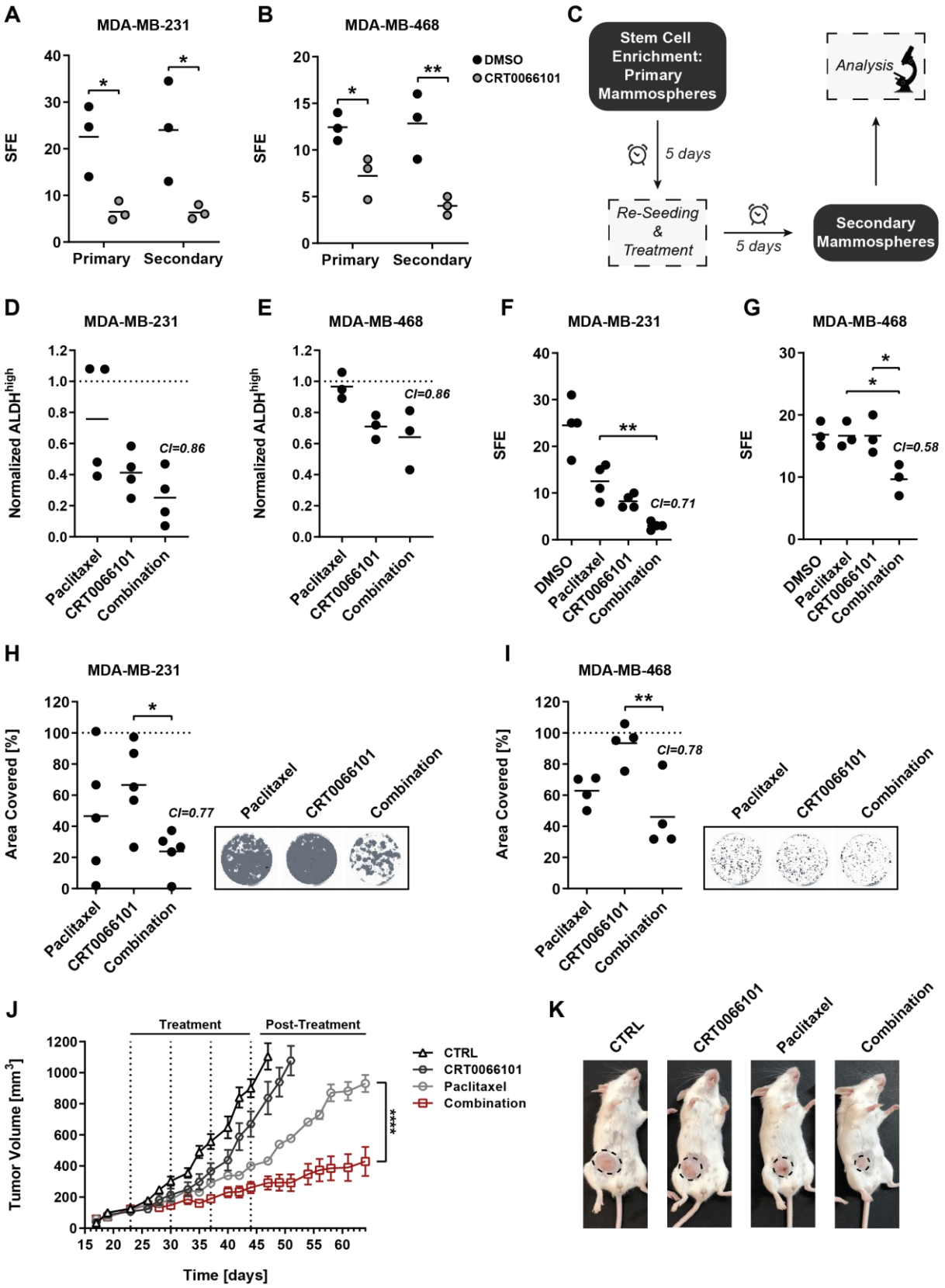

Figure 17 | The combination of paclitaxel and CRT0066101 synergistically reduces sphere formation in vitro and tumor growth as well as tumor recurrence in vivo. (A-B) Counting of primary and secondary oncospheres of (A) MDA-MB-231 or (B) MDA-MB-468 cells. Cells were treated with 1 µM CRT0066101 directly after seeding into the respective

oncosphere assay. Data is presented as mean sphere formation efficiency (SFE), n=3. Statistical comparison by one-way ANOVA and Bonferroni-test. **(C)** Workflow of paclitaxel and CRT0066101 oncosphere treatment. **(D-E)** Flow cytometry-based stemness analysis of (D) MDA-MB-231 or (E) MDA-MB-468 cells via ALDEFLUORTM. Directly after seeding into the secondary oncosphere assay, cells were treated with paclitaxel (5 nM) or CRT0066101 (MDA-MB-231: 1 µM; MDA-MB-468: 0.5 µM), or in combination. DMSO served as control. Data is presented as mean ALDHhigh population normalized to DMSO control, n=3-4. Statistical comparison by one-way ANOVA and Bonferroni-test. Combination index (CI) values were calculated via Webb's fractional product method using the respective mean of % ALDHhigh populations. CI<1 indicates synergism. **(F-G)** Counting of secondary oncospheres of (F) MDA-MB-231 or (G) MDA-MB-468 cells. Directly after seeding into the secondary oncosphere assay, cells were treated with paclitaxel (5 nM) or CRT0066101 (MDA-MB-231: 1 µM; MDA-MB-468: 0.5 µM), or in combination. DMSO served as control. Data is presented as mean sphere formation efficiency (SFE), n=3-4. Statistical comparison by one-way ANOVA and Bonferroni-test. Combination index (CI) values were calculated using Webb's fractional product method. CI<1 indicates synergism. **(H-I)** Left panels: colony formation of (H) MDA-MB-231 or (I) MDA-MB-468 cells. 24 h after seeding into 6-well culture dishes, MDA-MB-231 or MDA-MB-468 cells were treated for 48 h with paclitaxel (1 nM) or CRT0066101 (MDA-MB-231: 1 µM; MDA-MB-468: 0.1 µM), or the combination of both. DMSO served as control. Afterwards, cells were further cultured for 2 weeks and analyzed using the Odyssey imaging system. Data is presented as mean area covered. DMSO control was set to 100 %, n=4-5. Statistical comparison by one-way ANOVA and Bonferroni-test. Combination index (CI) values were calculated using Webb's fractional product method. CI<1 indicates synergism. Right panels: Representative pictures of the respective colony formation assays. **(J)** 8-week-old female SCID mice were injected with 2x106 MDA-MB-231 cells into the right fat pad of the 4th nipple. After the tumors had reached 100 mm3 mice were treated with either CRT0066101, paclitaxel or the combination of both. The combination of the respective carriers served as control. Data is presented as tumor volume (mm3), mean ± SEM, n=7. Statistical comparison by two-way ANOVA and Bonferroni-test. **(K)** Representative pictures of animals from the respective treatment groups. Tumors are indicated by dotted circles.

4 Discussion

The signaling pathways and cellular functions regulated by PKD family members have intensively been studied in the past years. PKDs are important for a variety of cellular processes, such as vesicular transport, migration, invasion and proliferation[11-14]. Important physiological roles identified so far are, for example, initiating host innate immune responses[219], regulation of memory formation[220] and muscle differentiation[177,221], and insulin secretion[127]. In addition, a switch in PKD isoform expression contributes to the development and progression of breast cancer. However, the physiological role and therapeutic significance of PKD enzymes *in vivo* is incompletely understood. Using established cell lines, primary cells and mouse models for *in vivo* studies I investigated the contribution of PKD to two different biological processes, namely the maintenance of pancreatic β-cell function and the breast cancer stem cell population.

4.1 Regulation of glucose homeostasis

The risk of suffering from T2D is highly associated with aging and HFD[85-87]. In this study, a critical role for PKD in the maintenance of β-cell function during aging and HFD, which depends on p16 expression, was defined for the first time. The functional knockout of all three PKD isoforms in PKDkd-EGFP mice led to an upregulation of p16, which induced a senescence program and resulted in increased glucose tolerance. More importantly, PKDkd-EGFP expression protected mice from HFD-induced insulin and glucose intolerance. Using the PKD inhibitor CRT0066101 these findings could be verified. In wildtype CRT0066101-fed mice, pancreatic beta-cells showed hallmarks of senescence and glucose tolerance was strongly improved. Strikingly, CRT0066101 demonstrated strong efficacy in rescuing HFD-fed mice from insulin and glucose intolerance. Thus, the inhibition of all PKD isoforms is highly beneficial for β-cell function during aging and HFD, and therefore represents a new strategy for the treatment of T2D.

The function of PKD1 in pancreatic β-cell has intensively been studied over the recent years. However, direct examination of PKD1 function in β-cells has almost exclusively been conducted in the rat insulinoma cell line INS-1[62,128,130]. Other studies have looked indirectly at PKD1 signaling *in vivo*, and demonstrated that GPR-40, p38MAPK and the M3-Muscarinic receptor regulate this kinase in β-cells[127,129,130]. So far only one

study assessed the direct effect of a β-cell specific PKD1 knockout in a mouse model and observed that PKD1 is dispensable for β-cells under basal conditions but necessary for the compensatory increase in GSIS in response to HFD[131]. Interestingly, the PKD isoforms have demonstrated to not only have redundant and specific functions, but in some instances even have opposing effects as observed in breast cancer[222]. Thus, I was interested in analyzing β-cell function in a β-cell specific triple-knockout of PKD. Therefore, a PKDkd-EGFP expressing mouse model was employed, which to my knowledge is the first model to functionally knockout all PKD isoforms in β-cells at the same time (Figure 5).

In HeLa cells, PKDkd is localized to the TGN and inhibits the fission of transport carriers destined for the plasma membrane[182,203]. In pancreatic β-cells, PKD1 controls insulin secretory granule biogenesis at the Golgi[62,127], however, it is likely that constitutive transport is regulated by the kinase as well. Expression of PKDkd-EGFP thus might impact the secretory phenotype of β-cells. Notably, SASP is characterized by increased secretion of proinflammatory cytokines[100]. These inflammatory proteins might disrupt β-cell function by impairing glucose homeostasis and reducing insulin secretion[223]. Inhibition of PKD function by CRT0066101 or expression of PKDkd-EGFP could counteract the secretion of these factors and thereby limit inflammation in the tissue environment.

In contrast to Sumara et. al, who claimed PKD1 to be the predominant isoform in β-cells[127], I observed that PKD2 and PKD3 were expressed at much higher levels. In adult animals, the expression of both PKD2 and PKD3 decreased, which correlated with observations that demonstrated a downregulation of PKD3 in islets during aging[185], suggesting a functional role of PKD2 and PKD3 during the aging process (Figure 6A).

Islets of PKDkd-EGFP mice displayed upregulated p16 expression levels in juvenile mice, which correlated with further markers of senescence, such as increased cell size, islet area and SA β-galactosidase activity as well as reduced proliferation (Figure 6B-G). Helman et. al demonstrated in a striking study that the forced expression of p16 in β-cells from juvenile mice induced features of senescence, such as increased β-cell size. Notably, p16 expression improved glucose tolerance in juvenile mice and GSIS increased during aging. Moreover, they observed that p16-dependent senescence

increased in aged humans[97]. Interestingly, Wang et al. showed in rats that islet sizes were the same in young adult (4-5 months) and senescent (21-22 months) animals. Moreover, senescent islets secreted less insulin, compared to adult islets[224]. Focusing on p16 expression may only imitate one aspect of cellular senescence to partially reflect β-cell senescence and aging related effects. However, I could show that employing both the transgenic approach as well as the inhibitor CRT0066101 promoted a senescent phenotype and thereby increased glucose tolerance and decreased insulin resistance (Figure 7, Figure 8).

Inducing PKDkd-EGFP expression improved glucose tolerance and GSIS in juvenile mice (Figure 7A, F, H). Interestingly, I did not observe the same effects in adult mice (Figure 7C, G, J). However, as p16 expression physiologically increases with aging[109], the expression of PKDkd-EGFP had putatively no “on-top” effect.

To exclude off-target effects of transgene (PKDkd-EGFP) expression I treated wildtype mice with the pan PKD inhibitor CRT0066101[133] and analyzed β-cell function. Strikingly, CRT0066101 triggered the same effects and caused senescence, coupled to improved glucose tolerance and *in vivo* GSIS (Figure 8). Of note, in this setting the inhibition of PKD was global and not restricted to pancreatic β-cells. PKD is expressed in almost every tissue. Thus, it is likely that CRT0066101 blocked PKD activity in additional cell types that might affect β-cell function. For example, the AMP-activated protein kinase (AMPK) induces cellular energy generation in muscle-, β-cells (MIN6 β-cells) and adipocytes but is inhibited in settings of insulin resistance. Interestingly, PKD was found to impair insulin signaling via AMPK inhibition[225-227]. It is thus possible that CRT0066101 inhibited PKD also in muscle cells thereby increasing their metabolism, which contributed to the improved glucose tolerance.

The expression of PKDkd-EGFP and the inhibition of PKD via CRT0066101 decreased SOD2 expression and increased ROS levels (Figure 7L, M and Figure 8H,I). Previous studies showed that ROS activates PKD, leading to the induction of SOD2 expression via the NF-κB transcription factor[44,64]. Interestingly, ROS promotes senescence via p16 upregulation in human epidermal keratinocytes[186] and mouse fibroblasts[187]. These findings thus mechanistically connect PKD inhibition/functional knockout to the upregulation of ROS and p16, which induces senescence and improves glucose tolerance and GSIS[97].

The results strongly suggest that PKDkd-EGFP expression and CRT0066101 altered the physiological glucose tolerance through inducing a senescent phenotype in β-cells. I next analyzed if PKD inhibition could improve insulin and glucose tolerance in a high-fat-diet mouse model. Therefore, I fed PKD-EGFP and control mice with HFD and LFD and compared β-cell function. I observed that PKDkd-EGFP mice weighted less and had improved glucose as well as insulin tolerance (Figure 9). A previous study showed that the β-cell specific knockout of PKD1 exacerbates high-fat-diet-induced glucose intolerance[131]. However, this study only analyzed PKD1 and did not take PKD2 and PKD3 into consideration.

To assess the effect of PKD inhibition on an already developed pathology, I put wildtype mice on a 16-week HFD. After insulin and glucose tolerance had formed, I treated the animals with CRT0066101, to mimic a potential therapeutic approach. Strikingly, this treatment could rescue the CRT0066101-treated animals from glucose and insulin intolerance (Figure 10). Due to the systemic effect of CRT0066101, these findings are most likely attributable to multiple tissues. For instance, the knockout of PKD1 in adipocytes improves insulin and glucose tolerance *in vivo*, protects from obesity and T2D, and increases the generation of beige adipocytes[227]. Additionally, CRT006101 induced β-cell senescence in these mice (Figure 8), which potentially contributed to the observed phenotype. My findings thus demonstrate that drug-induced senescence could have a beneficial effect for pre-diabetic or diabetic patients. Currently, several drugs that induce senescence are under development, but so far they have mainly been used for the treatment of cancer, e.g. CDK4 and CDK6 inhibitors[228].

These findings highlight, that the combinatory inhibition/functional knockout of all PKD isoforms improves glucose tolerance, GSIS and protects from insulin intolerance in an HFD mouse model. These features are most likely dependent on p16-mediated senescence. The administration of CRT0066101 to animals with established glucose and insulin intolerance completely rescued β-cell function. I therefore established PKD as a critical regulator of insulin secretion and glucose homeostasis. My results further suggest that senescence-inducing drugs should be taken into consideration to regulate glucose homeostasis.

4.2 PKD3 signaling in TNBC stem cells

PKD3 has been associated with TNBC progression[14,133] but so far, a specific role for PKD3 in the TNBC stem cell population has not been described. In this study, I have defined a critical role for PKD3 in the maintenance and propagation of TNBC stem cells *in vitro* and *in vivo*, which depends on GEF-H1-mediated PKD3 activation. The PKD inhibitor CRT0066101 demonstrated strong efficacy in eliminating TNBC stem cells *in* vitro. More importantly, CRT0066101 synergistically increased the response to paclitaxel *in vitro* and *in vivo*. These findings are of high clinical relevance as taxanes alone have shown to increase the TNBC stem cell population[142,143,229]. Thus, inhibiting PKD3 in combination with paclitaxel has a dual effect by targeting differentiated cancer cells and at the same time eradicating the cell population responsible for chemoresistance and tumor recurrence.

The role of PKD3 in cancer stemness was specific for TNBC cell lines as in luminal A MCF7 cells with only marginal PKD3 expression depletion of the kinase did not affect oncosphere formation (Figure 15F). Our findings further support the postulated isoform switch from PKD1 to PKD3 in breast tumor progression. While PKD1 is a negative regulator of cell motility and invasion and contributes to the maintenance of the epithelial phenotype of breast cells, PKD3 supports all aspects of oncogenic signaling thereby contributing to proliferation, migration, invasion[133] and, as shown in this study, cancer stem cell maintenance.

In monolayer cultured MDA-MB-231 cells PKD3 knockdown was accompanied by decreased proliferation[133]. However, while oncosphere formation was less efficient in the absence of PKD3, the size of spheres was not significantly affected. Likewise, only the number but not the size of tumors growing from PKD3 depleted implanted cells was reduced. Because MDA-MB-231_shPKD3 cells still express low levels of PKD3 (Figure 12A-B) I suggest that a selection process takes place, in which the small fraction of PKD3 positive cells survive to initiate oncosphere and tumor growth *in vitro* and *in vivo*, respectively.

Taxanes have shown to increase the cancer stem cell population in patients with invasive breast cancer[142,143,145]. In contrast to our studies, Bhola et al. observed an increase of BT-549 oncosphere formation after paclitaxel treatment. However, they allowed the cells in the oncosphere assay to recover for 4 days after treatment[230]

whereas I immediately analyzed the SFE and ALDH activity after 5 days of paclitaxel treatment. Moreover, paclitaxel was reported to increase the ALDH-positive population in MDA-MB-231 cells via increased expression levels of SOX2, ABCG2 and TWIST1, unraveling an interconnected pluripotency-chemoresistance-EMT axis[144]. Strikingly, PKD3 depletion in MDA-MB-231 cells decreased SOX2, ABCG2 and the EMT marker SNAIL (Figure 11E, Figure 12K, O). Moreover, PKD3 positively regulates EMT, as treating MDA-MB-231 cells with CTR0066101 resulted in a reduction of SNAIL[222]. EMT is linked to breast cancer stem cell regulation, thereby controlling self-renewal and the tumor initiation capacity[231]. In line with this, exposing TNBC cells to the EMT inducer transforming growth factor beta (TGF-β) increased oncosphere formation and the $CD44^+/CD24^-$ stem cell signature[232]. Expression of SNAIL alone, which is upregulated upon TGF-ß-mediated EMT-induction, induced an increase in oncosphere formation[232]. PKD3 inhibition thus likely counteracts the paclitaxel-induced upregulation of EMT genes such as SNAIL, thereby inhibiting oncosphere formation *in vitro*. Consequently, breaking up the pluripotency-chemoresistance-EMT axis might contribute to the strong response to combined CRT0066101 and paclitaxel treatment *in vivo*.

How does PKD3 contribute to the maintenance of TNBC stem cells? I identified GEF-H1 to be upstream of PKD3 activity in oncosphere formation and it was recently shown that PKD signaling through a GEF-H1-RhoA-PLCε pathway regulates the fission of exocytic vesicles at the Golgi complex[36]. The changes in surface protein expression upon PKD3 depletion could thus be a result of deregulated exocytosis. In addition, various secreted factors derived from the bulk tumor and the cancer stem cells acting in paracrine and autocrine manners, respectively, are required for the survival of cancer stem cells. For example, in basal-like breast cancer the mesenchymal-like tumor cells produce high levels of WNT2, CXCL12, and IL6, which drive the self-renewal of the cancer stem cells[128]. Furthermore, activation via TGF-β together with canonical and non-canonical WNT signaling through autocrine signaling controls migratory and self-renewal ability of cancer stem cells thereby contributing to metastases and tumorigenicity of breast cancer[233]. Moreover, signaling by these autocrine and paracrine loops promotes the expression of EMT-associated transcription factors e.g. Twist, SLUG and ZEB1/2[233]. By blocking secretion and eventually extracellular autocrine and paracrine signaling of the stem and the bulk

tumor cells, inhibition of PKD3 signaling may interfere with the expression of EMT-associated transcription factors ultimately leading to the destabilization of the cancer stem cell state. Our data further prove that YAP/TAZ signaling was downregulated upon PKD3 depletion (Figure 12O), congruent with the reported regulation of YAP/TAZ signaling by PKD in pancreatic cancer cells[234]. EMT induces and requires YAP/TAZ for triggering breast cancer stemness and metastasis[213] and vice versa, YAP/TAZ are active inducers of EMT[235,236]. This suggests that several positive and negative feedback loops are in place to sustain the maintenance of cancer stem cells.

Breast cancer stem cells display increased expression of free radical scavenging systems to maintain low levels of reactive oxygen species (ROS) that result in less DNA damage and radioprotection[237], providing a possible explanation for tumor recurrence after radiation therapy. Consequently, low ROS promote the breast cancer stem cell phenotype. Notably, as PKD is involved in ROS-detoxification[64], amplified ROS levels could contribute to the alterations in the stem cell status upon loss of PKD3 activity as well. PKD3 phosphorylates GIT1, a regulator of cell shape and motility[24]. Interestingly, GIT1 appears to play a major role in breast cancer metastasis formation and is associated with advanced stages of breast cancer[238]. However, how PKD3 exactly maintains the TNBC stem cell population remains to be identified in future studies.

TNBC surviving patients have a high probability of tumor recurrence within the first five years after the end of treatment[239], which is largely driven by cancer stem cell activity[145]. The development of new therapeutic strategies targeting TNBC stem cells has thus been intensified over the last years. *In* vivo targeting of active CD44 decreased MDA-MB-231-mediated tumor growth[240]. Other studies have focused on targeting the WNT/β-CATENIN pathway[241], degradation of Krüppel-like factor 5 by metformin[242] or interferon-beta signaling[243]. Just recently, the combination of the BCR-ABL inhibitor dasatinib and paclitaxel has shown promising results in reducing TNBC tumor formation and TNBC stem cell prevalence. Although the single treatment with paclitaxel increased ALDH positivity, the combination with dasatinib significantly reduced the TNBC stem cell population[244]. Moreover, the inhibition of the TGF-β pathway enhanced the responsiveness to paclitaxel treatment in TNBC and prevented tumor recurrence[230].

Thus, these studies and our results demonstrate that combining paclitaxel with therapeutic antibodies or small molecule inhibitors such as CRT0066101 has tremendous clinical potential through the superior targeting of both TNBC bulk and stem cell populations.

5 Conclusion

In my doctoral thesis I investigated the role of PKD in β-cell function and TNBC stem cell maintenance. Using state of the art *in vivo* and *ex vivo* approaches, I discovered a novel function for PKD in the regulation of β-cell senescence and GSIS. My data proved that not PKD1, but PKD2 and PKD3 are the major isoforms in mouse islets. I showed that the functional knockout of all three PKD isoforms increased β-cell senescence in juvenile mice, which resulted in increased glucose tolerance. I further provided evidence that the functional knockout of PKD protected from HFD-induced glucose and insulin intolerance. Significantly, the administration of the selective PKD inhibitor CRT0066101 did not only upregulate senescence but also rescued mice from HFD-induced insulin and glucose intolerance. My results thus demonstrate the importance of PKD for the maintenance of β-cell function, not only during healthy aging but also during HFD. Although PKDkd-EGFP expression allows for a simultaneous functional knockdown of all PKD isoforms, off-target effects cannot be ruled out. For example, substrate competition with other PKD-related kinases such as Ca2+/calmodulin-dependent protein kinase could blur the interpretation of observed phenotypes. Therefore, further studies should analyze the role of PKD using an inducible tissue specific CRISPR/cas9[245] knockout to rule out aforementioned off-target effects. Moreover, the SASP[100] should be further examined. The modified secretion of cytokines during senescence could at least partially be responsible for the observed effects. Additionally, human material should be employed to study the efficacy of CRT0066101 on human β-cells.

Moreover, I could show via targeted cell surface screening, that PKD3 plays a major role in the maintenance of cancer stem cells in TNBC. I found that the loss of PKD3 in TNBC cell lines reduced the stem cell frequency *in vitro* and decreased the tumor initiation potential of implanted MDA-MB-231 cells *in vivo*. I further provided evidence that the function of PKD3 in the maintenance of cancer stem cells requires upstream activation by the Rho guanine nucleotide exchange factor 2 GEF-H1. Significantly, the combinatorial treatment with the pharmacological PKD inhibitor CRT0066101 and the chemotherapeutic agent paclitaxel was superior in reducing oncosphere formation *in vitro* and tumor recurrence *in vivo* when compared to monotherapy. My findings thus reveal the importance of PKD3-mediated cancer stem cell regulation and provide a

rationale for targeting the GEF-H1/PKD3 signaling pathway to eliminate the tumor initiating cell population in TNBC.

In sum, I developed an innovative treatment that rescued HFD-mediated glucose intolerance and insulin resistance, and established a therapeutic strategy that specifically targeted TNBC stem cells and thereby markedly reduced recurrence *in vivo.*

6 Supplements

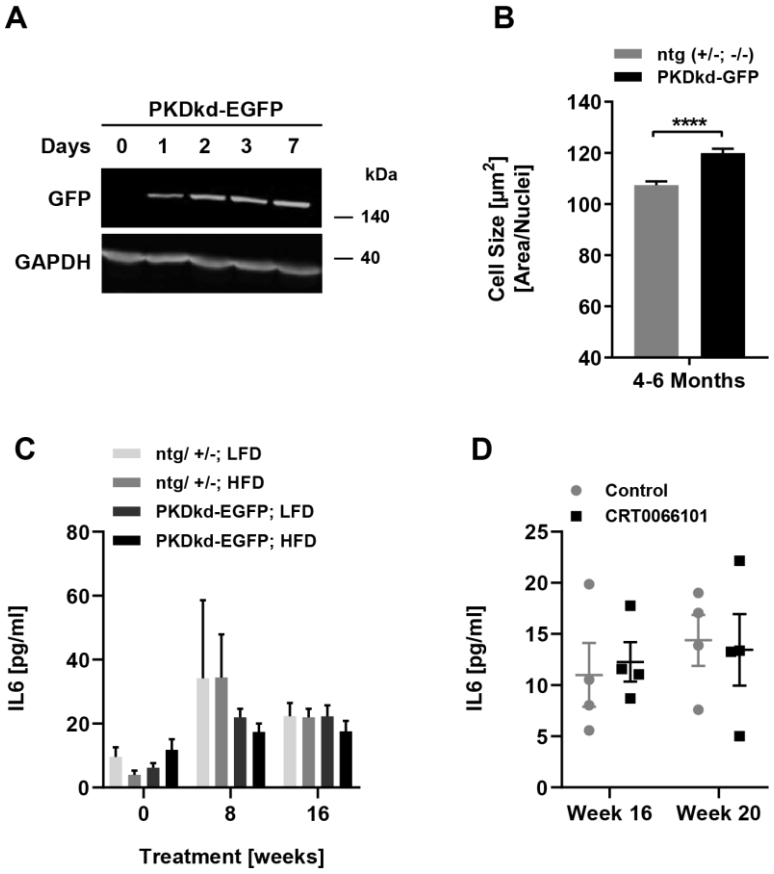

Supplemental Figure S1 | PKD inhibition increases β-cell size but does not promote IL6 secretion. (A) Western blot of PKDkd-EGFP expression in the pancreas. Doxycycline was given to PKDkd-EGFP mice in the drinking water for indicated time points. Pancreata were isolated and western blot was conducted, and membranes were probed with specific antibodies as indicated. GAPDH was used as loading control. Experiment and analysis by Kornelia Ellwanger **(B)** Quantification of the beta cell area. Pancreas was sectioned via cryosectioning. Beta cell area was calculated by dividing the cross-section area of an islet by the nuclei number. Data is presented as mean cell size (μm^2) ± SEM, n=64. Statistical comparison by t-test. **(C)** Plasma IL6 of HFD and LFD treated transgenic mice via ELISA. Data is presented as mean IL6 (pg/ml) ± SEM, n=4-7. Statistical comparison by two-way ANOVA. **(D)** Plasma IL6 before (16 weeks) and after (20 weeks) CRT0066101 treated mice via ELISA. Data is presented as mean IL6 (pg/ml) ± SEM, n=4. Statistical comparison by two-way ANOVA.

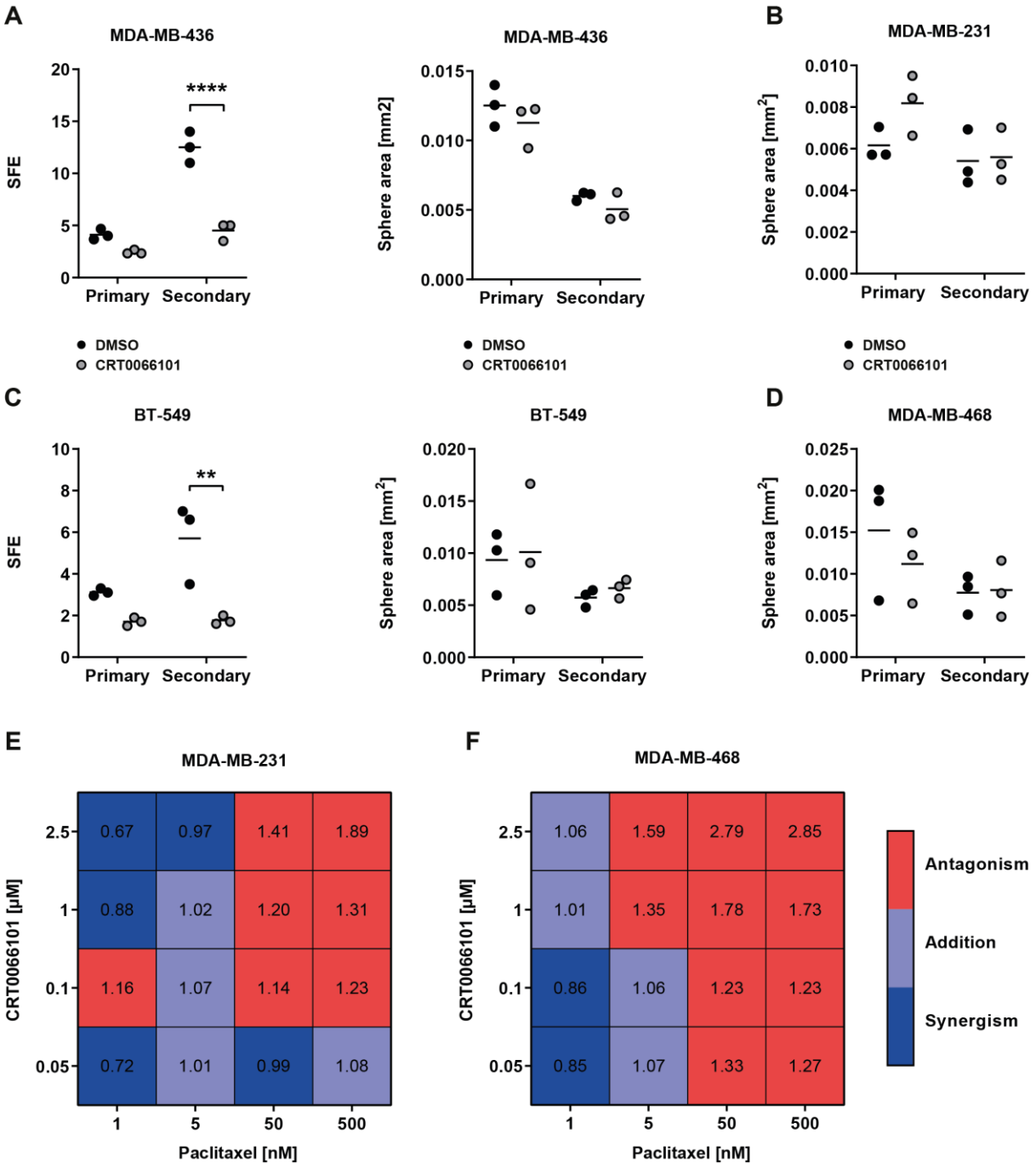

Supplemental Figure S2 | CRT0066101 decreases sphere forming efficiency in TNBC cell lines. (A-D) Oncosphere count or sphere area of primary and secondary oncosphere assays of (A) MDA-MB-436, (B) MDA-MB-231, (C) BT-549 and (D) MDA-MB-468 cells. Cells were treated with 1 µM CRT0066101 directly after seeding into the respective oncosphere assay. Data is presented as mean sphere area (mm^2) or as mean sphere formation efficiency (SFE), n=3. Statistical comparison by one-way ANOVA and Bonferroni-test. **(E-F)** Synergy scores of treated (E) MDA-MB-231 or (F) MDA-MB-468 cells. Cells were seeded in poly-HEMA 96-well plates and treated for 72 h with the indicated combinations of paclitaxel and CRT0066101. Analysis was conducted using the CellTiter-Glo reagent. Luminescence scores were normalized to the DMSO control. Data is presented as mean combination index (CI), n=2-3. Combination index (CI) values were calculated using Webb's fractional product method. CI<1 indicates synergism. 1≤CI≤1.09 indicates addition. CI>1.09 indicates antagonism.

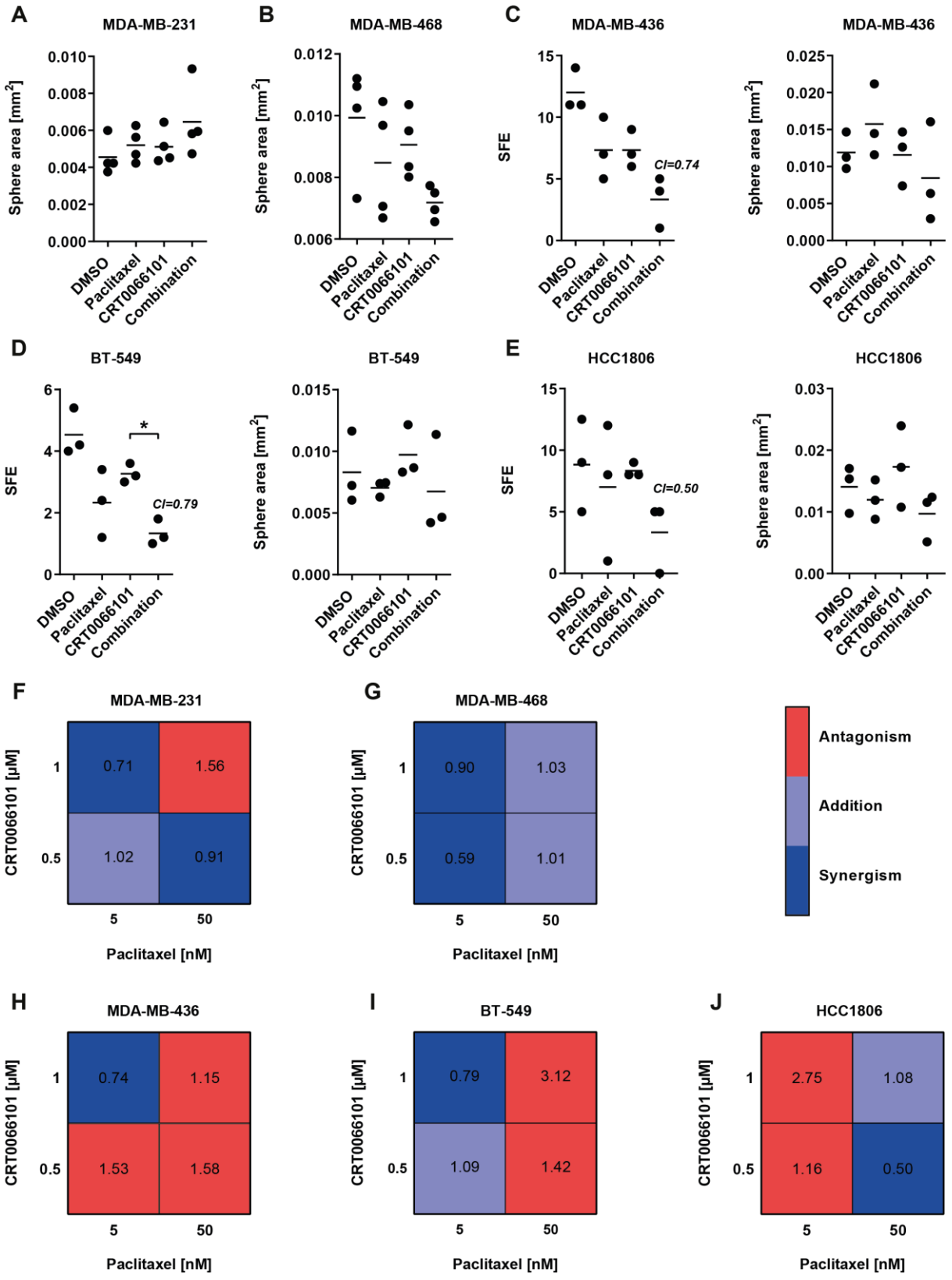

Supplemental Figure S3 | Combinatory inhibition using CRT0066101 and paclitaxel results in a synergistic decrease of sphere formation. (A-B) Sphere area of secondary oncospheres of (A) MDA-MB-231 or (B) MDA-MB-468 cells. Directly after seeding into the secondary oncosphere assay, cells were treated with paclitaxel (5 nM) or CRT0066101 (MDA-

MB-231: 1 µM; MDA-MB-468: 0.5 µM), or in combination. DMSO served as control. Data is presented as mean sphere area (mm^2), n=4. Statistical comparison by one-way ANOVA and Bonferroni-test. **(C-E)** *Left panels:* counting of secondary oncospheres of (C) MDA-MB-436, (D) BT-549 or (E) HCC1806 cells. Directly after seeding into the secondary oncosphere assay, cells were treated with paclitaxel (MDA-MB-436: 5 nM; BT-549: 5nM; HCC1806: 50 nM) or CRT0066101 (MDA-MB-436: 1 µM; BT-549: 1 µM; HCC1806: 0.5 µM), or in combination. DMSO served as control. Data is presented as mean sphere formation efficiency (SFE), n=3. Statistical comparison by one-way ANOVA and Bonferroni-test. Combination index (CI) values were calculated using Webb's fractional product method. CI<1 indicates synergism. *Right panels:* sphere area of secondary oncospheres of (C) MDA-MB-436, (D) BT-549 or (E) HCC1806 cells. Data is presented as mean sphere area (mm^2), n=3. Statistical comparison by one-way ANOVA and Bonferroni-test. **(F-J)** Synergy scores of secondary oncosphere formation assays of (F) MDA-MB-231, (G) MDA-MB-468, (H) MDA-MB-436, (I) BT-549 or (J) HCC1806 cells. Directly after seeding into the secondary oncosphere assay, cells were treated with paclitaxel and CRT0066101 using the indicated concentrations. SFE counts were normalized to the DMSO control. Data is presented as mean combination index (CI), n=3-4. Combination index (CI) values were calculated using Webb's fractional product method. CI<1 indicates synergism. 1≤CI≤1.09 indicates addition. CI>1.09 indicates antagonism.

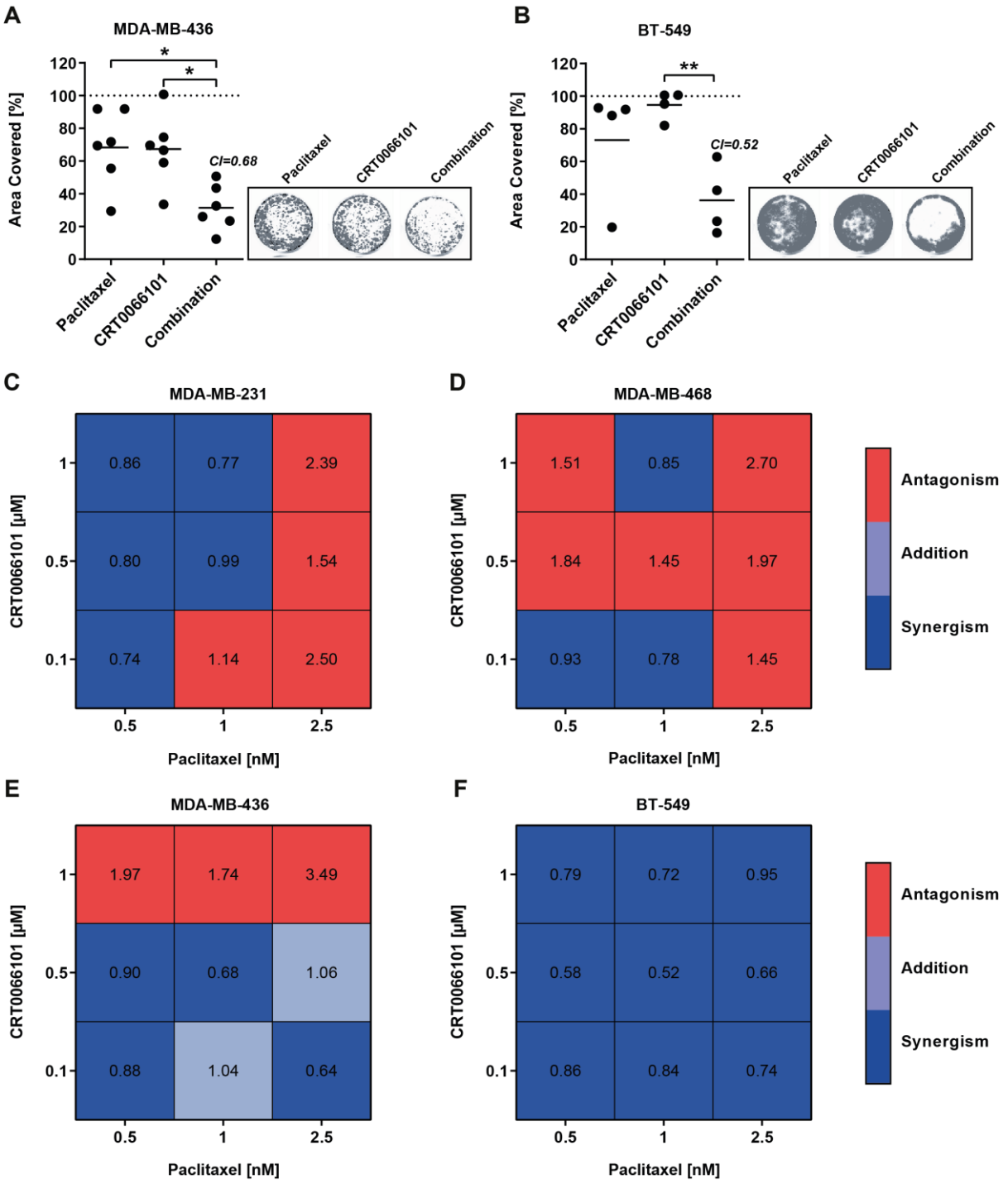

Supplemental Figure S4 | Combination of paclitaxel and CRT0066101 synergistically decreases colony formation. (A-B) *Left panels:* Colony formation of (A) MDA-MB-436 or (B) BT-549 cells. 24 h after seeding in 6-well culture dishes, MDA-MB-436 or BT-549 cells were treated for 48 h with paclitaxel (1 nM) or CRT0066101 (0.5 µM), or the combination of both. DMSO served as control. Afterwards, cells were further cultured for 2 weeks and analyzed using the Odyssey imaging system. Data is presented as mean area covered, normalized to the respective DMSO control, n=4-6. Statistical comparison by one-way ANOVA and Bonferroni-test. Combination index (CI) values were calculated using Webb's fractional product method. CI<1 indicates synergism. *Right panels:* Representative pictures of the respective colony formation assays. **(C-F)** Synergy scores of colony formation assays of (C) MDA-MB-231, (D) MDA-MB-468, (E) MDA-MB-436 or (F) BT-549 cells. Data is presented as

mean combination index (CI), n=4-6. Combination index (CI) values were calculated using Webb's fractional product method. CI<1 indicates synergism. 1≤CI≤1.09 indicates addition. CI>1.09 indicates antagonism.

7 References

1. Ficarro SB, McCleland ML, Stukenberg PT, et al. Phosphoproteome analysis by mass spectrometry and its application to Saccharomyces cerevisiae. *Nat Biotechnol.* 2002;20(3):301-305.

2. Cohen P. The regulation of protein function by multisite phosphorylation--a 25 year update. *Trends Biochem Sci.* 2000;25(12):596-601.

3. Manning G, Whyte DB, Martinez R, Hunter T, Sudarsanam S. The protein kinase complement of the human genome. *Science.* 2002;298(5600):1912-1934.

4. Muller S, Chaikuad A, Gray NS, Knapp S. The ins and outs of selective kinase inhibitor development. *Nat Chem Biol.* 2015;11(11):818-821.

5. Levitzki A. Protein kinase inhibitors as a therapeutic modality. *Acc Chem Res.* 2003;36(6):462-469.

6. Rozengurt E, Rey O, Waldron RT. Protein kinase D signaling. *J Biol Chem.* 2005;280(14):13205-13208.

7. Johannes FJ, Prestle J, Eis S, Oberhagemann P, Pfizenmaier K. PKCu is a novel, atypical member of the protein kinase C family. *J Biol Chem.* 1994;269(8):6140-6148.

8. Valverde AM, Sinnett-Smith J, Van Lint J, Rozengurt E. Molecular cloning and characterization of protein kinase D: a target for diacylglycerol and phorbol esters with a distinctive catalytic domain. *Proc Natl Acad Sci U S A.* 1994;91(18):8572-8576.

9. Sturany S, Van Lint J, Muller F, et al. Molecular cloning and characterization of the human protein kinase D2. A novel member of the protein kinase D family of serine threonine kinases. *J Biol Chem.* 2001;276(5):3310-3318.

10. Hayashi A, Seki N, Hattori A, Kozuma S, Saito T. PKCnu, a new member of the protein kinase C family, composes a fourth subfamily with PKCmu. *Biochim Biophys Acta.* 1999;1450(1):99-106.

11. Van Lint J, Rykx A, Maeda Y, et al. Protein kinase D: an intracellular traffic regulator on the move. *Trends Cell Biol.* 2002;12(4):193-200.

12. Olayioye MA, Barisic S, Hausser A. Multi-level control of actin dynamics by protein kinase D. *Cell Signal.* 2013;25(9):1739-1747.

13. Rykx A, De Kimpe L, Mikhalap S, et al. Protein kinase D: a family affair. *FEBS Lett.* 2003;546(1):81-86.

14. Huck B, Duss S, Hausser A, Olayioye MA. Elevated protein kinase D3 (PKD3) expression supports proliferation of triple-negative breast cancer cells and contributes to mTORC1-S6K1 pathway activation. *J Biol Chem.* 2014;289(6):3138-3147.

15. Iglesias T, Rozengurt E. Protein kinase D activation by mutations within its pleckstrin homology domain. *J Biol Chem.* 1998;273(1):410-416.

16. Iglesias T, Rozengurt E. Protein kinase D activation by deletion of its cysteine-rich motifs. *FEBS Lett.* 1999;454(1-2):53-56.

17. Maeda Y, Beznoussenko GV, Van Lint J, Mironov AA, Malhotra V. Recruitment of protein kinase D to the trans-Golgi network via the first cysteine-rich domain. *EMBO J.* 2001;20(21):5982-5990.

18. Rey O, Young SH, Cantrell D, Rozengurt E. Rapid protein kinase D translocation in response to G protein-coupled receptor activation. Dependence on protein kinase C. *J Biol Chem.* 2001;276(35):32616-32626.

19. Nishikawa K, Toker A, Johannes FJ, Songyang Z, Cantley LC. Determination of the specific substrate sequence motifs of protein kinase C isozymes. *J Biol Chem.* 1997;272(2):952-960.

20. Hutti JE, Jarrell ET, Chang JD, et al. A rapid method for determining protein kinase phosphorylation specificity. *Nat Methods.* 2004;1(1):27-29.

21. Doppler H, Storz P, Li J, Comb MJ, Toker A. A phosphorylation state-specific antibody recognizes Hsp27, a novel substrate of protein kinase D. *J Biol Chem.* 2005;280(15):15013-15019.

22. Hausser A, Link G, Bamberg L, et al. Structural requirements for localization and activation of protein kinase C mu (PKC mu) at the Golgi compartment. *J Cell Biol.* 2002;156(1):65-74.

23. Sanchez-Ruiloba L, Cabrera-Poch N, Rodriguez-Martinez M, et al. Protein kinase D intracellular localization and activity control kinase D-interacting substrate of 220-kDa traffic through a postsynaptic density-95/discs large/zonula occludens-1-binding motif. *J Biol Chem.* 2006;281(27):18888-18900.

24. Huck B, Kemkemer R, Franz-Wachtel M, Macek B, Hausser A, Olayioye MA. GIT1 phosphorylation on serine 46 by PKD3 regulates paxillin trafficking and cellular protrusive activity. *J Biol Chem.* 2012;287(41):34604-34613.

25. Roy A, Ye J, Deng F, Wang QJ. Protein kinase D signaling in cancer: A friend or foe? *Biochim Biophys Acta Rev Cancer.* 2017;1868(1):283-294.

26. Zugaza JL, Waldron RT, Sinnett-Smith J, Rozengurt E. Bombesin, vasopressin, endothelin, bradykinin, and platelet-derived growth factor rapidly activate protein kinase D through a protein kinase C-dependent signal transduction pathway. *J Biol Chem.* 1997;272(38):23952-23960.

27. Newton AC. Protein kinase C: structural and spatial regulation by phosphorylation, cofactors, and macromolecular interactions. *Chem Rev.* 2001;101(8):2353-2364.

28. Waldron RT, Iglesias T, Rozengurt E. Phosphorylation-dependent protein kinase D activation. *Electrophoresis.* 1999;20(2):382-390.

29. Matthews SA, Rozengurt E, Cantrell D. Protein kinase D. A selective target for antigen receptors and a downstream target for protein kinase C in lymphocytes. *J Exp Med.* 2000;191(12):2075-2082.

30. Yuan J, Slice L, Walsh JH, Rozengurt E. Activation of protein kinase D by signaling through the alpha subunit of the heterotrimeric G protein G(q). *J Biol Chem.* 2000;275(3):2157-2164.

31. Yuan J, Rey O, Rozengurt E. Protein kinase D3 activation and phosphorylation by signaling through G alpha q. *Biochem Biophys Res Commun.* 2005;335(2):270-276.

32. Waldron RT, Rozengurt E. Protein kinase C phosphorylates protein kinase D activation loop Ser744 and Ser748 and releases autoinhibition by the pleckstrin homology domain. *J Biol Chem.* 2003;278(1):154-163.

33. Wong C, Jin ZG. Protein kinase C-dependent protein kinase D activation modulates ERK signal pathway and endothelial cell proliferation by vascular endothelial growth factor. *J Biol Chem.* 2005;280(39):33262-33269.

34. Matthews SA, Rozengurt E, Cantrell D. Characterization of serine 916 as an in vivo autophosphorylation site for protein kinase D/Protein kinase Cmu. *J Biol Chem.* 1999;274(37):26543-26549.

35. Li J, O'Connor KL, Hellmich MR, Greeley GH, Jr., Townsend CM, Jr., Evers BM. The role of protein kinase D in neurotensin secretion mediated by protein kinase C-alpha/-delta and Rho/Rho kinase. *J Biol Chem.* 2004;279(27):28466-28474.

36. Eisler SA, Curado F, Link G, et al. A Rho signaling network links microtubules to PKD controlled carrier transport to focal adhesions. *Elife.* 2018;7.

37. Endo K, Oki E, Biedermann V, et al. Proteolytic cleavage and activation of protein kinase C [micro] by caspase-3 in the apoptotic response of cells to 1-beta -D-arabinofuranosylcytosine and other genotoxic agents. *J Biol Chem.* 2000;275(24):18476-18481.

38. Lemonnier J, Ghayor C, Guicheux J, Caverzasio J. Protein kinase C-independent activation of protein kinase D is involved in BMP-2-induced activation of stress mitogen-activated protein kinases JNK and p38 and osteoblastic cell differentiation. *J Biol Chem.* 2004;279(1):259-264.

39. Doppler H, Storz P. A novel tyrosine phosphorylation site in protein kinase D contributes to oxidative stress-mediated activation. *J Biol Chem.* 2007;282(44):31873-31881.

40. Wang QJ. PKD at the crossroads of DAG and PKC signaling. *Trends Pharmacol Sci.* 2006;27(6):317-323.

41. Hausser A, Storz P, Martens S, Link G, Toker A, Pfizenmaier K. Protein kinase D regulates vesicular transport by phosphorylating and activating phosphatidylinositol-4 kinase IIIbeta at the Golgi complex. *Nat Cell Biol.* 2005;7(9):880-886.

42. Peterburs P, Heering J, Link G, Pfizenmaier K, Olayioye MA, Hausser A. Protein kinase D regulates cell migration by direct phosphorylation of the cofilin phosphatase slingshot 1 like. *Cancer Res.* 2009;69(14):5634-5638.

43. Eiseler T, Hausser A, De Kimpe L, Van Lint J, Pfizenmaier K. Protein kinase D controls actin polymerization and cell motility through phosphorylation of cortactin. *J Biol Chem.* 2010;285(24):18672-18683.

44. Doppler H, Storz P. Mitochondrial and Oxidative Stress-Mediated Activation of Protein Kinase D1 and Its Importance in Pancreatic Cancer. *Front Oncol.* 2017;7:41.

45. Dequiedt F, Van Lint J, Lecomte E, et al. Phosphorylation of histone deacetylase 7 by protein kinase D mediates T cell receptor-induced Nur77 expression and apoptosis. *J Exp Med.* 2005;201(5):793-804.

46. Eiseler T, Schmid MA, Topbas F, Pfizenmaier K, Hausser A. PKD is recruited to sites of actin remodelling at the leading edge and negatively regulates cell migration. *FEBS Lett.* 2007;581(22):4279-4287.

47. Eiseler T, Doppler H, Yan IK, Kitatani K, Mizuno K, Storz P. Protein kinase D1 regulates cofilin-mediated F-actin reorganization and cell motility through slingshot. *Nat Cell Biol.* 2009;11(5):545-556.

48. Barisic S, Nagel AC, Franz-Wachtel M, et al. Phosphorylation of Ser 402 impedes phosphatase activity of slingshot 1. *EMBO Rep.* 2011;12(6):527-533.

49. Ziegler S, Eiseler T, Scholz RP, Beck A, Link G, Hausser A. A novel protein kinase D phosphorylation site in the tumor suppressor Rab interactor 1 is critical for coordination of cell migration. *Mol Biol Cell.* 2011;22(5):570-580.

50. De Kimpe L, Janssens K, Derua R, et al. Characterization of cortactin as an in vivo protein kinase D substrate: interdependence of sites and potentiation by Src. *Cell Signal.* 2009;21(2):253-263.

51. Jaggi M, Rao PS, Smith DJ, et al. E-cadherin phosphorylation by protein kinase D1/protein kinase C{mu} is associated with altered cellular aggregation and motility in prostate cancer. *Cancer Res.* 2005;65(2):483-492.

52. Du C, Zhang C, Hassan S, Biswas MH, Balaji KC. Protein kinase D1 suppresses epithelial-to-mesenchymal transition through phosphorylation of snail. *Cancer Res.* 2010;70(20):7810-7819.

53. Heerboth S, Housman G, Leary M, et al. EMT and tumor metastasis. *Clin Transl Med.* 2015;4:6.

54. Yeaman C, Ayala MI, Wright JR, et al. Protein kinase D regulates basolateral membrane protein exit from trans-Golgi network. *Nat Cell Biol.* 2004;6(2):106-112.

55. Hausser A, Link G, Hoene M, Russo C, Selchow O, Pfizenmaier K. Phospho-specific binding of 14-3-3 proteins to phosphatidylinositol 4-kinase III beta protects from dephosphorylation and stabilizes lipid kinase activity. *J Cell Sci.* 2006;119(Pt 17):3613-3621.

56. Graham TR, Burd CG. Coordination of Golgi functions by phosphatidylinositol 4-kinases. *Trends Cell Biol.* 2011;21(2):113-121.

57. Levine TP, Munro S. The pleckstrin homology domain of oxysterol-binding protein recognises a determinant specific to Golgi membranes. *Curr Biol.* 1998;8(13):729-739.

58. Toth B, Balla A, Ma H, Knight ZA, Shokat KM, Balla T. Phosphatidylinositol 4-kinase IIIbeta regulates the transport of ceramide between the endoplasmic reticulum and Golgi. *J Biol Chem.* 2006;281(47):36369-36377.

59. Hanada K, Kumagai K, Tomishige N, Yamaji T. CERT-mediated trafficking of ceramide. *Biochim Biophys Acta.* 2009;1791(7):684-691.

60. Fugmann T, Hausser A, Schoffler P, Schmid S, Pfizenmaier K, Olayioye MA. Regulation of secretory transport by protein kinase D-mediated phosphorylation of the ceramide transfer protein. *The Journal of cell biology.* 2007;178(1):15-22.

61. Nhek S, Ngo M, Yang X, et al. Regulation of oxysterol-binding protein Golgi localization through protein kinase D-mediated phosphorylation. *Mol Biol Cell.* 2010;21(13):2327-2337.

62. Gehart H, Goginashvili A, Beck R, et al. The BAR domain protein Arfaptin-1 controls secretory granule biogenesis at the trans-Golgi network. *Dev Cell.* 2012;23(4):756-768.

63. Cruz-Garcia D, Ortega-Bellido M, Scarpa M, et al. Recruitment of arfaptins to the trans-Golgi network by PI(4)P and their involvement in cargo export. *EMBO J.* 2013;32(12):1717-1729.

64. Storz P, Doppler H, Toker A. Protein kinase D mediates mitochondrion-to-nucleus signaling and detoxification from mitochondrial reactive oxygen species. *Mol Cell Biol.* 2005;25(19):8520-8530.

65. Ha CH, Wang W, Jhun BS, et al. Protein kinase D-dependent phosphorylation and nuclear export of histone deacetylase 5 mediates vascular endothelial growth factor-induced gene expression and angiogenesis. *J Biol Chem.* 2008;283(21):14590-14599.

66. Ferrara N, Davis-Smyth T. The biology of vascular endothelial growth factor. *Endocr Rev.* 1997;18(1):4-25.

67. Xu W, Qian J, Zeng F, et al. Protein kinase Ds promote tumor angiogenesis through mast cell recruitment and expression of angiogenic factors in prostate cancer microenvironment. *J Exp Clin Cancer Res.* 2019;38(1):114.

68. Cheatham B, Kahn CR. Insulin action and the insulin signaling network. *Endocr Rev.* 1995;16(2):117-142.

69. Marchetti P, and Ferrannini, E. Beta cell mass and function in human type 2 diabetes. *International Textbook of Diabetes Mellitus*. New York: John Wiley & Sons; 2015:354–370.

70. Ohlsson H, Karlsson K, Edlund T. IPF1, a homeodomain-containing transactivator of the insulin gene. *EMBO J.* 1993;12(11):4251-4259.

71. Naya FJ, Huang HP, Qiu Y, et al. Diabetes, defective pancreatic morphogenesis, and abnormal enteroendocrine differentiation in BETA2/neuroD-deficient mice. *Genes Dev.* 1997;11(18):2323-2334.

72. Pino MF, Ye DZ, Linning KD, et al. Elevated glucose attenuates human insulin gene promoter activity in INS-1 pancreatic beta-cells via reduced nuclear factor binding to the A5/core and Z element. *Mol Endocrinol.* 2005;19(5):1343-1360.

73. Shi Y, Vattem KM, Sood R, et al. Identification and characterization of pancreatic eukaryotic initiation factor 2 alpha-subunit kinase, PEK, involved in translational control. *Mol Cell Biol.* 1998;18(12):7499-7509.

74. Delepine M, Nicolino M, Barrett T, Golamaully M, Lathrop GM, Julier C. EIF2AK3, encoding translation initiation factor 2-alpha kinase 3, is mutated in patients with Wolcott-Rallison syndrome. *Nat Genet.* 2000;25(4):406-409.

75. Zhang W, Feng D, Li Y, Iida K, McGrath B, Cavener DR. PERK EIF2AK3 control of pancreatic beta cell differentiation and proliferation is required for postnatal glucose homeostasis. *Cell Metab.* 2006;4(6):491-497.

76. Kahn SE, Hull RL, Utzschneider KM. Mechanisms linking obesity to insulin resistance and type 2 diabetes. *Nature.* 2006;444(7121):840-846.

77. Haeusler RA, McGraw TE, Accili D. Biochemical and cellular properties of insulin receptor signalling. *Nat Rev Mol Cell Biol.* 2018;19(1):31-44.

78. American Diabetes A. Diagnosis and classification of diabetes mellitus. *Diabetes Care.* 2014;37 Suppl 1:S81-90.

79. Craig ME, Hattersley A, Donaghue KC. Definition, epidemiology and classification of diabetes in children and adolescents. *Pediatr Diabetes.* 2009;10 Suppl 12:3-12.

80. Galtier F. Definition, epidemiology, risk factors. *Diabetes Metab.* 2010;36(6 Pt 2):628-651.

81. WHO. Diabetes. 2018; https://www.who.int/news-room/fact-sheets/detail/diabetes, 2019.

82. Devendra D, Liu E, Eisenbarth GS. Type 1 diabetes: recent developments. *BMJ.* 2004;328(7442):750-754.

83. Halban PA, Polonsky KS, Bowden DW, et al. beta-cell failure in type 2 diabetes: postulated mechanisms and prospects for prevention and treatment. *Diabetes Care.* 2014;37(6):1751-1758.

84. Dabelea D, Mayer-Davis EJ, Saydah S, et al. Prevalence of type 1 and type 2 diabetes among children and adolescents from 2001 to 2009. *JAMA.* 2014;311(17):1778-1786.

85. Donath MY, Shoelson SE. Type 2 diabetes as an inflammatory disease. *Nat Rev Immunol.* 2011;11(2):98-107.

86. Almaca J, Molina J, Arrojo EDR, et al. Young capillary vessels rejuvenate aged pancreatic islets. *Proc Natl Acad Sci U S A.* 2014;111(49):17612-17617.

87. Meneilly GS, Tessier D. Diabetes in elderly adults. *J Gerontol A Biol Sci Med Sci.* 2001;56(1):M5-13.

88. Naser KA, Gruber A, Thomson GA. The emerging pandemic of obesity and diabetes: are we doing enough to prevent a disaster? *Int J Clin Pract.* 2006;60(9):1093-1097.

89. Karpe F, Dickmann JR, Frayn KN. Fatty acids, obesity, and insulin resistance: time for a reevaluation. *Diabetes.* 2011;60(10):2441-2449.

90. Szendroedi J, Yoshimura T, Phielix E, et al. Role of diacylglycerol activation of PKCtheta in lipid-induced muscle insulin resistance in humans. *Proc Natl Acad Sci U S A.* 2014;111(26):9597-9602.

91. Yu C, Chen Y, Cline GW, et al. Mechanism by which fatty acids inhibit insulin activation of insulin receptor substrate-1 (IRS-1)-associated phosphatidylinositol 3-kinase activity in muscle. *J Biol Chem.* 2002;277(52):50230-50236.

92. Kim JK, Zisman A, Fillmore JJ, et al. Glucose toxicity and the development of diabetes in mice with muscle-specific inactivation of GLUT4. *J Clin Invest.* 2001;108(1):153-160.

93. Samuel VT, Shulman GI. The pathogenesis of insulin resistance: integrating signaling pathways and substrate flux. *J Clin Invest.* 2016;126(1):12-22.

94. Tchkonia T, Kirkland JL. Aging, Cell Senescence, and Chronic Disease: Emerging Therapeutic Strategies. *JAMA.* 2018;320(13):1319-1320.

95. Chia CW, Egan JM, Ferrucci L. Age-Related Changes in Glucose Metabolism, Hyperglycemia, and Cardiovascular Risk. *Circ Res.* 2018;123(7):886-904.

96. Kalyani RR, Golden SH, Cefalu WT. Diabetes and Aging: Unique Considerations and Goals of Care. *Diabetes Care.* 2017;40(4):440-443.

97. Helman A, Klochendler A, Azazmeh N, et al. p16(Ink4a)-induced senescence of pancreatic beta cells enhances insulin secretion. *Nat Med.* 2016;22(4):412-420.

98. Hayflick L, Moorhead PS. The serial cultivation of human diploid cell strains. *Exp Cell Res.* 1961;25:585-621.

99. Hayflick L. The Limited in Vitro Lifetime of Human Diploid Cell Strains. *Exp Cell Res.* 1965;37:614-636.

100. Herranz N, Gil J. Mechanisms and functions of cellular senescence. *J Clin Invest.* 2018;128(4):1238-1246.

101. Storer M, Mas A, Robert-Moreno A, et al. Senescence is a developmental mechanism that contributes to embryonic growth and patterning. *Cell.* 2013;155(5):1119-1130.

102. Munoz-Espin D, Canamero M, Maraver A, et al. Programmed cell senescence during mammalian embryonic development. *Cell.* 2013;155(5):1104-1118.

103. Demaria M, Ohtani N, Youssef SA, et al. An essential role for senescent cells in optimal wound healing through secretion of PDGF-AA. *Dev Cell.* 2014;31(6):722-733.

104. Collado M, Serrano M. Senescence in tumours: evidence from mice and humans. *Nat Rev Cancer.* 2010;10(1):51-57.

105. d'Adda di Fagagna F. Living on a break: cellular senescence as a DNA-damage response. *Nat Rev Cancer.* 2008;8(7):512-522.

106. d'Adda di Fagagna F, Reaper PM, Clay-Farrace L, et al. A DNA damage checkpoint response in telomere-initiated senescence. *Nature.* 2003;426(6963):194-198.

107. Gil J, Peters G. Regulation of the INK4b-ARF-INK4a tumour suppressor locus: all for one or one for all. *Nat Rev Mol Cell Biol.* 2006;7(9):667-677.

108. Bracken AP, Kleine-Kohlbrecher D, Dietrich N, et al. The Polycomb group proteins bind throughout the INK4A-ARF locus and are disassociated in senescent cells. *Genes Dev.* 2007;21(5):525-530.

109. Krishnamurthy J, Torrice C, Ramsey MR, et al. Ink4a/Arf expression is a biomarker of aging. *The Journal of clinical investigation.* 2004;114(9):1299-1307.

110. Yamakoshi K, Takahashi A, Hirota F, et al. Real-time in vivo imaging of p16Ink4a reveals cross talk with p53. *J Cell Biol.* 2009;186(3):393-407.

111. Burd CE, Sorrentino JA, Clark KS, et al. Monitoring tumorigenesis and senescence in vivo with a p16(INK4a)-luciferase model. *Cell.* 2013;152(1-2):340-351.

112. Kurz DJ, Decary S, Hong Y, Erusalimsky JD. Senescence-associated (beta)-galactosidase reflects an increase in lysosomal mass during replicative ageing of human endothelial cells. *J Cell Sci.* 2000;113 (Pt 20):3613-3622.

113. Lee BY, Han JA, Im JS, et al. Senescence-associated beta-galactosidase is lysosomal beta-galactosidase. *Aging Cell.* 2006;5(2):187-195.

114. Adams PD. Remodeling chromatin for senescence. *Aging Cell.* 2007;6(4):425-427.

115. Narita M, Nunez S, Heard E, et al. Rb-mediated heterochromatin formation and silencing of E2F target genes during cellular senescence. *Cell.* 2003;113(6):703-716.

116. Chandra T, Ewels PA, Schoenfelder S, et al. Global reorganization of the nuclear landscape in senescent cells. *Cell Rep.* 2015;10(4):471-483.

117. Ivanov A, Pawlikowski J, Manoharan I, et al. Lysosome-mediated processing of chromatin in senescence. *J Cell Biol.* 2013;202(1):129-143.

118. Dou Z, Ghosh K, Vizioli MG, et al. Cytoplasmic chromatin triggers inflammation in senescence and cancer. *Nature.* 2017;550(7676):402-406.

119. Sun N, Youle RJ, Finkel T. The Mitochondrial Basis of Aging. *Mol Cell.* 2016;61(5):654-666.

120. Correia-Melo C, Marques FD, Anderson R, et al. Mitochondria are required for pro-ageing features of the senescent phenotype. *EMBO J.* 2016;35(7):724-742.

121. Rankin MM, Kushner JA. Adaptive beta-cell proliferation is severely restricted with advanced age. *Diabetes.* 2009;58(6):1365-1372.

122. Tyrberg B, Eizirik DL, Hellerstrom C, Pipeleers DG, Andersson A. Human pancreatic beta-cell deoxyribonucleic acid-synthesis in islet grafts decreases with increasing organ donor age but increases in response to glucose stimulation in vitro. *Endocrinology.* 1996;137(12):5694-5699.

123. De Tata V. Age-related impairment of pancreatic Beta-cell function: pathophysiological and cellular mechanisms. *Frontiers in endocrinology.* 2014;5:138.

124. Krishnamurthy J, Ramsey MR, Ligon KL, et al. p16INK4a induces an age-dependent decline in islet regenerative potential. *Nature.* 2006;443(7110):453-457.

125. Chen H, Gu X, Su IH, et al. Polycomb protein Ezh2 regulates pancreatic beta-cell Ink4a/Arf expression and regeneration in diabetes mellitus. *Genes Dev.* 2009;23(8):975-985.

126. Pascoe J, Hollern D, Stamateris R, et al. Free fatty acids block glucose-induced beta-cell proliferation in mice by inducing cell cycle inhibitors p16 and p18. *Diabetes.* 2012;61(3):632-641.

127. Sumara G, Formentini I, Collins S, et al. Regulation of PKD by the MAPK p38delta in insulin secretion and glucose homeostasis. *Cell.* 2009;136(2):235-248.

128. Goginashvili A, Zhang Z, Erbs E, et al. Insulin granules. Insulin secretory granules control autophagy in pancreatic beta cells. *Science.* 2015;347(6224):878-882.

129. Ferdaoussi M, Bergeron V, Zarrouki B, et al. G protein-coupled receptor (GPR)40-dependent potentiation of insulin secretion in mouse islets is mediated by protein kinase D1. *Diabetologia.* 2012;55(10):2682-2692.

130. Kong KC, Butcher AJ, McWilliams P, et al. M3-muscarinic receptor promotes insulin release via receptor phosphorylation/arrestin-dependent activation of protein kinase D1. *Proc Natl Acad Sci U S A.* 2010;107(49):21181-21186.

131. Bergeron V, Ghislain J, Vivot K, et al. Deletion of Protein Kinase D1 in Pancreatic beta-Cells Impairs Insulin Secretion in High-Fat Diet-Fed Mice. *Diabetes.* 2018;67(1):71-77.

132. Jemal A, Bray F, Center MM, Ferlay J, Ward E, Forman D. Global cancer statistics. *CA Cancer J Clin.* 2011;61(2):69-90.

133. Borges S, Perez EA, Thompson EA, Radisky DC, Geiger XJ, Storz P. Effective Targeting of Estrogen Receptor-Negative Breast Cancers with the Protein Kinase D Inhibitor CRT0066101. *Mol Cancer Ther.* 2015;14(6):1306-1316.

134. McGuire A, Brown JA, Malone C, McLaughlin R, Kerin MJ. Effects of age on the detection and management of breast cancer. *Cancers (Basel).* 2015;7(2):908-929.

135. Anders CK, Carey LA. Biology, metastatic patterns, and treatment of patients with triple-negative breast cancer. *Clin Breast Cancer.* 2009;9 Suppl 2:S73-81.

136. Perou CM, Sorlie T, Eisen MB, et al. Molecular portraits of human breast tumours. *Nature.* 2000;406(6797):747-752.

137. Goldhirsch A, Winer EP, Coates AS, et al. Personalizing the treatment of women with early breast cancer: highlights of the St Gallen International Expert Consensus on the Primary Therapy of Early Breast Cancer 2013. *Ann Oncol.* 2013;24(9):2206-2223.

138. Liedtke C, Mazouni C, Hess KR, et al. Response to neoadjuvant therapy and long-term survival in patients with triple-negative breast cancer. *J Clin Oncol.* 2008;26(8):1275-1281.

139. Smid M, Wang Y, Zhang Y, et al. Subtypes of breast cancer show preferential site of relapse. *Cancer Res.* 2008;68(9):3108-3114.

140. Foulkes WD, Smith IE, Reis-Filho JS. Triple-negative breast cancer. *N Engl J Med.* 2010;363(20):1938-1948.

141. von Minckwitz G, Schneeweiss A, Loibl S, et al. Neoadjuvant carboplatin in patients with triple-negative and HER2-positive early breast cancer (GeparSixto; GBG 66): a randomised phase 2 trial. *Lancet Oncol.* 2014;15(7):747-756.

142. Creighton CJ, Li X, Landis M, et al. Residual breast cancers after conventional therapy display mesenchymal as well as tumor-initiating features. *Proc Natl Acad Sci U S A.* 2009;106(33):13820-13825.

143. Li X, Lewis MT, Huang J, et al. Intrinsic resistance of tumorigenic breast cancer cells to chemotherapy. *J Natl Cancer Inst.* 2008;100(9):672-679.

144. Mukherjee P, Gupta A, Chattopadhyay D, Chatterji U. Modulation of SOX2 expression delineates an end-point for paclitaxel-effectiveness in breast cancer stem cells. *Sci Rep.* 2017;7(1):9170.

145. Lin Y, Zhong Y, Guan H, Zhang X, Sun Q. CD44+/CD24- phenotype contributes to malignant relapse following surgical resection and chemotherapy in patients with invasive ductal carcinoma. *J Exp Clin Cancer Res.* 2012;31:59.

146. Adamczyk A, Niemiec JA, Ambicka A, Mucha-Malecka A, Mitus J, Rys J. CD44/CD24 as potential prognostic markers in node-positive invasive ductal breast cancer patients treated with adjuvant chemotherapy. *J Mol Histol.* 2014;45(1):35-45.

147. Ma F, Li H, Li Y, et al. Aldehyde dehydrogenase 1 (ALDH1) expression is an independent prognostic factor in triple negative breast cancer (TNBC). *Medicine (Baltimore).* 2017;96(14):e6561.

148. Abraham BK, Fritz P, McClellan M, Hauptvogel P, Athelogou M, Brauch H. Prevalence of CD44+/CD24-/low cells in breast cancer may not be associated with clinical outcome but may favor distant metastasis. *Clin Cancer Res.* 2005;11(3):1154-1159.

149. Bao B, Ahmad A, Azmi AS, Ali S, Sarkar FH. Overview of cancer stem cells (CSCs) and mechanisms of their regulation: implications for cancer therapy. *Curr Protoc Pharmacol.* 2013;Chapter 14:Unit 14 25.

150. Kakarala M, Wicha MS. Implications of the cancer stem-cell hypothesis for breast cancer prevention and therapy. *J Clin Oncol.* 2008;26(17):2813-2820.

151. Ahmed MA, Aleskandarany MA, Rakha EA, et al. A CD44(-)/CD24(+) phenotype is a poor prognostic marker in early invasive breast cancer. *Breast Cancer Res Treat.* 2012;133(3):979-995.

152. Lindahl R. Aldehyde dehydrogenases and their role in carcinogenesis. *Crit Rev Biochem Mol Biol.* 1992;27(4-5):283-335.

153. Chute JP, Muramoto GG, Whitesides J, et al. Inhibition of aldehyde dehydrogenase and retinoid signaling induces the expansion of human hematopoietic stem cells. *Proc Natl Acad Sci U S A.* 2006;103(31):11707-11712.

154. Kida K, Ishikawa T, Yamada A, et al. Effect of ALDH1 on prognosis and chemoresistance by breast cancer subtype. *Breast Cancer Res Treat.* 2016;156(2):261-269.

155. Al-Hajj M, Wicha MS, Benito-Hernandez A, Morrison SJ, Clarke MF. Prospective identification of tumorigenic breast cancer cells. *Proc Natl Acad Sci U S A.* 2003;100(7):3983-3988.

156. Reya T, Morrison SJ, Clarke MF, Weissman IL. Stem cells, cancer, and cancer stem cells. *Nature.* 2001;414(6859):105-111.

157. Gupta PB, Fillmore CM, Jiang G, et al. Stochastic state transitions give rise to phenotypic equilibrium in populations of cancer cells. *Cell.* 2011;146(4):633-644.

158. Zhao W, Li Y, Zhang X. Stemness-Related Markers in Cancer. *Cancer Transl Med.* 2017;3(3):87-95.

159. Takahashi K, Yamanaka S. Induction of pluripotent stem cells from mouse embryonic and adult fibroblast cultures by defined factors. *Cell.* 2006;126(4):663-676.

160. Capaccione KM, Pine SR. The Notch signaling pathway as a mediator of tumor survival. *Carcinogenesis.* 2013;34(7):1420-1430.

161. Hassan KA, Wang L, Korkaya H, et al. Notch pathway activity identifies cells with cancer stem cell-like properties and correlates with worse survival in lung adenocarcinoma. *Clin Cancer Res.* 2013;19(8):1972-1980.

162. Liu X, Fan D. The epithelial-mesenchymal transition and cancer stem cells: functional and mechanistic links. *Curr Pharm Des.* 2015;21(10):1279-1291.

163. Koury J, Zhong L, Hao J. Targeting Signaling Pathways in Cancer Stem Cells for Cancer Treatment. *Stem Cells Int.* 2017;2017:2925869.

164. Borges S, Doppler H, Perez EA, et al. Pharmacologic reversion of epigenetic silencing of the PRKD1 promoter blocks breast tumor cell invasion and metastasis. *Breast Cancer Res.* 2013;15(2):R66.

165. Hao Q, McKenzie R, Gan H, Tang H. Protein kinases D2 and D3 are novel growth regulators in HCC1806 triple-negative breast cancer cells. *Anticancer Res.* 2013;33(2):393-399.

166. Chen J, Lu L, Feng Y, et al. PKD2 mediates multi-drug resistance in breast cancer cells through modulation of P-glycoprotein expression. *Cancer Lett.* 2011;300(1):48-56.

167. Eiseler T, Doppler H, Yan IK, Goodison S, Storz P. Protein kinase D1 regulates matrix metalloproteinase expression and inhibits breast cancer cell invasion. *Breast Cancer Res.* 2009;11(1):R13.

168. Yang ZF, Zhang H, Ma L, et al. GABP transcription factor is required for development of chronic myelogenous leukemia via its control of PRKD2. *Proc Natl Acad Sci U S A.* 2013;110(6):2312-2317.

169. Liao YC, Ruan JW, Lua I, et al. Overexpressed hPTTG1 promotes breast cancer cell invasion and metastasis by regulating GEF-H1/RhoA signalling. *Oncogene.* 2012;31(25):3086-3097.

170. Meiri D, Greeve MA, Brunet A, et al. Modulation of Rho guanine exchange factor Lfc activity by protein kinase A-mediated phosphorylation. *Mol Cell Biol.* 2009;29(21):5963-5973.

171. Masoud V, Pages G. Targeted therapies in breast cancer: New challenges to fight against resistance. *World J Clin Oncol.* 2017;8(2):120-134.

172. FDA FaDA. FDA approves atezolizumab for PD-L1 positive unresectable locally advanced or metastatic triple-negative breast cancer. 2019; https://www.fda.gov/drugs/drug-approvals-and-databases/fda-approves-atezolizumab-pd-l1-positive-unresectable-locally-advanced-or-metastatic-triple-negative. Accessed 07/2019, 2019.

173. Dawood S. Triple-negative breast cancer: epidemiology and management options. *Drugs.* 2010;70(17):2247-2258.

174. Wahba HA, El-Hadaad HA. Current approaches in treatment of triple-negative breast cancer. *Cancer Biol Med.* 2015;12(2):106-116.

175. Sparano JA, Wang M, Martino S, et al. Weekly paclitaxel in the adjuvant treatment of breast cancer. *N Engl J Med.* 2008;358(16):1663-1671.

176. Eitaki M, Yamamori T, Meike S, Yasui H, Inanami O. Vincristine enhances amoeboid-like motility via GEF-H1/RhoA/ROCK/Myosin light chain signaling in MKN45 cells. *BMC Cancer.* 2012;12:469.

177. Ellwanger K, Kienzle C, Lutz S, et al. Protein kinase D controls voluntary-running-induced skeletal muscle remodelling. *Biochem J.* 2011;440(3):327-324.

178. Hu Y, Smyth GK. ELDA: extreme limiting dilution analysis for comparing depleted and enriched populations in stem cell and other assays. *J Immunol Methods.* 2009;347(1-2):70-78.

179. Rajavelu A, Lungu C, Emperle M, et al. Chromatin-dependent allosteric regulation of DNMT3A activity by MeCP2. *Nucleic Acids Res.* 2018;46(17):9044-9056.

180. Rathert P, Roth M, Neumann T, et al. Transcriptional plasticity promotes primary and acquired resistance to BET inhibition. *Nature.* 2015;525(7570):543-547.

181. Fellmann C, Hoffmann T, Sridhar V, et al. An optimized microRNA backbone for effective single-copy RNAi. *Cell Rep.* 2013;5(6):1704-1713.

182. Liljedahl M, Maeda Y, Colanzi A, Ayala I, Van Lint J, Malhotra V. Protein kinase D regulates the fission of cell surface destined transport carriers from the trans-Golgi network. *Cell.* 2001;104(3):409-420.

183. Gossen M, Bujard H. Tight control of gene expression in mammalian cells by tetracycline-responsive promoters. *Proceedings of the National Academy of Sciences of the United States of America.* 1992;89(12):5547-5551.

184. Koch C. Role of PKD in Glucose Metabolism and Insulin Secretion – Studies in vivo and ex vivo. *Diploma Thesis.* 2014.

185. Avrahami D, Li C, Zhang J, et al. Aging-Dependent Demethylation of Regulatory Elements Correlates with Chromatin State and Improved beta Cell Function. *Cell Metab.* 2015;22(4):619-632.

186. Sasaki M, Kajiya H, Ozeki S, Okabe K, Ikebe T. Reactive oxygen species promotes cellular senescence in normal human epidermal keratinocytes through epigenetic regulation of p16(INK4a.). *Biochem Biophys Res Commun.* 2014;452(3):622-628.

187. Saxena S, Vekaria H, Sullivan PG, Seifert AW. Connective tissue fibroblasts from highly regenerative mammals are refractory to ROS-induced cellular senescence. *Nat Commun.* 2019;10(1):4400.

188. Song M, Franco A, Fleischer JA, Zhang L, Dorn GW, 2nd. Abrogating Mitochondrial Dynamics in Mouse Hearts Accelerates Mitochondrial Senescence. *Cell Metab.* 2017;26(6):872-883 e875.

189. Kim HS, Kim Y, Lim MJ, Park YG, Park SI, Sohn J. The p38-activated ER stress-ATF6alpha axis mediates cellular senescence. *FASEB J.* 2019;33(2):2422-2434.

190. Wiley CD, Campisi J. From Ancient Pathways to Aging Cells-Connecting Metabolism and Cellular Senescence. *Cell Metab.* 2016;23(6):1013-1021.

191. Velarde MC, Flynn JM, Day NU, Melov S, Campisi J. Mitochondrial oxidative stress caused by Sod2 deficiency promotes cellular senescence and aging phenotypes in the skin. *Aging (Albany NY).* 2012;4(1):3-12.

192. Tirosh O, Pardo M, Schwartz B, Miskin R. Long-lived alphaMUPA transgenic mice show reduced SOD2 expression, enhanced apoptosis and reduced susceptibility to the carcinogen dimethylhydrazine. *Mech Ageing Dev.* 2005;126(12):1262-1273.

193. Nomiyama T, Tanaka Y, Piao L, et al. The polymorphism of manganese superoxide dismutase is associated with diabetic nephropathy in Japanese type 2 diabetic patients. *J Hum Genet.* 2003;48(3):138-141.

194. Wang CY, Liao JK. A mouse model of diet-induced obesity and insulin resistance. *Methods Mol Biol.* 2012;821:421-433.

195. Yoshida H, Miura S, Kishikawa H, et al. Fatty acids enhance GRO/CINC-1 and interleukin-6 production in rat intestinal epithelial cells. *J Nutr.* 2001;131(11):2943-2950.

196. Xu H, Barnes GT, Yang Q, et al. Chronic inflammation in fat plays a crucial role in the development of obesity-related insulin resistance. *J Clin Invest.* 2003;112(12):1821-1830.

197. Hotamisligil GS, Shargill NS, Spiegelman BM. Adipose expression of tumor necrosis factor-alpha: direct role in obesity-linked insulin resistance. *Science.* 1993;259(5091):87-91.

198. Jais A, Bruning JC. Hypothalamic inflammation in obesity and metabolic disease. *J Clin Invest.* 2017;127(1):24-32.

199. Hoffler U, Hobbie K, Wilson R, et al. Diet-induced obesity is associated with hyperleptinemia, hyperinsulinemia, hepatic steatosis, and glomerulopathy in C57Bl/6J mice. *Endocrine.* 2009;36(2):311-325.

200. Kraemer FB, Takeda D, Natu V, Sztalryd C. Insulin regulates lipoprotein lipase activity in rat adipose cells via wortmannin- and rapamycin-sensitive pathways. *Metabolism.* 1998;47(5):555-559.

201. Jiao P, Ma J, Feng B, et al. FFA-induced adipocyte inflammation and insulin resistance: involvement of ER stress and IKKbeta pathways. *Obesity (Silver Spring).* 2011;19(3):483-491.

202. Lieb WS, Lungu C, Tamas R, et al. The GEF-H1/PKD3 signaling pathway promotes the maintenance of triple-negative breast cancer stem cells. *Int J Cancer.* 2019.

203. Bossard C, Bresson D, Polishchuk RS, Malhotra V. Dimeric PKD regulates membrane fission to form transport carriers at the TGN. *J Cell Biol.* 2007;179(6):1123-1131.

204. Dubrovska A, Hartung A, Bouchez LC, et al. CXCR4 activation maintains a stem cell population in tamoxifen-resistant breast cancer cells through AhR signalling. *British Journal Of Cancer.* 2012;107:43.

205. Vaillant F, Asselin-Labat ML, Shackleton M, Forrest NC, Lindeman GJ, Visvader JE. The mammary progenitor marker CD61/beta3 integrin identifies cancer stem cells in mouse models of mammary tumorigenesis. *Cancer Res.* 2008;68(19):7711-7717.

206. Harrison H, Farnie G, Howell SJ, et al. Regulation of breast cancer stem cell activity by signaling through the Notch4 receptor. *Cancer Res.* 2010;70(2):709-718.

207. Glinka Y, Mohammed N, Subramaniam V, Jothy S, Prud'homme GJ. Neuropilin-1 is expressed by breast cancer stem-like cells and is linked to NF-kappaB activation and tumor sphere formation. *Biochem Biophys Res Commun.* 2012;425(4):775-780.

208. Yen WC, Fischer MM, Axelrod F, et al. Targeting Notch signaling with a Notch2/Notch3 antagonist (tarextumab) inhibits tumor growth and decreases tumor-initiating cell frequency. *Clin Cancer Res.* 2015;21(9):2084-2095.

209. Leis O, Eguiara A, Lopez-Arribillaga E, et al. Sox2 expression in breast tumours and activation in breast cancer stem cells. *Oncogene.* 2012;31(11):1354-1365.

210. Iriondo O, Rabano M, Domenici G, et al. Distinct breast cancer stem/progenitor cell populations require either HIF1alpha or loss of PHD3 to expand under hypoxic conditions. *Oncotarget.* 2015;6(31):31721-31739.

211. Ginestier C, Hur MH, Charafe-Jauffret E, et al. ALDH1 is a marker of normal and malignant human mammary stem cells and a predictor of poor clinical outcome. *Cell Stem Cell.* 2007;1(5):555-567.

212. Cioce M, Gherardi S, Viglietto G, et al. Mammosphere-forming cells from breast cancer cell lines as a tool for the identification of CSC-like- and early progenitor-targeting drugs. *Cell Cycle.* 2010;9(14):2878-2887.

213. Cordenonsi M, Zanconato F, Azzolin L, et al. The Hippo transducer TAZ confers cancer stem cell-related traits on breast cancer cells. *Cell.* 2011;147(4):759-772.

214. Fu Y, Rubin CS. Protein kinase D: coupling extracellular stimuli to the regulation of cell physiology. *EMBO Rep.* 2011;12(8):785-796.

215. Hu T, Liu S, Breiter DR, Wang F, Tang Y, Sun S. Octamer 4 small interfering RNA results in cancer stem cell-like cell apoptosis. *Cancer Res.* 2008;68(16):6533-6540.

216. McAndrew N, DeMichele A. Neoadjuvant Chemotherapy Considerations in Triple-Negative Breast Cancer. *J Target Ther Cancer.* 2018;7(1):52-69.

217. Zasadil LM, Andersen KA, Yeum D, et al. Cytotoxicity of paclitaxel in breast cancer is due to chromosome missegregation on multipolar spindles. *Sci Transl Med.* 2014;6(229):229ra243.

218. Rajendran V, Jain MV. In Vitro Tumorigenic Assay: Colony Forming Assay for Cancer Stem Cells. *Methods Mol Biol.* 2018;1692:89-95.

219. Ren M, Feng H, Fu Y, Land M, Rubin CS. Protein kinase D is an essential regulator of C. elegans innate immunity. *Immunity.* 2009;30(4):521-532.

220. Bencsik N, Sziber Z, Liliom H, et al. Protein kinase D promotes plasticity-induced F-actin stabilization in dendritic spines and regulates memory formation. *J Cell Biol.* 2015;210(5):771-783.

221. Fielitz J, Kim MS, Shelton JM, et al. Requirement of protein kinase D1 for pathological cardiac remodeling. *Proc Natl Acad Sci U S A.* 2008;105(8):3059-3063.

222. Durand N, Borges S, Storz P. Protein Kinase D Enzymes as Regulators of EMT and Cancer Cell Invasion. *J Clin Med.* 2016;5(2).

223. Larsen CM, Faulenbach M, Vaag A, et al. Interleukin-1-receptor antagonist in type 2 diabetes mellitus. *N Engl J Med.* 2007;356(15):1517-1526.

224. Wang SY, Halban PA, Rowe JW. Effects of aging on insulin synthesis and secretion. Differential effects on preproinsulin messenger RNA levels, proinsulin biosynthesis, and secretion of newly made and preformed insulin in the rat. *J Clin Invest.* 1988;81(1):176-184.

225. Garcia-Haro L, Garcia-Gimeno MA, Neumann D, Beullens M, Bollen M, Sanz P. Glucose-dependent regulation of AMP-activated protein kinase in MIN6 beta cells is not affected by the protein kinase A pathway. *FEBS Lett.* 2012;586(23):4241-4247.

226. Coughlan KA, Valentine RJ, Sudit BS, et al. PKD1 Inhibits AMPKalpha2 through Phosphorylation of Serine 491 and Impairs Insulin Signaling in Skeletal Muscle Cells. *J Biol Chem.* 2016;291(11):5664-5675.

227. Loffler MC, Mayer AE, Trujillo Viera J, et al. Protein kinase D1 deletion in adipocytes enhances energy dissipation and protects against adiposity. *EMBO J.* 2018;37(22).

228. Nardella C, Clohessy JG, Alimonti A, Pandolfi PP. Pro-senescence therapy for cancer treatment. *Nat Rev Cancer.* 2011;11(7):503-511.

229. Gomez-Miragaya J, Palafox M, Pare L, et al. Resistance to Taxanes in Triple-Negative Breast Cancer Associates with the Dynamics of a CD49f+ Tumor-Initiating Population. *Stem Cell Reports.* 2017;8(5):1392-1407.

230. Bhola NE, Balko JM, Dugger TC, et al. TGF-beta inhibition enhances chemotherapy action against triple-negative breast cancer. *J Clin Invest.* 2013;123(3):1348-1358.

231. Hollier BG, Evans K, Mani SA. The epithelial-to-mesenchymal transition and cancer stem cells: a coalition against cancer therapies. *J Mammary Gland Biol Neoplasia.* 2009;14(1):29-43.

232. Mani SA, Guo W, Liao MJ, et al. The epithelial-mesenchymal transition generates cells with properties of stem cells. *Cell.* 2008;133(4):704-715.

233. Scheel C, Eaton EN, Li SH, et al. Paracrine and autocrine signals induce and maintain mesenchymal and stem cell states in the breast. *Cell.* 2011;145(6):926-940.

234. Wang J, Sinnett-Smith J, Stevens JV, Young SH, Rozengurt E. Biphasic Regulation of Yes-associated Protein (YAP) Cellular Localization, Phosphorylation, and Activity by G Protein-coupled Receptor Agonists in Intestinal Epithelial Cells: A NOVEL ROLE FOR PROTEIN KINASE D (PKD). *J Biol Chem.* 2016;291(34):17988-18005.

235. Shao D, Zhai P, Del Re DP, et al. A functional interaction between Hippo-YAP signalling and FoxO1 mediates the oxidative stress response. *Nature communications.* 2014;5:3315.

236. Zhao B, Wei X, Li W, et al. Inactivation of YAP oncoprotein by the Hippo pathway is involved in cell contact inhibition and tissue growth control. *Genes & development.* 2007;21(21):2747-2761.

237. Diehn M, Cho RW, Lobo NA, et al. Association of reactive oxygen species levels and radioresistance in cancer stem cells. *Nature.* 2009;458(7239):780-783.

238. Chan SH, Huang WC, Chang JW, et al. MicroRNA-149 targets GIT1 to suppress integrin signaling and breast cancer metastasis. *Oncogene.* 2014;33:4496.

239. Reddy SM, Barcenas CH, Sinha AK, et al. Long-term survival outcomes of triple-receptor negative breast cancer survivors who are disease free at 5 years and relationship with low hormone receptor positivity. *Br J Cancer.* 2018;118(1):17-23.

240. Yang C, He Y, Zhang H, et al. Selective killing of breast cancer cells expressing activated CD44 using CD44 ligand-coated nanoparticles in vitro and in vivo. *Oncotarget.* 2015;6(17):15283-15296.

241. Lin CC, Lo MC, Moody R, et al. Targeting LRP8 inhibits breast cancer stem cells in triple-negative breast cancer. *Cancer Lett.* 2018;438:165-173.

242. Shi P, Liu W, Tala, et al. Metformin suppresses triple-negative breast cancer stem cells by targeting KLF5 for degradation. *Cell Discovery.* 2017;3:17010.

243. Doherty MR, Cheon H, Junk DJ, et al. Interferon-beta represses cancer stem cell properties in triple-negative breast cancer. *Proc Natl Acad Sci U S A.* 2017;114(52):13792-13797.

244. Tian J, Raffa FA, Dai M, et al. Dasatinib sensitises triple negative breast cancer cells to chemotherapy by targeting breast cancer stem cells. *British Journal of Cancer.* 2018;119(12):1495-1507.

245. Katigbak A, Robert F, Paquet M, Pelletier J. Inducible Genome Editing with Conditional CRISPR/Cas9 Mice. *G3 (Bethesda).* 2018;8(5):1627-1635.

Acknowledgements

PD Dr. Angelika Hausser and Prof. Dr. Monilola Olayioye: My doctoral thesis was a joint project between the Hausser and Olayioye laboratories. Therefore, I would like to greatly acknowledge PD Dr. Angelika Hausser and Prof. Dr. Monilola Olayioye for their support and guidance during my doctoral thesis. Both of you gave me plenty of "space" to develop myself, to test new hypothesis and to follow my ideas. Thank you for the marvelous atmosphere that both of you created amongst the lab members. I especially enjoyed our off-site events, like barbecuing at your places. Both of you made my doctorate a very special time, that I will never forget. Thank You!

Prof. Dr. Roland Kontermann: Thank you for the joint paper and for chairing my doctoral defence.

Prof. Dr. Tilman Brummer: Thank you for being my second examiner.

Carlos Omar Oueslati Morales: Despite of my part-time studies in Frankfurt, I could run my experiments without interruption. All thanks to you. Thank you for your support during my projects. Thank you for being my friend… So many things I have to thank you for…

Biswajit Podder: When I first met Biswajit, I asked whether he was the new PhD student from India. A big mistake… At some point he forgave me that affront and we spend many hours, discussing science and life. Thank you for your friendship. I know you will make it at UCL!

Alexander Rau: Thank you for the joint paper and your positivity. I wish you great success in the future.

Gisela Link: Thank you for helping me with cloning and keeping my "tidiness" in check. Every lab really needs someone like you.

Sylke Lutz: Thank you for teaching me the islet isolation method and for supporting me during many animal studies. I wish you good health.

Thank you to all the people at **IZI** who supported me (Gabi, Josip, Vesna, Olli, Nadine…) and worked on my projects: T2D (Carlos, Kornelia, Sylke, Claudia, Angelika); TNBC stem cells (Cristiana, Raluca, Hannah, Philipp, Peter, Moni, Angelika,

Gisela, Yannick); Special thanks to Dr. Cristiana Lungu for conducting the review of the TNBC stem cell paper.

AMoR: Thank you to the AMoR-Team for great discussions and ideas!

Things I learned at IZI and will never forget:

- Don`t get into people's way if they crave for coffee.
- Don't tell people that they are from India if they are not.
- Pronounce "Biswajit" correctly.
- If you need someone to carry a cupboard (weighing tons) 3 stories up, call Josip.

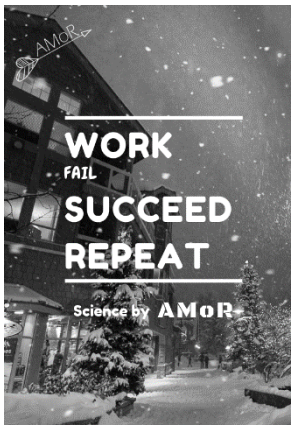

And lastly, I want to thank my **family** for their never-ending support during my doctoral studies. Thanks to my mum and dad I could entirely focus on my studies and never had to worry about anything. Thank you, Sarah, for pulling me through all my ups and downs (and there were many downs), and for being my save harbor. Thank you, Merlin, Franziska and Frederik for always believing in me!

Thank you!

Sebastian

Curriculum Vitae

SEBASTIAN **LIEB**

MANAGEMENT TRAINEE | MBA | PHD CANDIDATE

AT A GLANCE

ABOUT ME

I am an exceptionally driven consulting enthusiast and combine strong analytical expertise with agile management skills and an entrepreneurial mindset. I want to work in an agile, divers and vibrant environment. Developing new business strategies for customers to adapt to future challenges is my aspiration.

PERSONAL DATA

LANGUAGES

- German
- English
- French
- Spanish

SKILLS

- Leadership
- Project Mgmt
- Strategy Dev.
- Agile Methods
- Public Speaking
- MS Office
- Adobe Illustrator
- DaVinci Resolve

EXPERIENCES

MANAGEMENT TRAINEE BIOPHARMA
08/2019 -

BOEHRINGER INGELHEIM BIOPHARMA

Project lead strategy development for focus factory drug product. Project lead risk assessment essential technology for focus factory drug product. Project lead employer branding strategy development for Boehringer Ingelheim, Biopharma. Leading cross-functional teams (from trainee to senior management). Continuous feedback loops with/ and reporting to senior management. Scrum Master.

DOCTORATE/ DR. RER. NAT.
12/2015 - 07/2019

UNIVERSITY OF STUTTGART

Basic research and treatment development for breast cancer and diabetes mellitus. Project lead for *in vivo* studies. Planning, budgeting, coordination, execution, analysis, presentation and publishing of research.

MBA-THESIS
03/2018 - 09/2018

FRANKFURT SCHOOL & CEIBS

Entrepreneurial business plan, "PerfectWave". Project lead. Market analysis and development of business model, UX design, go-to-market strategy as well as financial model & projection. *Award for the best MBA-Thesis.*

MASTER THESIS
04/2014 - 09/2014

HARVARD MEDICAL SCHOOL

Treatment development for glaucoma. Planning, coordination, execution, analysis, presentation and publishing of research.

EDUCATION

UNIVERSITY OF STUTTGART DEPARTMENT: IZI
12/2015 - 07/2019

PHD (DR. RER. NAT.)

Emphasis: Triple-Negative Breast Cancer
Diabetes Mellitus
Final Grade: Thesis defense in March-April 2020

FRANKFURT SCHOOL OF FINANCE AND MANAGEMENT
10/2016 - 09/2018

MBA (PART-TIME)

Emphasis: Leadership & Change Management
Entrepreneurial Management
Marketing & Innovation Management
Final Grade: 1.5

CERTIFICATES & AWARDS

SCRUM MASTER
Scrum PSMI, Scrum.org, December 2019

BEST MBA-THESIS
Frankfurt School of Finance & Management, October 2018

SEBASTIAN **LIEB**

MANAGEMENT TRAINEE | MBA | PHD CANDIDATE

ADDITIONAL INFORMATION

PUBLICATIONS

LIEB ET AL. 2020

"Inhibition of protein kinase D induces β-cell senescence and thereby protects from high-fat-diet-induced glucose and insulin intolerance". *in preparation*.

RAU & LIEB ET AL. 2020

"A new bispecific antibody, targeting EGFRxHER3". *in preparation*.

LIEB ET AL. 2019

"The GEF-H1/PKD3 signaling pathway promotes the maintenance of triple negative breast cancer stem cells". *International Journal of Cancer*.

MUENSTER & LIEB ET AL. 2017

"The Ability of Nitric Oxide to Lower Intraocular Pressure Is Dependent on Guanylyl Cyclase". *Invest. Ophthalmol. Vis. Sci.*

BRÉGÈRE ET AL. 2017

"Neonatal hypoxia-ischemia in rat disrupts the developmental time course of doublecortin release in the cerebrospinal fluid". *European Journal of Neuroscience*.

HOERBER ET AL. 2016

"The atypical inhibitor of κB isoform ζ (I κBζ) regulates the anti-inflammatory response via interleukine 10 in macrophages". *Journal of Biological Chemistry*.

BRÉGÈRE ET AL. 2015

"Doublecortin in the Cerebrospinal Fluid Is a Candidate Biomarker of Neurogenesis after Neonatal Hypoxia Ischemia Brain Injury in Rats". *J Neurol Surg A Cent Eur Neurosurg*.

BRANER ET AL. 2012

"Hydrolysis of fatty acid esters by Candida antarctica lipase B (Novozym 435) dissolved in anhydrous triethylamine". *ChemCatChem*.

FURTHER EXPERIENCES

RESEARCH ASSISTANT
02/2015 - 11/2015
UNIVERSITY OF TUEBINGEN, IFIB
Prof. Dr. Klaus Schulze-Osthoff. Basic research on inflammatory diseases. Planning, coordination, execution, analysis, presentation and publishing of research.

INTERNSHIP
01/2014 - 03/2014
UNIVERSITY HOSPITAL BASEL, BIOMEDICINE
Prof. Dr. Raphael Guzman. Basic research on neurological diseases. Biomarker development for stroke patients. Execution, analysis and presentation of research.

BACHELOR THESIS
06/2012 - 08/2012
UNIVERSITY OF APPLIED SCIENCES, DA
Prof. Dr. Stephan Huettenhain. Organic chemistry. Research on homochiral-3-hydroxy fatty acid esters. Execution, analysis and presentation of research.

INTERNSHIP
03/2012 - 05/2012
NATIONAL UNIVERSITY OF SINGAPORE
Prof. Dr. Stephan Jaenicke. Organic chemistry. Research on catalytic and biocatalytic systems. Execution, analysis and presentation of research.

FURTHER EDUCATION

CHINA EUROPE INTERNATIONAL BUSINESS SCHOOL
07/2017
INTERNATIONAL MANAGEMENT
Part of the Frankfurt School of Finance & Management Part-Time MBA curriculum.
Final Grade: 1.0

UNIVERSITY OF TUEBINGEN & HARVARD MEDICAL SCHOOL
10/2012 - 03/2015
MSc BIOCHEMISTRY
Emphasis: Molecular Medicine, Phamracology
Final Grade: 1.4

UNIVERSITY OF APPLIED SCIENCES DARMSTADT
10/2009 - 09/2012
BSc BIOTECHNOLOGY
Emphasis: Biochemistry, Organic Chemistry
Final Grade: 1.5

CERTIFICATES & AWARDS

SCRUM MASTER
Scrum PSMI, Scrum.org, December 2019

DIGITAL TRANSFORMATION FOR LEADERS
LinkedIn Learning Certificate, February 2019

BEST MBA-THESIS
Frankfurt School of Finance & Management, October 2018

BEST SCIENTIFIC TALK
University of Stuttgart, IZI, September 2018